EXPERIMENTAL AND SIMULATION BASED DYNAMIC ASSESSMENT OF FLEXION AND EXTENSION MOVEMENTS OF TORSO

Pranitha Gottipati

Dissertation submitted to the faculty of the

Virginia Polytechnic Institute and State University

in partial fulfillment of the requirements for the degree of

Doctor of Philosophy

in

Engineering Mechanics

Kevin P. Granata, PhD, Co-Chair

Raymond H. Plaut, PhD, Co-Chair

Raffaella De Vita

J. Wally Grant

Scott L. Hendricks

Robert L. West

December 4th, 2009

Blacksburg, VA

Keywords: Spine, fatigue, stability, muscle forces

EXPERIMENTAL AND SIMULATION BASED DYNAMIC ASSESSMENT OF FLEXION AND EXTENSION MOVEMENTS OF TORSO

Pranitha Gottipati

ABSTRACT

Low back disorders (LBDs) comprise one of the major health issues in the United States. Previous research used isometric studies to understand the mechanisms that cause LBDs. Occupational tasks involving dynamic trunk movements, muscle fatigue, and spinal instability are identified as major risk factors for developing low back pain. Dynamic stability and muscle forces during trunk flexion-extension movements are studied in this dissertation.

Torso muscle fatigue is known to affect the neuromuscular muscle recruitment that influences spinal stability. The first part of this dissertation investigates the effect of muscle fatigue on the stability of dynamic trunk flexion-extension movements. Participants with no self-reported low back pain history performed repetitive trunk flexion-extension exercises before and after extensor muscle fatigue. The extensor muscles were fatigued to 60% of their unfatigued isometric maximum voluntary exertion force. The maximum finite-time Lyapunov exponent, λ_{Max}, was used to quantify the dynamic stability. Values of λ_{Max} increased with fatigue, suggesting dynamic stability of the torso decreases with muscle fatigue. Fatigue-by-task asymmetry interactions did not influence spinal stability.

The purpose of the second part of this dissertation was to predict time-dependent muscle forces and spinal loads during symmetric flexion-extension movements. A 2-dimensional sagittal plane, lumped parameter model was built with one thorax and five lumbar vertebrae stacked upon a stationary pelvis. Kinematics driven optimization was used to estimate time-dependent muscle forces. Muscle forces were determined by minimizing the metabolic power while satisfying the equations of motion. Spinal loads were calculated as the vector sum of the muscle

forces and the trunk weight. Abdominal activity was observed at the onset of flexion and at the end of extension. The multifidus and psoas muscles played a major role in the spine dynamics. The compressive spinal loads were found to reach highest values at the onset of flexion, while the shear loads reached the highest values at large flexion angles.

Acknowledgements

First of all I would like to thank my co-advisor Dr. Kevin Granata for introducing me to the field of musculoskeletal biomechanics. Without your vision and contributions this dissertation would not have been complete. Your knowledge and passion in this field have been a great inspiration for me. You have been a role model both in my professional and personal life.

I would like to thank my co-advisor Dr. Raymond Plaut for his invaluable support during the second part of my research. Thank you very much for taking up the responsibility and providing the required technical advice and feedback throughout my dissertation.

My advisory committee included Dr. Wallace Grant, Dr. Robert West, Dr. Raffaella DeVita, and Dr. Scott Hendricks. Your input and help at every step of my dissertation were very valuable. I would also like to thank Dr. Glenn Kraige for being a good friend and for providing valuable suggestions with regard to both the professional and personal life of a teacher. I will always cherish the days I worked for you as a GTA. I am thankful to Dr. Michael Madigan for being there for us in difficult times and always lending me a friendly hand whenever I needed it.

I am very thankful to Mrs. Linda Granata and to Mike and Lois Diersing for their continuous encouragement and support during the past four years. Mike and Lois, I am very indebted to you for all you did for me in my last semester. I would like to thank Anna for helping me with the writing. Thanks to ESM graduate enrollment specialists Mrs. Joyce Smith and Mrs. Lisa Smith for taking care of my academic paper work throughout my PhD.

I am very thankful to my friends Greg and Steve for helping me with data collection, and to Sunny for helping me with coding. My friends in Norris Hall, Corrie, Jul, Katie, Tim, Greg, Steve, Martin, Nick, Hyun, Brad, Dennis, Sara, and Emily, have helped me throughout my Ph.D. with their friendship and valuable inputs. I appreciate all you did for me and will always cherish

your friendship. I would like to thank my good friends, Rani and Shashi, for always being a phone call away irrespective of the time of day. I am very thankful to my friends in Blacksburg, Phani, Kalpana, Kiran, Priya, Smitha, Sheetal, Corrie, Sunny, Naresh, Vyas, Satyam, Neeta, Sachi, Prathyusha, Chaitanya, Tila, and Abhranil. Thanks for your love and care, especially in the last semester.

Thanks to my immediate and extended family for always believing in me and encouraging me in whatever I pursued. Thanks to peddamma and peddananna for being my proxy parents in the U.S. I am very indebted to my parents, Ragini and Aravind, for their unconditional love and support. I would not have been what I am if not for them. And to my brother, Roopu, who is my good friend. Thanks Roopu for being there to always lend your listening ear in good and bad times.

Finally, I would like to thank my husband, Vamsi, for his support and encouragement. Your love and patience especially during the last few months has been invaluable. You have worked hard to make it easier to live away from you during this long journey.

Table of Contents

List of Figures

List of Tables

Attributions

Dr. Kevin Granata contributed greatly to the work described in chapter 3. His interpretation of the results was helpful in developing the article and understanding the implications of the research. I thank him for his innovative ideas and inputs at every part of this work.

Chapter 1 - Significance

In the human body, the torso comprises two-thirds of the body weight. The spinal column is an important skeletal part of the torso. The spine consists of four types of vertebrae: (1) Cervical vertebrae; (2) Thoracic vertebrae; (3) Lumbar vertebrae; and (4) Sacrum. The lower-back or lumbar spine consists of five vertebrae, L1, L2, L3, L4 and L5. The movements of the lower-back vertebrae mainly influence the large angular displacements of the torso.

Low back pain is one of the most prevalent health issues in the United States. 85% of the U.S. population suffers from low back pain sometime in their lifetime (Pai and Sundaram, 2004). 85% of the time, the cause for back injuries is unknown (McGill, 2007). For the past few decades, active research has been conducted in the field of biomechanics to understand the cause for low back disorders and to develop prevention techniques.

Past work shows that the lack of stability is one of the major causes for low back injuries. Stability studies have demonstrated that certain factors such as muscle recruitment, spinal posture, and sudden external loads influence the static stability of the spine (Gardner-Morse et al., 1995b; Granata and Wilson, 2001). Recently researchers showed a link between muscle fatigue and stability (Granata et al., 2004). However, little has been investigated about the influence of muscle fatigue on the dynamic stability of musculoskeletal systems. Empirical investigation of the influence of fatigue on dynamic stability may help us in developing ways to control low back pain.

It is known that most of the low back disorders occur while performing dynamic tasks in industry and sports. Even though spine research has been active for decades, there is very little knowledge of the dynamic behavior of the spine. Many researchers have studied the isometric muscle recruitment patterns due to various postures and sudden load application. These studies

enabled us to understand the muscle co-activation and spine stability during certain postures and applications of sudden loads (McCook et al., 2009; Cholewicki and McGill, 1996; Dolan and Adams, 1993; Gardner-Morse et al., 1995b; Granata et al., 2005; Granata and Orishimo, 2001). Lately, there has been some emphasis on the dynamics of the low back. It was shown that the movement pace and direction during trunk flexion and extension movements affect spinal stability (Granata and England, 2006). Spinal loads and muscle forces increase considerably with movement velocity, acceleration, and sudden loading conditions (Bazrgari et al., 2008; Bazrgari et al., 2009 a,b; Lavender et al., 2003). Hence, there is a further need to study spine mechanics more in the dynamic sense than in the isometric sense.

Specific Aims

Many fundamental tasks that use large trunk movements involve flexion and extension. Therefore, this research study is focused on the mechanics of sagittal plane flexion and extension movements of the trunk. The dissertation research consists of two major parts: (1) the experimental part, and (2) the modeling part.

Experimental Study

Experiments were conducted to study empirically the effect of lumbar fatigue on the dynamic stability of trunk flexion and extension movements. The empirical measurements that quantify the stability are used in the study.

Model

A new mathematical simulation model has been developed. The model uses the recorded data from the experiments to estimate dynamic muscle forces. The dynamic forces during continuous flexion and extension movements are determined using optimization techniques.

Documentation Organization

This dissertation consists of six chapters. Chapter 1 gives brief information on the motivation for the research. Chapter 2 introduces the literature review and analytical background for the experimental study. Chapter 3 presents the detailed experimental study, "Fatigue Influences the Dynamic Stability of the Torso". Chapter 4 introduces the literature review and background for the simulation study. Chapter 5 presents the detailed methods for simulation study. Chapter 6 presents the study "Estimating Dynamic Muscle Forces of the Torso during Flexion and Extension Movements: A Mathematical Simulation". Finally, Chapter 7 summarizes the results of the work and presents ideas for possible future research.

References

BAZRGARI, B., SHIRAZI-ADL, A. & LARIVIERE, C. (2009a) Trunk response analysis under sudden forward perturbations using a kinematics-driven model. *J Biomech,* 42**,** 1193-200.

BAZRGARI, B., SHIRAZI-ADL, A. & PARNIANPOUR, M. (2009b) Transient analysis of trunk response in sudden release loading using kinematics-driven finite element model. *Clin Biomech,* 24**,** 341-7.

BAZRGARI, B., SHIRAZI-ADL, A. & KASRA, M. (2008) Computation of trunk muscle forces, spinal loads and stability in whole-body vibration. *J Sound Vib,* 318**,** 1334-47.

BAZRGARI, B., SHIRAZI-ADL, A., TROTTIER, M. & MATHIEU, P. (2008) Computation of trunk equilibrium and stability in free flexion-extension movements at different velocities. *J Biomech,* 41**,** 412-21.

CHOLEWICKI, J. & MCGILL, S. M. (1996) Mechanical stability of the in vivo lumbar spine: implications for injury and chronic low back pain. *Clin Biomech,* 11**,** 1-15.

DOLAN, P. & ADAMS, M. A. (1993) The relationship between EMG activity and extensor moment generation in the erector spinae muscles during bending and lifting activities. *J Biomech,* 26**,** 513-22.

GARDNER-MORSE, M. G., STOKES, I. A. F. & LAIBLE, J. P. (1995) Role of muscles in lumbar spine stability in maximum extension efforts. *J Orthop Res,* 13**,** 802-8.

GRANATA, K. P. & ENGLAND, S. A. (2006) Stability of dynamic trunk movement. *Spine,* 31**,** E271-6.

GRANATA, K. P., LEE, P. E. & FRANKLIN, T. C. (2005) Co-contraction recruitment and spinal load during isometric trunk flexion and extension. *Clin Biomech,* 20**,** 1029-37.

GRANATA, K. P. & ORISHIMO, K. F. (2001) Response of trunk muscle coactivation to changes in spinal stability. *J Biomech,* 34**,** 1117-23.

GRANATA, K. P., SLOTA, G. P. & WILSON, S. E. (2004) Influence of fatigue in neuromuscular control of spinal stability. *Hum Factors,* 46**,** 81-91.

GRANATA, K. P. & WILSON, S. E. (2001) Trunk posture and spinal stability. *Clin Biomech,* 16**,** 650-9.

LAVENDER, S. A., ANDERSSON, G. B. J., SCHIPPLEIN, O. D. & FUENTES, H. J. (2003) The effects of initial lifting height, load magnitude, and lifting speed on the peak dynamic L5/S1 moments. *Int J Indus Ergonom,* 31**,** 51-9.

MCCOOK, D. T., VICENZINO, B. & HODGES, P. W. (2009) Activity of deep abdominal muscles increases during submaximal flexion and extension efforts but antagonist co-contraction remains unchanged. *J Electromyogr Kinesiol,* 19**,** 754-62.

MCGILL, S. M. (2007) *Low Back Disorders: Evidence-Based Prevention and Rehabilitation.* Champaign (IL), Human Kinematics.

PAI, S. & SUNDARAM, L. J. (2004) Low back pain: an economic assessment in the United States. *Orthop Clin North Am,* 35**,** 1-5.

Chapter 2 – Muscle Fatigue and Spinal Stability

Introduction

Muscle fatigue can be defined as a reduction in capacity of a muscle to produce tension or contraction (Cailliet, 2003). Muscle fatigue has been identified as a risk factor for developing low back pain. Researchers have been investigating various mechanisms to understand how muscle fatigue influences low back disorders. Muscle fatigue may influence the stability of a musculoskeletal system, which may lead to injury and pain. The following section gives an overview of muscle fatigue studies in the literature. The section after that presents an overview of past studies in which the stability of musculoskeletal systems was investigated analytically and empirically. The final section gives the analytical background related to this study.

Muscle Fatigue Linked to Low Back Pain

For decades, muscle fatigue has been considered to be a major factor in causing low back pain by affecting the neuro-musculoskeletal functions. As a result, in the past two decades researchers have shown growing interest in studying the role of muscle fatigue in developing low back disorders. One of the early studies demonstrated that isometric endurance tests can predict the onset of low back pain (Biersing-Sorensen, 1984). Roy et al. (1989) showed that muscle fatigue could serve as a measure of low back pain. Electromyograms of multiple back muscles were recorded during sustained isometric trunk extensions. These tests predicted the onset of low back pain in the subjects with approximately 90% reliability. Luoto et al. (1995) conducted static back endurance tests to measure the risk of developing low back pain. It was found that poor endurance may lead to physical fatigue and thus may increase the risk of developing low back disorders. Thomas et al. (2000) studied muscle fatigue associated with loading of the trunk in the coronal plane, and found that all the trunk muscles are susceptible to fatigue. This study concluded that endurance training of paraspinal and abdominal muscles may reduce the risk of low back pain.

Taimela et al. (1999) showed that lumbar fatigue impairs the ability to sense a change in lumbar position. This phenomenon was found to be even worse in patients with low back pain. The task in that study involved reacting to the perception of lumbar movement (flexion and extension) as soon as possible. During the test, the participants were seated on a specially manufactured trunk rotation measurement unit that induced dynamic movement to the trunk while restricting the movement of the pelvis and lower limbs. In Sparto and Parnianpour (1998), the effects of torso extensor muscle fatigue on muscle forces and spinal loading were investigated during the performance of repetitive dynamic trunk extensions. Fatigue was quantified using endurance time and rate of decline of dynamic maximum voluntary contraction in trunk extension. This study showed that the risk of low back pain could be due to the effect of muscle fatigue on muscle recruitment patterns, and thus due to the spinal loads.

Recent investigations suggested that torso muscle fatigue may affect spinal stability and as a result may increase the risk of low back pain. In Granata et al. (2004), the subjects were asked to maintain a static posture against a sudden horizontal flexion force before and after muscle fatigue. Electromyographic and kinematics data during the trial were recorded to assess the change in spinal stability with fatigue. The investigators also developed a mathematical model of the spine with 6 degrees of freedom and 12 deformable muscles. Using optimization techniques and sensitivity analyses, they investigated the effect of fatigue on spinal stability analytically. It was found that the empirical analyses supported the model predictions.

In Herrmann et al. (2006), 10 male participants were subjected to perturbation during quiet standing before and after muscle fatigue. Reflexes of paraspinal muscles during these trials were recorded. Fatigue of paraspinal muscles increased the amplitude of the muscle reflexes to compensate for the loss of the muscle force capacity to maintain spinal stability. A similar study was conducted to investigate the effect of fatigue on postural sway and joint kinematics during quiet standing (Madigan et al., 2006). It was found that after muscle fatigue the participant had a slight forward lean posture and that the variability of the joint angle had increased. However, none of these studies reported empirical evidence that shows the influence of torso muscle fatigue on dynamic stability of the torso.

Stability

Many investigators in the past two decades have focused on finding the mechanisms causing instability of musculoskeletal systems. Stability is necessary to avoid pain and injury (Reeves et al., 2007). For years, the effect of fatigue on spinal stability has been studied using empirical data on changes in postural sway or muscular responses to sudden perturbations (Davidson et al., 2004).

Bergmark (1989) was the first investigation of the stability of the spine, and involved minimizing the potential energy of the system. Crisco and Panjabi (1992) modeled the spine as an Euler column. They used Euler buckling theory to investigate the mechanical stability of the spine. The stability and the load bearing capacity of the spine decreased after buckling. This model was validated by experiments.

Meakin et al. (1996) built two models: a static model and a dynamic model. The standing posture in the sagittal plane was modeled as an Euler beam in the second mode. The flexed spine was modeled as an Euler beam in the first mode. Stability was investigated using the changes in the bending stiffnesses of the beams.

Later researchers started investigating stability changes in musculoskeletal systems empirically based on experimental studies. Sparto and Parnianpour (1998) used center of pressure measurements to quantify postural stability. In 2003 investigations showed that the center of pressure (COP) quantifies the postural sway, whereas the center of mass (COM) quantifies the postural stability. However, COP and COM measurements limit one to investigate the postural stability, but not dynamic stability. To investigate dynamic stability, kinematic variability has been used as the quantifying factor in some studies (Holt et al., 1995; Yack and Berger, 1993). In general, dynamic stability is considered to be the ability of a system to resist kinematic perturbations. However, Dingwell and Cusumano (2000) showed that kinematic variability cannot be a quantifying measure of this dynamic stability. They showed that greater kinematic variability does not suggest lower stability. In their study, nonlinear dynamics concepts were

applied to empirically investigate the local dynamic stability of human walking. Maximum finite-time Lyapunov exponents were calculated to quantify local dynamic stability of continuous overground walking in patients with diabetic neuropathy. Granata and England (2006) applied these concepts to investigate the dynamic stability of repetitive trunk movements. The kinematic trajectories of torso flexion and extension movements were recorded using motion sensors. The maximum finite-time Lyapunov exponents of these trajectories were calculated. The larger the maximum Lyapunov exponent is, the lower the dynamic stability of the system. That study found that the torso's dynamic stability decreases with movement velocity. It also found that symmetric movements of the torso are less stable than asymmetric movements. These dynamic stability assessment methods can also be used to investigate the effect of muscle fatigue on the stability of the torso.

Analysis Background

Local Dynamic Stability

Stability can be defined in many ways depending on the problem that is considered. For the scope of this work, the concept of Lyapunov stability is used. A movement trajectory of a system is considered stable if all movement trajectories that are sufficiently close to the reference path continue to remain close for all time (Strogatz, 1994). This kind of stability can be quantified using Lyapunov exponents. The following paragraphs describe the theory of Lyapunov exponents.

Dynamical systems are represented by state vectors in a state space that change with time. The evolution of the state vectors is sensitive to initial conditions. This sensitivity to initial conditions can be quantified by the Lyapunov exponents. The state vectors of a system define the movement trajectories. If a trajectory diverges (converges) from (towards) the reference trajectory at time *'t'*, then the rate of divergence (convergence) gives the measure of local instability (stability) of the system at that time. This rate of divergence (convergence) is quantified using Lyapunov exponents, i.e., the measure of divergence (convergence) is

proportional to $e^{\lambda t}$, where λ is the Lyapunov exponent. A positive λ represents divergence, whereas a negative λ represents convergence. An *n*-dimensional dynamical system has *n* state vectors, hence *n* Lyapunov exponents (Lyapunov spectrum). For a system to be globally stable, the sum of all the Lyapunov exponents should be less than zero (Rosenstein et al., 1993).

The entire Lyapunov spectrum of a system can be calculated from the dynamic equations of the system. However, in most experimental studies the dynamic equations of the system are not available. In such cases the maximum finite-time Lyapunov exponent can be used to quantify the level of local dynamic stability. It has been suggested that according to the multiplicative ergodic theorem two randomly chosen initial trajectories will diverge on average exponentially at a rate given by the maximum Lyapunov exponent (Rosenstein et al., 1993). This maximum finite-time Lyapunov exponent is defined as the average rate of divergence of neighboring trajectories in a state space at time *t* (Dingwell and Cusumano, 2000).

Reconstruction Dynamics

To calculate the maximum Lyapunov exponent, information on the complete dynamics of the system is necessary, which can be achieved by reconstruction dynamics. In general, musculoskeletal systems are complex systems for which multiple dimensions are required to represent the complete dynamics. However, it is not always easy to record the complete dynamics of a system experimentally. In such cases, it can be reconstructed from a single time series vector. In this research, the method of delays (Granata and England, 2006; Rosenstein et al., 1993) was used to reconstruct the *n*-dimensional state space from a single time series. The number '*n*' is called the embedding dimension. If *x(t)* is the single time series vector available and T_d is the chosen time delay, then the reconstructed state space can be expressed as

$$\mathbf{Y}(t) = [x(t), x(t+T_d), x(t+2T_d) \ldots x(t+(n-1)\cdot T_d)] \qquad (2.1)$$

The following sub-sections describe how to calculate the embedding dimension and time delay for a given experimental time series vector.

How to find time delay?

The reconstructed dynamics using the method of delays are sensitive to time delay (Rosenstein et al., 1993). For noise-free data, the time delay can be chosen arbitrarily; however, for experimental data, the time delay has to be chosen such that it is neither too small nor too large (Fraser and Swinney, 1986b). If the time delay is too small, it may result in redundancy, and if the time delay is too large, it will cause irrelevance (England and Granata, 2006; Rosenstein et al., 1993). Fraser and Swinney (1986) introduced the average mutual information (AMI) criterion to calculate the time delay for experimental data. In this method, the time delays are calculated from the first minimum of the AMI function (Dingwell and Cusumano, 2000). The AMI is defined as the information in two trajectories of a reconstructed state space that is mutual. The time delay at the minimum AMI function gives state space vectors with minimum redundancy.

How to find embedded dimension?

The embedding dimension of reconstruction dynamics can be estimated from the global false nearest neighbor analysis (Kennel and Isabelle, 1992b). The nearest neighbor of a point on a trajectory *i* is defined as a point on a neighboring trajectory *j* which is at the minimum Euclidean distance. When the dynamics of a system are represented in a lower dimensional space than required, the trajectories overlap. Due to such overlap of trajectories, the state space may represent false nearest neighbors. False nearest neighbors are defined as the set of neighbors that appear to be close at a lower dimensional state space, but not at the higher dimensions (England and Granata, 2006). The global false nearest neighbors algorithm (Kennel and Isabelle, 1992b) incrementally increases the dimensions while comparing the distances between the trajectories until the number of false nearest neighbors approaches zero (Dingwell and Cusumano, 2000; England and Granata, 2006). The number of dimensions at which the false nearest neighbors are zero is called the embedding dimension.

Maximum Lyapunov exponent

Once the embedding dimension '*n*' and the time delay 'T_d' are estimated, the single time series vector can be reconstructed into *n*-dimensional state space. From the reconstructed dynamics, the maximum Lyapunov exponent can be estimated using Rosenstein's nearest neighbors algorithm (Rosenstein et al., 1993). The algorithm finds the nearest neighbors of points on a trajectory and calculates the Euclidean distance between them. This Euclidean distance is proportional to $e^{\lambda t}$, where λ is the Lyapunov exponent at time t. The largest Lyapunov exponent is then calculated as the average rate of the Euclidean distance between the nearest neighbors in a finite time (Rosenstein et al., 1993). Then the separation $d_j(t)$ of the j^{th} nearest neighbors at time *t* can be given as

$$d_j(t) = C_j e^{\lambda_j t} \tag{2.2}$$

If Δt is the sampling period of the data set, then the above equation can be written as

$$d_j(i) = C_j e^{\lambda_j . i . \Delta t} \tag{2.3}$$

By taking the natural logarithm on both sides of the above equation, we get a set of lines with slopes equal to the Lyapunov exponents λ_j:

$$\ln d_j(i) = \ln C_j + \lambda_j . i . \Delta t \tag{2.4}$$

Then the maximum Lyapunov exponent is estimated from an average line of these sets of lines that can be estimated with a least squares fit, which gives

$$y(i) = \frac{1}{\Delta t} \left\langle \ln d_j(i) \right\rangle \tag{2.5}$$

where $\langle \ldots \rangle$ represents the average of the separations of all nearest neighbors. Empirically the algorithm calculates $\ln d_j(i)$ as $\ln\{d_j(t+\Delta t) / d_j(t)\}$. Then the above equation can be written as

$$\left\langle \ln \{d_j(t+\Delta t)/d_j(t)\} \right\rangle = \lambda_{Max} \Delta t \tag{2.6}$$

The slope of this line gives the finite-time maximum Lyapunov exponent λ_{Max} of a single time series vector. λ_{Max} is the mean rate of divergence of initially neighboring trajectories along the least stable dimension.

Example: Lorentz Attractor

The above described method is explained with the example of the Lorenz attractor below. Figure 2.1 shows the 2-dimensional Lorenz attractor with σ = 10, ρ = 28 and β = 8/3.

$$\begin{aligned} \dot{x} &= \sigma(y - x) \\ \dot{y} &= (-xz + \rho x - y) \\ \dot{z} &= (xy - \beta z) \end{aligned} \tag{2.7}$$

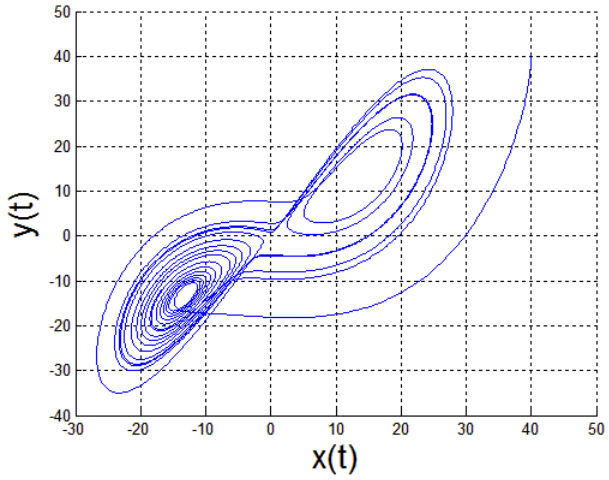

Figure 2.1: Lorenz attractor in 2D state space with σ = 10, ρ = 28 and β = 8/3

If only one state space vector *x(t)* is available, then the complete dynamics of the attractor can be represented using reconstructed dynamics. To reconstruct the dynamics, first the time delay and embedding dimension are calculated. Figures 2.2 and 2.3 show the graphs of the average mutual information function vs. time delay and the percentage of false nearest neighbors vs. embedding dimension, respectively. The first minimum AMI occurs at time lag 90, i.e., 0.09ms, and the embedding dimension is found to be 2.

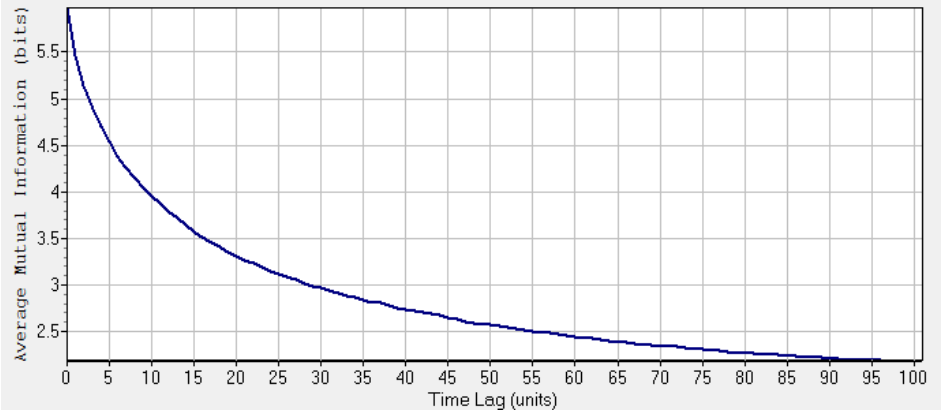

Figure 2.2: AMI vs. Time Lag: The AMI algorithm estimated time delay for Lorenz attractor as 0.09ms

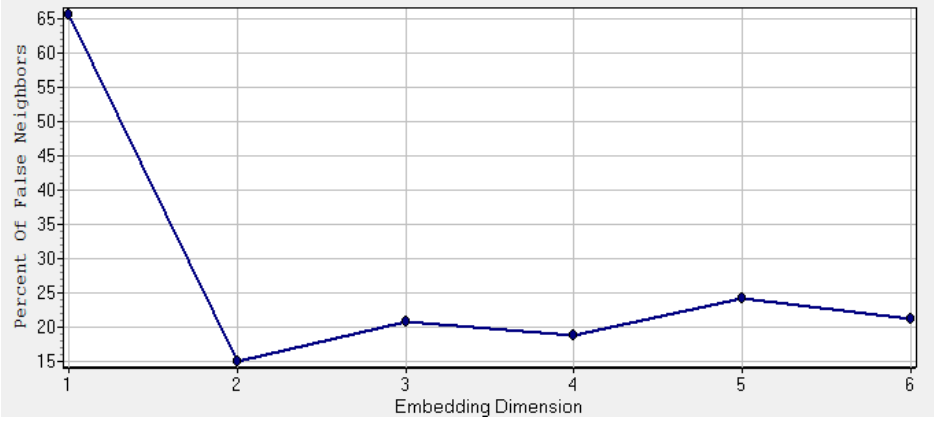

Figure 2.3: Percent of false neighbors vs. embedding dimension: The Global false nearest neighbor analysis estimated the embedding dimension of Lorenz attractor as 2

Once the embedding dimension and the time delay are calculated, the dynamics are reconstructed using the method of delays. Figure 2.4 shows the reconstructed dynamics in 2-dimensional state space. It also shows how the separation of nearest neighbors is calculated at time t. After reconstruction of the dynamics, the average logarithmic divergence of all the nearest neighbors is calculated and plotted against time (Figure 2.5). The slope of the initial linear region of the curve using a least squares best fit gives the maximum finite-time Lyapunov exponent.

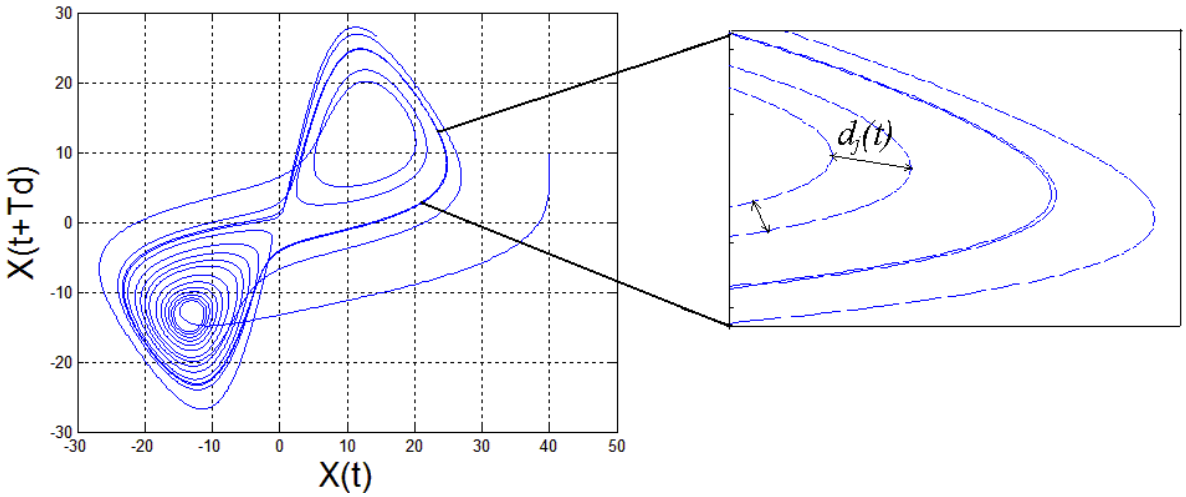

Figure 2.4: Reconstructed dynamics of Lorenz attractor and representation of Euclidean distance between nearest neighbors

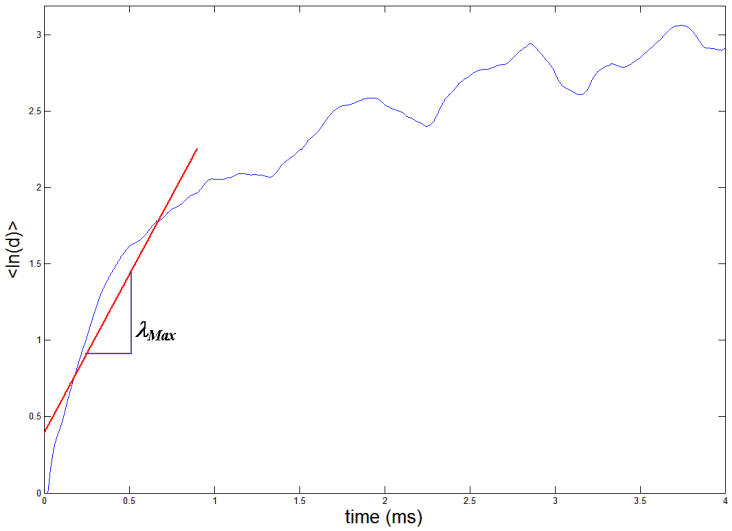

Figure 2.5: Average logarithmic divergence vs. time: The slope of the initial linear region of the curve is estimated as the maximum Lyapunov exponent

References

BERGMARK, A. (1989) Stability of the lumbar spine. A study in mechanical engineering. *Acta Orthop Scand,* 60 Suppl 230**,** 3-54.

BIERSING-SORENSEN, F. (1984) Physical measurements as risk indicators for low-back trouble over a one-year period. *Spine,* 9**,** 106-19.

CAILLIET, R., (2003) *Low back disorders A medical enigma,* Philadelphia, PA, Wolters Kluwer.

CRISCO, J. J. & PANJABI, M. M. (1992) Euler stability of the human ligamentous lumbar spine. Part I: Theory. *Clin Biomech,* 7**,** 19-26.

DAVIDSON, B. S., MADIGAN, M. L. & NUSSBAUM, M. A. (2004) Effects of lumbar extensor fatigue and fatigue rate on postural sway. *Eur J Appl Physiol,* 93**,** 183-9.

DINGWELL, J. B. & CUSUMANO, J. P. (2000) Nonlinear time series analysis of normal and pathological human walking. *Chaos,* 10**,** 848-63.

ENGLAND, S. A. & GRANATA, K. P. (2006) The influence of gait speed on local dynamic stability of walking. *Gait Posture,* 25, 172-8.

FRASER, A. M. & SWINNEY, H. L. (1986) Independent coordinates for strange attractors from mutual information. *Phys Rev A,* 33**,** 1134-40.

GRANATA, K. P. & ENGLAND, S. A. (2006) Stability of dynamic trunk movement. *Spine,* 31**,** E271-6.

GRANATA, K. P., SLOTA, G. P. & WILSON, S. E. (2004) Influence of fatigue in neuromuscular control of spinal stability. *Hum Factors,* 46**,** 81-91.

HERRMANN, C. M., MADIGAN, M. L., DAVIDSON, B. S. & GRANATA, K. P. (2006) Effect of lumbar extensor fatigue on paraspinal muscle reflexes. *J Electromyogr Kinesiol,* 16, 637-41.

HOLT, K. G., JENG, S. F., RATCLIFFE, R. & HAMILL, J. (1995) Energetic cost and stability during human walking at the preferred stride frequency. *J Motor Behavior,* 27**,** 164-78.

KENNEL, M. B. & ISABELLE, S. (1992) Method to distinguish possible chaos from colored noise and to determine embedding parameters. *Phys Rev A,* 46**,** 3111-8.

LUOTO, S., HELIOVAARA, M. H., HURRI, H. & ALARANTA, H. (1995) Static back endurance and the risk of low-back-pain. *Clin Biomech,* 10**,** 323-4.

MADIGAN, M. L., DAVIDSON, B. S. & NUSSBAUM, M. A. (2006) Postural sway and joint kinematics during quiet standing are affected by lumbar extensor fatigue. *Hum Mov Sci,* 25, 788-99.

MEAKIN, J. R., HUKINS, D. W. & ASPDEN, R. M. (1996) Euler buckling as a model for the curvature and flexion of the human lumbar spine. *Proc Roy Soc B - Biol Sci,* 263**,** 1383-7.

REEVES, N. P., NARENDRA, K. S. & CHOLEWICKI, J. (2007) Spine stability: the six blind men and the elephant. *Clin Biomech,* 22**,** 266-74.

ROSENSTEIN, M. T., COLLINS, J. J. & DE LUCA, C. J. (1993) A practical method for calculating largest Lyapunov exponents from small data sets. *Physica D,* 65**,** 117-34.

ROY, S. H., DE LUCA, C. J. & CASAVANT, D. A. (1989) Lumbar muscle fatigue and chronic lower back pain. *Spine,* 14**,** 992–1001.

SPARTO, P. J. & PARNIANPOUR, M. (1998) Estimation of trunk muscle forces and spinal loads during fatiguing repetitive trunk exertions. *Spine,* 23**,** 2563-73.

STROGATZ, S. (1994) *Nonlinear Dynamics and Chaos - With Applications to Physics, Biology, Chemistry, and Engineering*, Cambridge, MA, Perseus Books.

TAIMELA, S., KANKAANPAA, M. & LUOTO, S. (1999) The effect of lumbar fatigue on the ability to sense a change in lumbar position - A controlled study. *Spine,* 24**,** 1322-7.

THOMAS, J. S., CORCOS, D. M. & HASAN, Z. (2003) Effect of movement speed on limb segment motions for reaching from a standing position. *Exp Brain Res,* 148**,** 377-87.

YACK, H. J. & BERGER, R. C. (1993) Dynamic stability in the elderly: identifying a possible measure. *J Gerontol: Med Sci,* 48**,** M225-30.

Chapter 3 - Fatigue Influences the Dynamic Stability of the Torso

Published in Ergonomics, Vol. 51, 2008, pp. 1258-1271, by Kevin P. Granata and P. Gottipati.

Abstract

Objective: Fatigue in the extensor muscles of the torso affects neuromuscular recruitment and control of the spine. The goal of this study was to test whether fatigue influences the stability of dynamic torso movements.

Research Design: A controlled laboratory experiment measured the change in the maximum finite-time Lyapunov exponent, λ_{Max}, before and after fatigue of the extensor muscles.

Methods: Nonlinear analyses were used to compute stability from the embedding dimension and Lyapunov exponent recorded during repetitive dynamic trunk flexion tasks. Torso extensor muscles were fatigued to 60% of their unfatigued isometric maximum voluntary exertion force and then stability was re-measured. Independent variables included fatigue, task asymmetry, and lower-limb constraint.

Results: λ_{Max} values increased with fatigue, suggesting poorer dynamic stability when fatigued. Embedding dimension declined with fatigue, indicating reduced dynamic complexity when fatigued.

Conclusions: Fatigue-related changes in spinal stability may contribute to the risk of low back injury during fatiguing occupational lifting tasks.

Keywords: Low Back, Fatigue, Stability, Dynamics.

Introduction

Lifting-induced fatigue can influence neuromuscular control of spinal stability. Endurance and fatigue of the trunk extensor muscles have been identified as risk factors for low back pain (Biering-Sorensen, 1984; Luoto et al., 1995), but the mechanisms of this risk are not well understood. It may be associated with compensatory muscle recruitment and changes in spinal load when fatigued (Sparto and Parnianpour, 1998). It may also be associated with decrements in the ratio of lift-strength versus task requirements (Keyserling et al., 1980). Recent studies suggest that fatigue of the torso muscles can affect spinal stability (Granata et al., 2004). If fatigue impairs stability, then small kinematic disturbances or neuromuscular errors can cause brief uncontrolled intervertebral movement and subsequent tissue strain injury. However, there are no existing direct empirical measurements of stability to test whether fatigue influences stability during dynamic torso movements.

Neuromuscular control factors that contribute to stability are influenced by fatigue. Control of stability is maintained by three biomechanical sub-systems (Panjabi, 1992a). First, the passive sub-system describes stabilizing contributions from spinal ligaments, discs, and bones. Second, open-loop recruitment of torso and paraspinal muscles contributes to the active viscoelastic stiffness necessary to maintain stability of the spinal column (Bergmark, 1989a). The stiffness of muscles increases with active recruitment (Morgan et al., 1978). For example, co-contraction can influence the bending stiffness of the torso (Lee et al., 2006). Therefore, appropriate open-loop recruitment may be used to control spinal stiffness and stability (Gardner-Morse and Stokes, 1998, Granata and Marras, 2000). Fatigue may influence both the intrinsic stiffness of actively contracting muscles (Gollhoffer et al., 1987) and the muscle recruitment patterns during steady-state exertions (Sparto and Parnianpour, 1998). Hence, fatigue may influence the open-loop control of spinal stability. The third sub-system for control of stability is provided by active feedback from reflex and voluntary modulation of muscle recruitment (Hogan, 1984). Recent studies demonstrate that the feedback provided by reflexes in the paraspinal muscles may account for up to 40% of the stabilizing control of the torso (Moorhouse and Granata, 2006). Fatigue influences the reflex response of torso control (Wilder et al., 1996). There is a disagreement whether fatigue causes reflex amplitude to increase or decrease (Avela et al., 1999;

Qita and Kearney, 2000) but most studies agree that fatigue causes increased myoelectric and electromechanical delay (Hagbarth et al., 1995; Hotobagyi et al., 1991). Changes in feedback delay can inhibit the neuromuscular control of spinal stability (Franklin and Granata, 2006). Therefore, fatigue may influence the feedback control of spinal stability. Although fatigue may influence several control sub-systems, it is difficult to predict whether these effects are sufficient to affect overall stability. Therefore, empirical measures of torso stability are necessary.

Stability of the torso can be estimated using analyses of nonlinear dynamics. A time-dependent kinematic reference trajectory represents the desired time-dependent movement path of the torso. It is considered stable if all trajectories that are sufficiently close to the reference path continue to remain close for all time (Strogatz, 1994). These conditions assure that small kinematic disturbances can be controlled and attenuated. By recording the time-dependent behavior of kinematic variance, one can quantify stability from analyses of whether or not movement trajectories approach the reference trajectory. This concept was applied to record stabilizing control of the torso in a seated posture (Cholewicki et al., 2000). Nonlinear methods can also be used to quantify stability during dynamic movements. In dynamic tasks, Lyapunov exponents are used to describe whether local kinematic errors grow in time or decay toward the reference trajectory, i.e., kinematic expansion versus kinematic contraction. For a system moving in n generalized dimensions, there must be one Lyapunov exponent λ_i for each of the n dimensions. Kinematic dispersion (contraction) of the i^{th} principal axis is proportional to $e^{\lambda_i t}$. The Lyapunov exponent is positive if there is kinematic expansion; it is negative if the kinematic perturbations grow smaller in time, i.e. contraction. For a dynamic system to be asymptotically stable (i.e., stable in a global sense), the sum of all the Lyapunov exponents must be less than zero. Unfortunately, it is infeasible to measure all of the Lyapunov exponents from experimental time series data. However, the largest Lyapunov exponent λ_{Max} quickly dominates the dynamic behaviour of the system and is readily computed from measured data (Rosenstein et al., 1993). The kinematics of each flexion and extension movement of the torso can be represented by a kinematic trajectory. Therefore, empirical measurement of λ_{Max} has proven to be a useful estimate of stability during torso movements (Granata and England, 2006).

The goal of this study was to test whether fatigue influences stability during dynamic torso movements. The task involved repetitive trunk flexion and extension movements in the mid-sagittal plane to repeatedly touch a target in front of the subject. We tested two hypotheses. First, stability of dynamic trunk flexion and extension movements decreases with fatigue. Second, task asymmetry influences fatigue-related changes in dynamic stability. Task asymmetry is considered to be a risk factor for occupationally-related low back pain (Fathallah et al., 1998). Evidence suggests that asymmetry influences stability during dynamic trunk movements (Granata and England, 2006). Moreover, effects of asymmetry may influence compensatory muscle recruitment associated with fatigue (Van Dieen and Heijblom, 1996). Therefore, fatigue-by-asymmetry interactions were expected in the stability of flexion tasks. To address the goals and hypotheses, we implemented nonlinear time-series analyses to characterize stability during repetitive trunk flexion tasks both before and immediately following fatigue of the trunk extensor muscles.

Materials and methods

Subjects

Ten healthy adults performed repetitive dynamic trunk flexion movements. The subjects were five men and five women with no self-reported history of low back pain (Table 3.1). Prior to participation in the experiment, each subject provided informed consent approved by the Virginia Tech institutional review board.

Table 3.1: Subject demographics and anthropometry. Values represent mean (standard deviation) of the subject pool.

	Males	Females
Number of Subjects	5	5
Age [yrs]	29.60 (5.23)	23.60 (4.51)
Height [cm]	178.04 (9.35)	166.07 (3.10)
Body Mass [kg]	72.30 (9.04)	61.24 (12.43)

Stability Assessment Protocol

The stability assessment required subjects to repetitively touch a target placed in the anterior mid-sagittal plane (Figure 3.1) as per protocols described in (Thomas et al., 2003). The target was located so that the subject could reach it by means of 60^0 of trunk flexion with elbow extended, shoulder flexed 90^o, and lower limbs vertical. Note that the target placement was determined by these postural constraints, but during data collection trials the subjects were free to move in a self-selected manner with no constraint on arm, shoulder, or torso posture. The task required the subjects to touch the flexion target with their hands and then return to the upright posture. To assure that the subjects returned to an upright posture during each cycle, a sphere was suspended such that it made contact with the posterior thorax when the subject was fully upright. Subjects moved in time with a metronome tone so as to achieve 30 flexion cycles per minute. The cyclic movements were performed repetitively and without pause for a trial duration of one minute.

Movement kinematics were recorded throughout each dynamic stability trial. Two electromagnetic sensors were secured to the skin by double-sided tape over the S1 and T10 spinous processes (Motionstar ERT, Ascension Technology, Natick, MA). Lumbar angles were computed from the Euler rotation matrices recorded from the T10 sensor with respect to the S1 sensor at a data collection rate of 100 Hz (Granata and Sanford, 2000). These provided time-series signals of 3-D lumbar angles including sagittal flexion, lateral flexion, and twist during the repetitive dynamic movements.

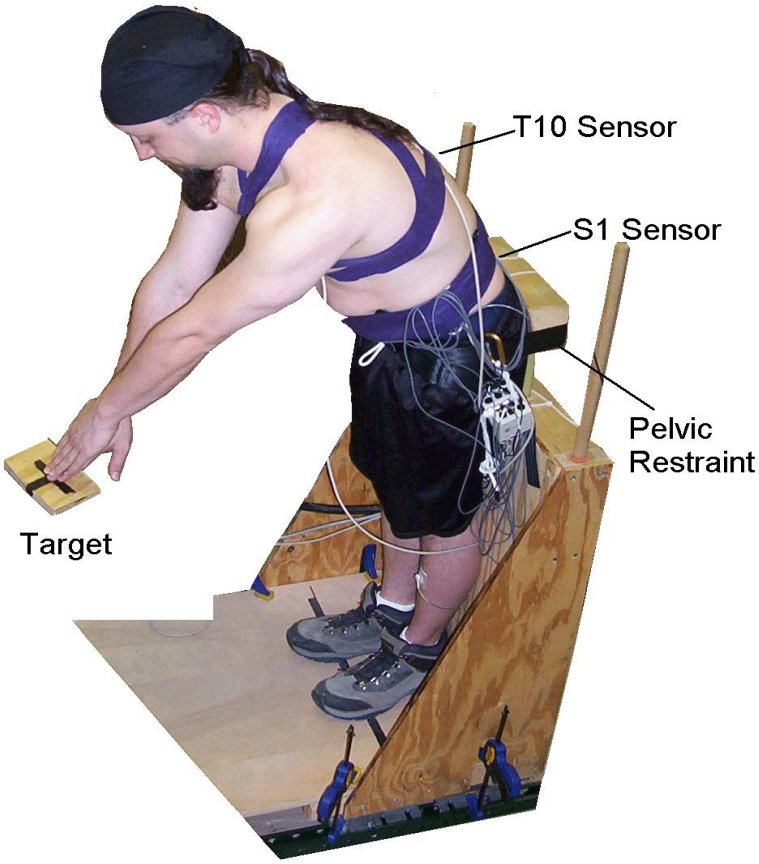

Figure 3.1: Stability Assessment Protocol: The task was to touch a target placed near knee level with their hands and then return to the upright posture in time with a metronome tone. The task required continuously repetitive movement patterns at a rate of 30 cycles per minute

Experimental conditions included task asymmetry, lower-limb constraint, and fatigue. During symmetric conditions, subjects were required to touch the target with both hands simultaneously. During asymmetric trials, they touched the target with their dominant hand only. Pilot measurements illustrated that one-handed reaching tasks produced asymmetric movement characterized by simultaneous torso flexion and axial rotation. Conditions of lower-limb constraint describe whether the subjects' legs and pelvis were constrained by strapping to a pelvic support structure. During constrained conditions, the pelvic support structure was designed to restrict the motion of the lower body, thereby isolating movement to the torso and arms (Figure 3.1). In the unconstrained trials, the legs and pelvis were free to move normally, but the subjects were instructed to keep their knees straight. Each experimental combination of

asymmetry and lower-limb constraint was performed twice, i.e., a total of 8 trials before fatigue and 8 trials after fatigue. Subjects were allowed to practice the movements until they were comfortable with the movement trajectory and movement pace before data collection for each trial. Experimental combinations of asymmetry and lower-limb constraint were presented in random order with at least one minute of rest between trials.

Fatigue Protocol

Stability was assessed before and immediately following a fatigue protocol. The fatigue protocol was performed immediately after the non-fatiguing protocol. The protocol required subjects to perform dynamic trunk extension exercises until the maximum voluntary trunk extension strength declined to 60% of the unfatigued strength. Subjects completed warm-up exercises including lumbar stretching and back extension movements on a 45^0 Roman chair. Following the warm up, isometric maximum voluntary exertion (MVE) force was recorded. To record the MVE, subjects were positioned on the Roman chair and they applied a maximum isometric trunk extension force against a cable strung between the thorax and the ground (Figure 3.2). The cable was connected to the subject via a modified construction harness so as to resist isometric trunk extension force when the torso was in a neutral posture. A load cell joined the cable to the ground so as to measure cable tension during the exertion (Interface Force, Scottsdale, AZ). Two isometric maximum exertions were performed with 1 minute of rest between exertions. The MVE force was recorded as the greatest peak of the two isometric trials. Following the MVE measurements, the cable was detached and fatigue was induced by performing dynamic trunk extension exercises on the Roman chair. During the initial exercise period, subjects completed 10 repetitions of torso flexion-extension at a rate of 30 cycles per minute in time with a metronome. After two minutes of exercise, the MVE extension force was re-recorded. With each measurement of maximum force, we expected a 5% decline in maximum force. This assures a final fatigued value of 60% MVE after 16 minutes of exercise. If the recorded force decayed less than 4.5% during any 2-minute exercise period, then the number of exercise repetitions was increased by 2 repetitions per minute. If the decline in force was greater than 5.5%, then the number of exercise repetitions was reduced by 2 repetitions per minute. This

assured a continuous and approximately linear fatigue onset. Detailed description and validation of the fatigue protocol is described in Davidson et al (2004).

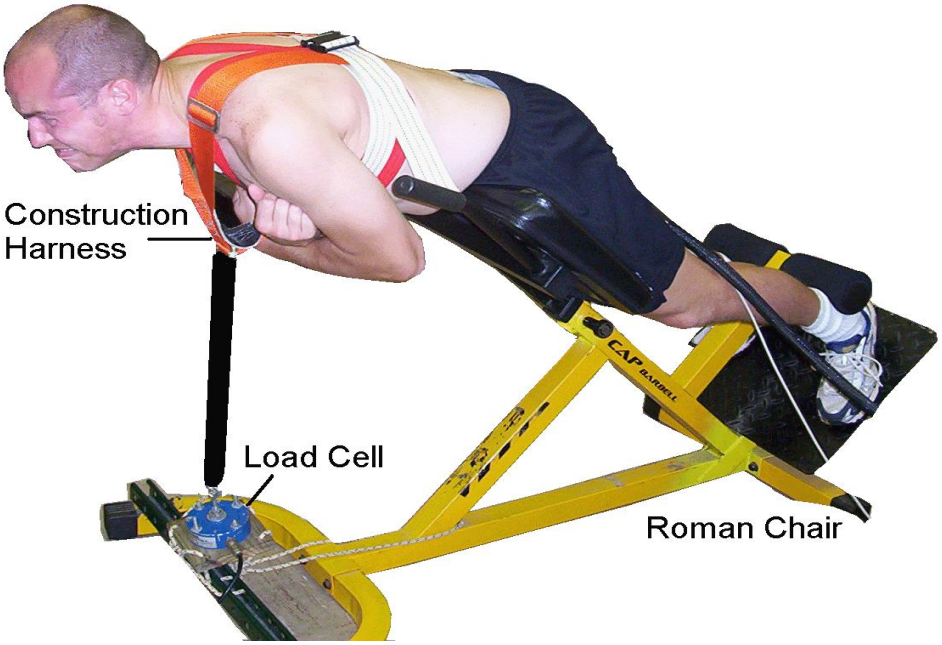

Figure 3.2: Fatigue Protocol: Subjects were asked to perform dynamic trunk extensions at a rate of 30 repetitions per minute on a Roman chair. Fatigue was documented by recording the change in maximum trunk extension strength throughout the exercise protocol. Once strength declined to 60% of the unfatigued level, the stability assessment was repeated.

Immediately following the fatigue protocol, the subjects repeated the dynamic stability assessment. The stability assessment protocol was identical to the protocol performed prior to fatigue, but there was no rest between trials so as to avoid fatigue recovery. Pilot studies indicated that there could be partial recovery after 4 trials of the stability assessment. Therefore, the subjects repeated the fatigue protocol after 4 trials of stability assessment. The re-fatigue was performed until the MVE force declined to less than 60% MVE. After completing the remainder of the stability measurement tasks, trunk extension MVE was again recorded to document fatigue at the end of the stability assessment.

Analysis

Stability was quantified from the maximum finite-time Lyapunov exponent, i.e., time-dependent expansion rate of kinematic variance. Kinematic data were filtered with a 10 Hz, low-pass, 2^{nd}-order Butterworth filter in preparation for calculation of dynamic stability. Nonlinear techniques often do not filter raw data to avoid removing physical artifact. However, the natural frequency of torso dynamics is approximately 1 Hz (Moorhouse and Granata, 2005), so torso movement artifact at frequencies greater than 10 Hz are attributable to noise and thereby removed from the signal. The first five and last five cycles of each trial were removed so as to focus on the steady-state dynamic movements. The data were re-sampled to 6000 data points per 20 movement cycles so that each cycle had a mean value of 300 data points. However, note that this re-sampling process retains cycle-to-cycle variation of cycle duration.

Expansion of kinematic variability in one dimension may be compensated by contraction in another dimension. Therefore, stability analyses were performed on a time signal representing the Euclidean norm of the three Euler angles at each time interval. This resulted in a one-dimensional time-series vector of kinematics data, $x(t)$. However, the system under consideration must be represented with a number of dimensions 'n' sufficient to represent the complete dynamics of the task (Takens, 1981). An n-dimensional Euclidean space, $\mathbf{Y}(t)$, can be created by reconstructing the dynamics of a system from the single time-series vector by the method of delays,

$$\mathbf{Y}(t) = [x(t),\ x(t+T_d),\ x(t+2T_d) \ldots x(t+(n-1)\cdot T_d)] \qquad (3.1)$$

where T_d is a constant time delay (Figure 3.3). Reconstructed dynamics represent information associated with previously unmeasured state dimensions of the complex system. The reconstruction delay, T_d, was estimated using the Average Mutual Information function (Fraser and Swinney, 1986a). This provides an appropriate time delay such that the information contained in vectors $x(t)$ and $x(t+T_d)$ are maximally uncorrelated (Rosenstein et al., 1994). Based upon these results, a constant delay of T_d = 200 msec was used to ensure that all trials were treated similarly. The embedding dimension, n, was determined from a Global False Nearest Neighbors analysis (Kennel and Isabelle, 1992a). This method incrementally increases the embedding dimension until the number of trajectory intersections is a minimum (England and

Granata, 2006). We found that an average embedding dimension for the analyzed data was n = 6. This indicates that we need at least 6 state variables (three lumbar angles and three angular velocities) to describe the complete dynamics of the torso movements in the present study.

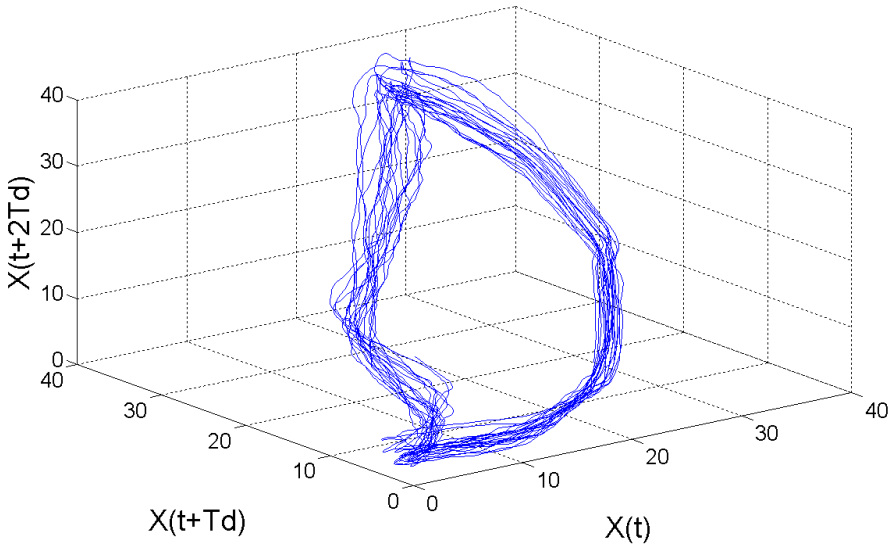

Figure 3.3: Reconstructed dynamics of repetitive torso flexion represented in 3 dimensions with Td = 200 msec. Although the movement data were analyzed with n=6, for purposes of demonstration, an embedding dimension of three is the largest that can be illustrated.

The largest Lyapunov exponent λ_{Max} was used to quantify and compare the local dynamic stability of the repetitive trunk movement represented in the reconstructed state-space matrix, $\mathbf{Y}(t)$. Local perturbations to a system cause displacements between kinematic trajectories. For every data point on a given trajectory (movement cycle), there is a data point on another trajectory that lies closest to it in the n-dimensional state-space. These are defined as nearest neighbors and will approach each other in time if the system is stable. The distance between each pair of nearest neighbors, $d_i(t)$, was recorded for all data points $i = 1 \ldots p$. Kinematic dispersion can be measured by noting the change in distance $d_i(t)$ to $d_i(t+\Delta t)$ as the trajectories moved forward in time by Δt. Two randomly selected neighboring trajectories diverge at a rate described by the largest Lyapunov exponent, λ_{Max} (Rosenstein et al., 1993). Therefore, the

maximum Lyapunov exponent was approximated as the slope of the linear best-fit line created by the equation

$$\langle \ln\{d_i(t+\Delta t) / d_i(t)\} \rangle = \lambda_{Max} \Delta t \quad (3.2)$$

The term $\langle \ln\{d_i(t+\Delta t) / d_i(t)\} \rangle$ represents the logarithmic of dispersion from $d_i(t)$ averaged across all pairs of nearest neighbors, *i* (Figure 3.3). The slope of this line is λ_{Max} and quantifies the mean rate of divergence of initially neighboring trajectories along the least stable dimension. λ_{Max} was recorded for each experimental trial.

Statistical analyses examined the effect of fatigue, asymmetry, and lower-limb constraint on the dependent variables of λ_{Max} and embedding dimension, n. Preliminary analyses revealed no significant gender differences in λ_{Max} ($p = 0.960$). Therefore, data were pooled across gender. The remaining independent variables were treated as within-subject effects in a repeated measures analysis of variance (ANOVA). Analyses were performed using commercial software (Statsoft, Inc., Tulsa, OK) using a significance level of $\alpha < 0.05$.

Results

Fatigue was characterized by the decline in maximum voluntary exertion recorded during isometric trunk extension tasks. The mean MVE force (± standard deviation) of all the subjects after the first fatigue protocol was 64.24 ±3.92% of the unfatigued trunk extension strength. Following the fatigue protocol, 4 stability assessment trials were performed and the MVE trunk extension strength was then re-tested. A significant strength recovery was observed after these 4 stability trials ($p = 0.0001$, $F(1, 9) = 52.890$). The mean of the MVE force after 4 trials was 75.01 ±4.26%. At this time, subjects were re-fatigued, after which they completed the remaining 4 stability assessment trials. After the final stability trial, a significant recovery was again noted ($p = 0.0001$, $F(1, 9) = 49.726$). The MVE force after these final stability assessments was 73.05 ±5.13%. Therefore, we are confident that the protocol successfully maintained a level of fatigue equivalent to at least 25% decrement in trunk extension strength throughout the post-fatigue stability assessments.

The average embedding dimension was n = 6.00 ± 0.91. This value was used for reconstruction of the state-space and calculation of the maximum finite-time Lyapunov exponent. However, the embedding dimension for the recorded trials ranged from 3 to 7, indicating that some conditions contained greater dynamic complexity than others (Table 3.2). The main effect of fatigue significantly influenced the embedding dimension ($p = 0.041$, $F(1, 9) = 5.709$). The embedding dimension of the dynamic movements before fatigue, n = 6.18 ±0.91, was greater than after fatigue, n = 5.83 ±0.88 (Figure 3.4). This indicated reduced dynamic complexity with fatigue. However, a trend was observed in the fatigue by lower-limb constraint interaction ($p = 0.082$, $F(1, 9) = 3.830$). Post-hoc analyses suggest that the fatigue effects on embedding dimension may be limited to conditions wherein subjects were fixed to the pelvic restraint structure ($p = 0.037$). In this condition the number of embedding dimensions was greater before fatigue, n = 6.38 ± 0.93, than after the fatiguing exercises, n = 5.78 ±1.00. When the flexion task was performed without lower-limb constraint, the embedding dimension was not significantly affected by fatigue ($p = 0.943$).

Dynamic stability of the torso was estimated from maximum Lyapunov exponents. Large values of λ_{Max} indicate less stable control of movement. λ_{Max} was significantly influenced by the main effect of fatigue ($p = 0.005$, $F(1, 9) = 13.950$). The mean kinematic rate of expansion before fatigue was $\lambda_{Max} = 0.87 \pm 0.12$. After the fatigue protocol it was 0.94 ±0.11, indicating poorer stability when fatigued (Figure 3.5). There was no significant main effect of asymmetry ($p=0.317$, $F(1, 9) = 1.124$) or lower-limb constraint ($p=0.282$, $F(1, 9) = 1.308$). Contrary to our second hypothesis, there was no significant interaction between fatigue and asymmetry. However, a significant interaction between asymmetry and lower-limb constraint was observed ($p = 0.047$, $F(1, 9) = 5.270$). When the movement was isolated to the torso and arms, asymmetric tasks were associated with a smaller $\lambda_{Max} = 0.90 \pm 0.15$ than symmetric tasks, 0.94 ± 0.14 ($p = 0.053$). Furthermore, λ_{Max} for the symmetric movements with lower-limb constraint, 0.94 ± 0.14, was greater ($p = 0.017$) than symmetric movements without lower-limb constraint, 0.89 ± 0.10.

Table 3.2: Statistical table for embedding dimension (n) and largest Lyapunov exponent (λ_{Max}). Numbers represent the type I statistical error, i.e., p-value. Significant effects ($p<0.05$) are highlighted in bold. Three-way interactions were not statistically significant.

	Embedding Dimension n		Lyapunov Exponent λ_{max}	
	F	P level	F	P level
Fatigue	5.709	**0.041**	13.950	**0.005**
Lower-Limb Constraint	0.663	0.437	1.308	0.282
Asymmetry	0.109	0.749	1.124	0.317
Fatigue x Constraint	3.830	0.082	0.457	0.516
Fatigue x Asymmetry	0.159	0.708	1.103	0.321

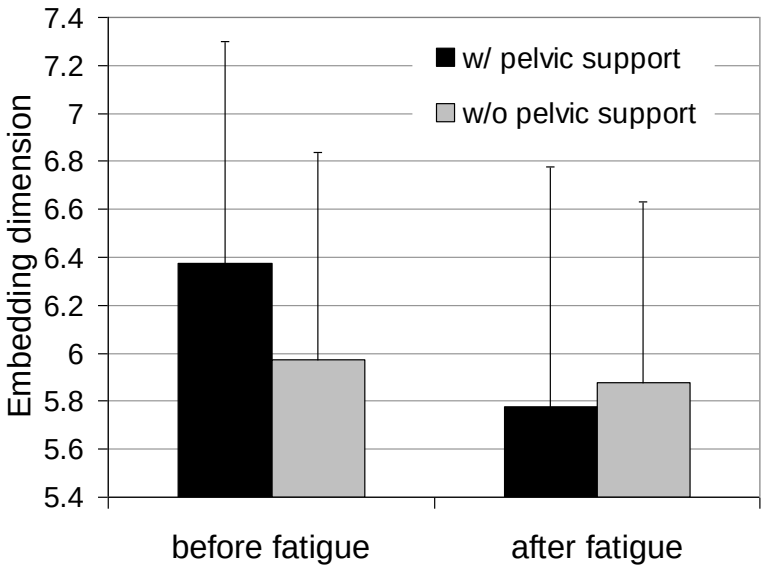

Figure 3.4: The embedding dimension 'n' indicates the dynamic complexity of the process. The number of embedding dimensions 'n' decreased with fatigue. (The errors bars are the standard deviations of the mean.)

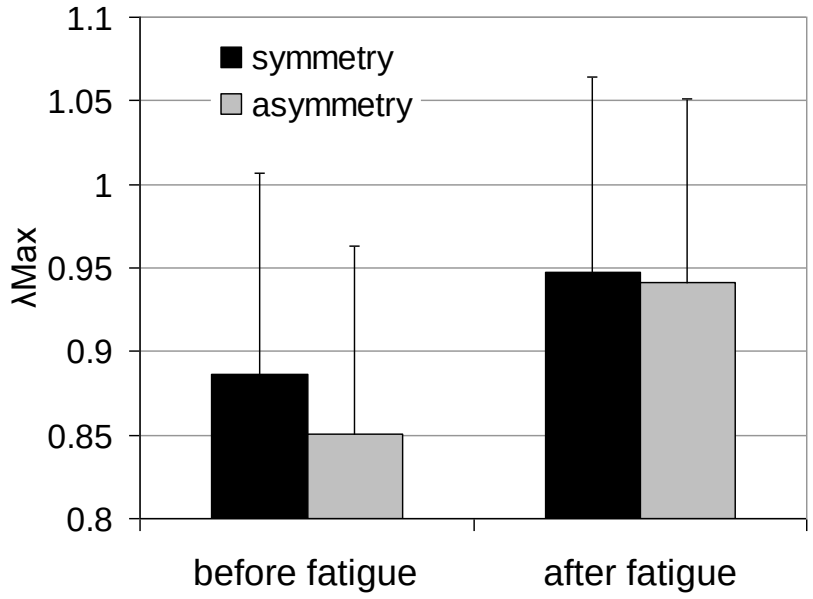

Figure 3.5: Large λMax values indicate poorer stability. λMax values were greater for the fatigued movements than for the unfatigued movements. (The errors bars are the standard deviations of the mean.)

Discussion

Workplace and personal factors that affect spinal load and stability contribute to mechanisms of biomechanical risk. Damage to the spine occurs when biomechanical loads exceed injury tolerance. Spinal loads during occupational lifting tasks are recognized as an important biomechanical risk factor for low back pain (Norman et al., 1998). Fatigue causes muscle recruitment to shift from the paraspinal muscles to more laterally situated muscles of the torso, but it remains unclear how this influences spinal load (Sparto and Parnianpour, 1998; Van Dieen and Heijblom, 1996). However, spinal load must be considered with respect to the loading tolerance. Multi-segment structural loading tolerance of the spine is measured in terms of its stable buckling load (Bergmark, 1989a). If spinal load exceeds this stability threshold then the spine cannot maintain its alignment (Crisco and Panjabi, 1992; Crisco et al., 1992) and a small disturbance or muscle recruitment error would cause brief uncontrolled intervertebral movement (Panjabi, 1992b). This may cause passive tissue strain injury and/or nerve-root impingement. Therefore, biomechanical tolerance to spinal overload injury can be attributed, in part, to the

ability of the neuromuscular system to maintain spinal stability. Fatigue influences the neuromuscular control factors that contribute to spinal stability (Hagbarth et al., 1995; Sparto and Parnianpour, 1998). Moreover, recruitment errors associated with fatigue may contribute to disturbance perturbations that precipitate unstable intervertebral movement. However, methods to empirically test the hypothesis that fatigue affects stability have only recently been developed.

Rosenstein et al. (1993) developed a method to calculate the maximum Lyapunov exponent, λ_{Max}, from experimental time-series data. This nonlinear dynamic analysis has previously been used to quantify dynamic stability of walking (Dingwell and Cusumano, 2000). In measurements of walking, λ_{Max} increases with subjective fatigue assessment (Yoshino et al., 2004). These nonlinear analyses can also be used to quantify the stability of the torso during dynamic movements (Granata and England, 2006) but the effects of fatigue have not been tested. The Lyapunov exponent represents the rate at which kinematic disturbances change with time. Clearly, the trunk flexion movements remained stable because the subjects successfully completed the experimental tasks. Therefore, during repetitive torso movements the stabilizing neuro-control system will cause the dynamics to be attracted toward the reference movement trajectory. This guarantees that the sum of Lyapunov exponents was less than zero, i.e. n-dimensional volume of kinematic dispersion contracts with time. However, while disturbances are attenuated in one dimension, they may grow in another as noted by positive values of λ_{Max}. These unstable dimensions may be characterized as a member of the uncontrolled manifold (Scholz and Schoner, 1999). Specifically, the neuromuscular controller does not need to assure stability in all of the dynamic movement dimensions to achieve stability of the repetitive task (Nayfeh and Balachandran, 1995). In fact, theoretical analyses suggest that optimal neuro-motor behaviour may allow kinematic variance in uncontrolled dimensions (Todorov and Jordan, 2002). Results suggest that the number of controlled dimensions was affected by fatigue.

The number of embedding dimensions decreased with fatigue of the trunk extensor muscles. Simple dynamical systems can be described with few state dimensions. Conversely, a larger number of embedding dimensions are required to describe complex dynamic systems: i.e. the number of state variables of a system increases with the dimensions. The average integer value

of state dimensions, n=6.0, agrees with previous measurements of torso dynamics (Granata and England, 2006). It suggests that the dynamic state at any instant in time requires a set of three lumbar angles and three angular velocities. Hence, sagittal plane dynamic analyses overlook important mechanical coupling. Fatigue appears to influence this coupling. When the extensor muscles were fatigued, the reduction of embedding dimensions indicates the reduction in complexity of the system (Figure 3.4). This may simplify the control of fatigued movements because systems with less complexity are intuitively easier to control. This effect may be explained by changes in muscle recruitment. When the paraspinal muscles become fatigued the recruitment shifts to greater co-activation of the lateral torso muscles to generate the trunk extension movement (Van Dieen and Heijblom, 1996). The oblique line-of-action of these muscles clearly provides the capacity to couple sagittal with lateral and axial control. Recruitment of these muscles as a consequence of fatigue may have resulted in constraining the torso movements to a lower dimensional state space causing the reduction in embedding dimension. However analyses were limited to integer dimensions. Fractal dimensions are often observed in nonlinear dynamic systems indicating deterministic chaos and strange attractor stability (Nayfeh and Balachandran, 1995). In fact, fractal dimensions are common in physiologic signals and provide predictive risk assessment (Goldberger et al., 2002). Further analyses should investigate the fractal characteristics of torso dynamics and its association with fatigue.

The maximum Lyapunov exponent, λ_{Max}, increased with fatigue. This suggests that the torso was less stable after the fatiguing protocol than during unfatigued measurements. The result agrees with the hypothesis. This effect may be attributed to previously reported fatigue-related changes in open-loop recruitment and changes in feedback neuro-control. However, results are limited to the interpretation of the λ_{Max} coefficient. Specifically, the maximum Lyapunov exponent, λ_{Max}, characterizes the maximum time-rate of expansion for the *n*-dimensional volume that describes kinematic variability. In other words, this value represents the least stable aspect of the movement dynamics (Rosenstein et al., 1993). Recognizing that kinematic dispersion of the i^{th} principal axis is proportional to $e^{\lambda i t}$, the positive values of λ_i quickly dominate the system dynamics. Unfortunately, current mathematical techniques do not permit us to determine the

direction of the least stable axis of movement. The results cannot guarantee that the least stable dimensions were along the same axes in fatigued and unfatigued conditions. For example, it is reasonable that the least stable dimension during symmetric unfatigued movements may exist along the twisting axis of the torso; whereas increased lateral muscle recruitment may improve axial control and the least stable dimension in fatigued conditions may have been aligned with the sagittal flexion axis. Moreover, the least stable direction may change with flexion angle throughout the dynamic movement trajectory. We hope to pursue further studies that will attempt to identify the local vector characteristics of instabilities thereby providing potential insight into the weakest control direction. Nonetheless, results demonstrate that the ability of the neuromuscular system to attenuate kinematic errors is impaired by fatigue of the trunk extensor muscles.

Contrary to our second hypothesis task asymmetry did not influence the fatigue-related change in stability. There were no significant main effects of task asymmetry. This was in contrast to our previous studies wherein movements in the mid-sagittal plane were less stable than when moving in a combined sagittal and twist trajectory (Granata and England, 2006). However, the asymmetric movement protocols in these two studies were different. Specifically, the asymmetric movement in the current protocol required touching a target in the mid-sagittal plane, whereas previous experimental designs placed the target to the left or right of the mid-sagittal plane. Moreover, in previous studies lower-limb constraint was imposed in all experimental conditions by strapping subject's legs and pelvis to a rigid structure so as to limit movement solely to the torso and arms. In this regard, results from the current study agree with previous analyses. A significant interaction between asymmetry and lower-limb constraint was observed in the current results. When the movement was isolated to the torso and arms there was a trend wherein asymmetric tasks were more stable than symmetric tasks. No effect of asymmetry was observed when subjects were free standing. This interaction indicates that dynamic coupling between the legs and torso contributes to the control of stability in asymmetric movements. Similarly, pair-wise analyses of embedding dimension revealed that fatigue-related changes in dynamic complexity were observed only if the legs were constrained. Future studies should investigate the dynamic coupling and control between the lower-limbs and torso stability.

Results provide insight into the mechanisms of fatigue, but limitations of the experimental design and analyses must be considered. The protocol rapidly introduced a very high level of fatigue. The protocol caused isometric MVE strength reduction to 60% of unfatigued strength within 16 minutes of exercise. This was done to investigate the fundamental hypotheses of fatigue and stability. However, workplace tasks are more likely to produce lower levels of fatigue over long time durations, e.g., accumulation of fatigue throughout an eight-hour work shift. Extrapolation of results to workplace conditions requires further experimental studies. Similarly, the experimental protocol was a single task, paced movement without a load in the hands. Manual materials' handling often requires multiple task components with a lifted load in the hands. Moreover, previous analyses showed that movement pace influences stability (Dingwell and Marin, 2006; Granata and England, 2006). The dynamic analyses can be extended to investigate multiple component movement patterns. The effect of lifting a box must be considered for a range of lifted weights. Small variations in embedding dimension, n, and time delay, T_d, were observed in each trial. However, the analyses implemented n = 6 and T_d=200 msec to assure consistent interpretation of every trial. Treating these parameters as trial-dependent co-factors may provide further information content when assessing dynamic stability using λ_{Max}. Evidence suggests that fatigue influences muscle recruitment. However, the present study did not investigate empirically the changes in muscle recruitment patterns due to lumbar fatigue.

In conclusion, fatigue of the trunk extensor muscles has been identified as a risk factor for low back injury (Biering-Sorensen, 1984; Luoto et al., 1995). Theoretical analyses suggest that the mechanism of this risk may be related to stability (Granata et al., 2004). Spinal instability is a common clinical condition associated with low back pain (Pope and Panjabi, 1985) wherein an unstable spine is susceptible to intersegmental hypermobility and tissue strain injury (Panjabi, 1992b). Results demonstrate that fatigue of the trunk extensor muscles impairs the neuromuscular stabilizing control of dynamic torso movement. Further studies must be conducted to examine whether torso and spinal stability can be used as a risk factor for discrimination and prediction of low back pain.

Acknowledgements

This study was supported by grants R01 AR46111 from NIAMS of the National Institute of Health and R01 OH07352 from NIOSH of the Centers for Disease Control and Prevention.

References

AVELA, J., KYROLAINEN, H., KOMI, P. V. & RAMA, D. (1999) Reduced reflex sensitivity persists several days after long-lasting stretch-shortening cycle exercise. *J Appl Physiol,* 86**,** 1292-300.

BERGMARK, A. (1989) Stability of the lumbar spine. A study in mechanical engineering. *Acta Orthop Scand,* 60 Suppl 230**,** 3-54.

BIERING-SORENSEN, F. (1984) Physical measurements as risk indicators for low-back trouble over a one-year period. *Spine,* 9**,** 106-19.

CHOLEWICKI, J., POLZHOFER, G. K. & RADEBOLD, A. (2000) Postural control of trunk during unstable sitting. *J Biomech,* 33**,** 1733-7.

CRISCO, J. J. & PANJABI, M. M. (1992) Euler stability of the human ligamentous lumbar spine. Part I: Theory. *Clin Biomech,* 7**,** 19-26.

CRISCO, J. J., PANJABI, M. M., YAMAMOTO, I. & OXLAND, T. R. (1992) Euler stability of the human ligamentous lumbar spine. Part II: Experiment. *Clin Biomech,* 7**,** 27-32.

DAVIDSON, B. S., MADIGAN, M. L. & NUSSBAUM, M. A. (2004) Effects of lumbar extensor fatigue and fatigue rate on postural sway. *Eur J Appl Physiol,* 93**,** 183-9.

DINGWELL, J. B. & CUSUMANO, J. P. (2000) Nonlinear time series analysis of normal and pathological human walking. *Chaos,* 10**,** 848-863.

DINGWELL, J. B. & MARIN, L. C. (2006) Kinematic variability and local dynamic stability of upper body motions when walking at different speeds. *J Biomech,* 39**,** 444-52.

ENGLAND, S. A. & GRANATA, K. P. (2006) The influence of gait speed on local dynamic stability of walking. *Gait Posture,* 25, 172-8.

FATHALLAH, F. A., MARRAS, W. S. & PARNIANPOUR, M. (1998) An assessment of complex spinal loads during dynamic lifting tasks. *Spine,* 23**,** 706-16.

FRANKLIN, T. C. & GRANATA, K. P. (2006) Role of reflex gain and reflex delay in spinal stability - A dynamic simulation. *J Biomech*, 40, 1762-7.

FRASER, A. M. & SWINNEY, H. L. (1986) Independent coordinates for strange attractors from mutual information. *Phys Rev A,* 33**,** 1134-40.

GARDNER-MORSE, M. G. & STOKES, I. A. (1998) The effects of abdominal muscle coactivation on lumbar spine stability. *Spine,* 23**,** 86-91; discussion 91-2.

GOLDBERGER, A. L., AMARAL, L. A., HAUSDORFF, J. M., IVANOV, P., PENG, C. K. & STANLEY, H. E. (2002) Fractal dynamics in physiology: alterations with disease and aging. *Proc Natl Acad Sci U S A,* 99 Suppl 1**,** 2466-72.

GOLLHOFER, A., KOMI, P. V., MIYASHITA, M. & AURA, O. (1987) Fatigue during stretch-shortening cycle exercises: Changes in mechanical performance of human skeletal-muscle. *Int J Sport Med,* 8**,** 71-8.

GRANATA, K. P. & ENGLAND, S. A. (2006) Stability of dynamic trunk movement. *Spine,* 31**,** E271-6.

GRANATA, K. P. & MARRAS, W. S. (2000) Cost-benefit of muscle cocontraction in protecting against spinal instability. *Spine,* 25**,** 1398-404.

GRANATA, K. P. & SANFORD, A. H. (2000) Lumbar-pelvic coordination is influenced by lifting task parameters. *Spine,* 25**,** 1413-8.

GRANATA, K. P., SLOTA, G. P. & WILSON, S. E. (2004) Influence of fatigue in neuromuscular control of spinal stability. *Hum Factors,* 46**,** 81-91.

HAGBARTH, K. E., BONGIOVANNI, L. G. & NORDIN, M. (1995) Reduced servo-control of fatigued human finger extensor and flexor muscles. *J Physiol,* 485**,** 865-72.

HERRMANN, C. M., MADIGAN, M. L., DAVIDSON, B. S. & GRANATA, K. P. (2006) Effect of lumbar extensor fatigue on paraspinal muscle reflexes. *J Electromyogr Kinesiol*, 16, 637-41.

HOGAN, N. (1984) Adaptive control of mechanical impedance by coactivation of antagonist muscles. *IEEE Trans Aut Control,* AC-29**,** 681-90.

HORTOBAGYI, T., LAMBERT, N. J. & KROLL, W. P. (1991) Voluntary and reflex responses to fatigue with stretch-shortening exercise. *Can J Sport Sci,* 16**,** 142-50.

KENNEL, M. B. & ISABELLE, S. (1992) Method to distinguish possible chaos from colored noise and to determine embedding parameters. *Phys Rev A,* 46**,** 3111-8.

KEYSERLING, W. M., HERRIN, G. D. & CHAFFIN, D. B. (1981) Isometric strength testing as a means of controlling medical incidents on strenuous jobs. *J Occup Env Med,* 22**,** 332-6.

LEE, P. J., ROGERS, E. L. & GRANATA, K. P. (2006) Active trunk stiffness increases with co-contraction. *J Electromyogr Kinesiol,* 16**,** 51-7.

LUOTO, S., HELIOVAARA, M. H., HURRI, H. & ALARANTA, H. (1995) Static back endurance and the risk of low-back-pain. *Clin Biomech,* 10**,** 323-4.

MADIGAN, M. L., DAVIDSON, B. S. & NUSSBAUM, M. A. (2006) Postural sway and joint kinematics during quiet standing are affected by lumbar extensor fatigue. *Hum Mov Sci, 25, 788-99.*

MEAKIN, J. R., HUKINS, D. W. & ASPDEN, R. M. (1996) Euler buckling as a model for the curvature and flexion of the human lumbar spine. *Proc Roy Soc B: Biol Sci,* 263**,** 1383-7.

MOORHOUSE, K. M. & GRANATA, K. P. (2005) Trunk stiffness and dynamics during active extension exertions. *J Biomech,* 38**,** 2000-7.

MOORHOUSE, K. M. & GRANATA, K. P. (2006) Role of reflex dynamics in spinal stability: Intrinsic muscle stiffness alone is insufficient for stability. *J Biomech,* 40, 1058-65.

MORGAN, D. L., PROSKE, U. & WARREN, D. (1978) Measurements of muscle stiffness and mechanism of elastic storage of energy in hopping kangaroos. *J Physiol,* 282**,** 253-61.

NAYFEH, A. H. & BALACHANDRAN, B. (1995) *Applied Nonlinear Dynamics: Analytical, Computational and Experimental Methods,* New York, Wiley.

NORMAN, R., WELLS, R., NEUMANN, P., FRANK, J., SHANNON, H. & KERR, M. (1998) A Comparison of peak vs cumulative physical work exposure risk factors for the reporting of low back pain in the automotive industry. *Clin Biomech,* 13**,** 561-73.

PANJABI, M. M. (1992a) The stabilizing system of the spine. Part I. Function, dysfunction, adaptation, and enhancement. *J Spinal Disord,* 5**,** 383-9; discussion 397.

PANJABI, M. M. (1992b) The stabilizing system of the spine. Part II. Neutral zone and instability hypothesis. *J Spinal Disord,* 5**,** 390-6; discussion 397.

POPE, M. H. & PANJABI, M. (1985) Biomechanical definitions of spinal instability. *Spine,* 10**,** 255-6.

QITA, W. A. & KEARNEY, R. E. (2000) Effects of triceps surae muscle fatigue on intrinsic and reflex contributions to dynamic ankle stiffness. *Proceedings of Annual International Conference of the IEEE Engineering in Medicine and Biology Society,* 22, 335-8.

REEVES, N. P., NARENDRA, K. S. & CHOLEWICKI, J. (2007) Spine stability: the six blind men and the elephant. *Clin Biomech,* 22**,** 266-74.

ROSENSTEIN M. T. & DE LUCA, C. J. (1993) A practical method for calculating largest Lyapunov exponent from small data sets. *Physica D,* 65**,** 117-34.

ROSENSTEIN, M. T., COLLINS, J. J. & DELUCA, C. J. (1994) Reconstruction expansion as a geometry-based framework for choosing proper delay times. *Physica D,* 73**,** 82-98.

SCHOLZ, J. P. & SCHONER, G. (1999) The uncontrolled manifold concept: identifying control variables for a functional task. *Exp Brain Res,* 126**,** 289-306.

SPARTO, P. J. & PARNIANPOUR, M. (1998) Estimation of trunk muscle forces and spinal loads during fatiguing repetitive trunk exertions. *Spine,* 23**,** 2563-73.

STROGATZ, S. (1994) *Nonlinear Dynamics and Chaos - With Applications to Physics, Biology, Chemistry, and Engineering,* Cambridge, MA, Perseus Books.

TAKENS, F. (1981) Detecting strange attractors in turbulence. In RAND, D. A. & YOUNG, L.-S. (Eds.) *Dynamical Systems and Turbulence.* New York, Springer, pp. 366-81.

THOMAS, J. S., CORCOS, D. M. & HASAN, Z. (2003) Effect of movement speed on limb segment motions for reaching from a standing position. *Exp Brain Res,* 148**,** 377-87.

TODOROV, E. & JORDAN, M. I. (2002) Optimal feedback control as a theory of motor coordination. *Nat Neurosci,* 5**,** 1226-35.

VAN DIEEN, J. & HEIJBLOM, P. (1996) Reproducibility of isometric trunk extension torque, trunk extensor endurance, and related electromyographic parameters in the context of their clinical applicability. *J Orthop Res,* 14**,** 139-43.

WILDER, D. G., ALEKSIEV, A. R., MAGNUSSON, M. L., POPE, M. H., SPRATT, K. F. & GOEL, V. K. (1996) Muscular response to sudden load - A tool to evaluate fatigue and rehabilitation. *Spine,* 21**,** 2628-39.

YOSHINO, K., MOTOSHIGE, T., ARAKI, T. & MATSUOKA, K. (2004) Effect of prolonged free-walking fatigue on gait and physiological rhythm. *J Biomech,* 37**,** 1271-80.

Chapter 4 – Biomechanical Modeling

The human musculoskeletal system is complex and often requires invasive methods to study its biomechanics. To avoid unethical invasive methods, mathematical biomechanics models are often used to study musculoskeletal systems. The first part of this chapter gives a brief history of past biomechanical models. The last part introduces the reader to the background of mathematical modeling.

Biomechanical Models

Biomechanical models are built using two methods, forward dynamics methods and inverse dynamics methods. Forward dynamics models take assumed forces and moments to predict the kinematics of the system. Such models help researchers study mechanisms that are impossible to test through in vivo testing (Potvin, 2008; Winter, 2005). Inverse dynamics models use known kinematics and anthropometric data to estimate the internal forces (Winter, 2005). The forward dynamics method is rarely used in the study of trunk biomechanics due to the complex nature of its structure. Most of the trunk models in the literature are inverse dynamics models. The following sections briefly present some of the previous models of the torso.

Early models

One of the early mathematical models was developed in (Schultz et al., 1982) to estimate the imposed loads on the lumbar structure and the internal lumbar muscle forces while performing various tasks. They used 6 equations and non-mechanical distribution laws to determine forces. Later, (Bergmark, 1989b) built a 3-D model with 6 rigid bodies (5 lumbar vertebrae and the thorax) and 18 degrees of freedom. The muscles were modelled as straight lines. The model studied the minimum intrinsic stiffness required for spinal stability. The study found that the minimum intrinsic stiffness required for stability is 40.

Gardner-Morse et al. (1995b) developed a model with 36 degrees of freedom (6 dof for each rigid body). The thorax and pelvis were modelled as rigid bodies. The 5 lumbar vertebrae and the intervertebral discs were modelled as 11 beams with 6 intervertebral joints. Each joint was given 6 degrees of freedom. 132 muscles fascicles were modelled as straight lines. The model estimated muscle forces for maximum extension efforts using linear optimization. The maximum displacements were limited to 5mm and 5^{o}.

Cholewicki and McGill (1996) developed a 3D trunk model with 7 rigid bodies: 5 lumbar vertebrae, a thorax, and a pelvis. The pelvis was constrained from moving. The intervertebral discs were modelled as lumped parameter discs with 3 rotational stiffnesses corresponding to 3 axes. Each intervertebral joint was given 3 rotational degrees of freedom, such that the total model had 18 degrees of freedom. The translations between the vertebrae were constrained to be zero. The model had 90 muscles with intermediate nodes in addition to origins and insertions to account for the curved lines of action. The kinematics for the model were taken from experimental data. Different dynamic tasks were analyzed in this study. However, each task was analyzed as a succession of static postures. EMG data was used with an optimization algorithm to find muscle activations at various postures, ensuring equilibrium kinematics at every posture.

Recent models

Shirazi-Adl et al. (2002) built two models, a detailed model using computer assisted tomography of a cadaver specimen and a simplified beam-rigid body model. The results of the simplified model were in agreement with those of the detailed model. In this model, the kinematics were also optimized along with muscle forces using a minimization approach. The translations between the vertebrae were taken into account. However, this study included only postural analysis, not a dynamic analysis.

Franklin and Granata (2007) investigated an inverse dynamic model similar to Cholewicki and McGill's with 7 rigid bodies and 18 degrees of freedom. The muscle model used was also similar to that of Cholewicki and McGill. Optimization was used to solve for muscle activations by

minimizing the metabolic power while linear stability was ensured. This study investigated how muscle recruitment patterns affect the reflex delay for certain prescribed stable kinematics. It also developed a similar forward dynamics model to examine the effect of reflex delays on muscle recruitment patterns and spinal stability. Again, this study did not investigate the large dynamic angular movements of the trunk.

Zeinali-Davarani et al. (2008) modelled the lumbar spine as a 3D inverted pendulum constrained at its base with a ball and socket joint, with three rotational degrees of freedom. 48 muscles were used in this study and the muscle model was similar to that of Cholewicki and McGill. The model was used to simulate 60^{o} flexion movement. The model used two processes, a feed-forward process (inverse dynamics) and a feed-back process (forward dynamics). In the feed-forward process, the muscle activations and the joint torque were calculated for the prescribed kinematics using static optimization. In the feed-back process, the kinematics were computed for given muscle spindle reflexes. The feed-forward process was used to predict the muscle activation with and without the stability constraints. This model estimated the activation patterns of flexor and extensor muscles during trunk flexion.

Bazrgari et al. (2008) built a kinematics-driven finite element model to evaluate the effects of the velocity of free flexion-extension movements on muscle forces and spinal loads. The model was sagittaly symmetric with T1-S1 motion segments and 56 muscles, and assumed constant shear between the vertebrae. The motion segments were represented by nonlinear deformable beams. The measured kinematics of one flexion-extension movement from the experiments were used to calculate the muscle forces while minimizing the cost function, which was the sum of the cubed muscle forces. This study showed that the effect of inertial forces on reaction forces was higher in the faster movements when compared to the slower movements. The faster movements exhibited higher muscle activation levels and spinal loads. The faster movements had considerable abdominal activity at the onset of flexion. There was no abdominal activity at the onset of slower movements; instead, abdominal activity was observed at larger flexion angles. The spinal loads increased from T12 to S1, being highest at the L5-S1 joint. The shearing between the vertebrae was kept constant in this study.

Except for two of the models, the previous models used pure rotational dynamics. Even the studies that considered axial translations ignored the shearing between the vertebrae. Moreover, except for two, most of the models were used for postural analyses or small-perturbation analyses. As mentioned before, the majority of low back disorders occur due to dynamic tasks, and it is necessary to study spine mechanics in the dynamic sense.

Muscle Forces

Muscle forces play a major role in spine mechanics. The muscular structure of the trunk provides mechanical support to the spine to avoid lateral and sagittal buckling (Bergmark 1989).

The ligamentous thoracic spine without muscular structure typically has a critical load around 20N, while the lumbar spine has a critical load around 80N (Crisco and Panjabi, 1991). However, the human spine can bear loads as large as twice the body weight with the help of the muscular structure (Crisco and Panjabi, 1991). Crisco and Panjabi (1991) also showed that stability of spine cannot be achieved without muscles.

In experimental studies, muscle forces are estimated using surface EMGs. However, surface EMG can only measure activation levels of the trunk muscles that are close to the skin surface, and also may have estimation errors (Staudenmann et al., 2007). Moreover, a single muscle or muscle group does not contribute sufficiently to achieve spinal stability; the combined contribution of a number of trunk muscles is required to maintain spinal stability (Cholewicki and VanVliet, 2002). Hence, it is important to study all the muscle groups that influence the trunk mechanics. Mathematical modeling helps one to estimate various muscle forces. In the current model, 90 trunk muscles are included and their internal forces are estimated.

Many past studies estimated trunk muscle forces for flexion-extension movements (Cholewicki and McGill, 1996; Dolan and Adams, 1993). However, these studies estimated isometric muscle forces. Small changes in posture can influence muscle forces and spinal loads (Shirazi-Adl et al.,

2005). Also, evidence shows that at large flexed angles, trunk muscle forces play a major role in stabilizing the spine, compared to passive tissues (Kong et al., 1996). While performing dynamic tasks, the vertebral positions continuously change, and it is necessary to understand the changes in muscles forces during a dynamic movement. Recently, two models investigated the dynamic muscle forces (Bazrgari et al., 2008; Zeinali-Davarani et al., 2008), as described earlier in this chapter.

References

BAZRGARI, B., SHIRAZI-ADL, A., TROTTIER, M. & MATHIEU, P. (2008) Computation of trunk equilibrium and stability in free flexion-extension movements at different velocities. *J Biomech,* 41**,** 412-21.

BERGMARK, A. (1989) Stability of the lumbar spine. A study in mechanical engineering. *Acta Orthop Scand Suppl,* 60**,** 1-54.

CHOLEWICKI, J. & MCGILL, S. M. (1996) Mechanical stability of the in vivo lumbar spine: implications for injury and chronic low back pain. *Clin Biomech,* 11**,** 1-15.

CHOLEWICKI, J. & VANVLIET, J. J. T. (2002) Relative contribution of trunk muscles to the stability of the lumbar spine during isometric exertions. *Clin Biomech,* 17**,** 99-105.

CRISCO, J. J., 3RD & PANJABI, M. M. (1991) The intersegmental and multisegmental muscles of the lumbar spine. A biomechanical model comparing lateral stabilizing potential. *Spine,* 16**,** 793-9.

DOLAN, P. & ADAMS, M. A. (1993) The relationship between EMG activity and extensor moment generation in the erector spinae muscles during bending and lifting activities. *J Biomech,* 26**,** 513-22.

FRANKLIN, T. C. & GRANATA, K. P. (2007) Role of reflex gain and reflex delay in spinal stability--a dynamic simulation. *J Biomech,* 40**,** 1762-7.

GARDNER-MORSE, M. G., STOKES, I. A. F. & LAIBLE, J. P. (1995) Role of muscles in lumbar spine stability in maximum extension efforts. *J Orthop Res,* 13**,** 802-8.

KONG, W. Z., GOEL, V. K., GILBERTSON, L. G. & WEINSTEIN, J. N. (1996) Effects of muscle dysfunction on lumbar spine mechanics - A finite element study based on a two motion segments model. *Spine,* 21**,** 2197-206.

POTVIN, J. R. (2008) Occupational spine biomechanics: a journey to the spinal frontier. *J Electromyogr Kinesiol,* 18**,** 891-9.

SCHULTZ, A. B., ANDERSSON, G. B. J., HADERSPECK, K., ORTENGREN, R., NORDIN, M. & BJORK, R. (1982) Analysis and measurement of lumbar trunk loads in tasks involving bends and twists. *J Biomech,* 15**,** 669-75.

SHIRAZI-ADL, A., EL-RICH, M., POP, D. G. & PARNIANPOUR, M. (2005) Spinal muscle forces, internal loads and stability in standing under various postures and loads--application of kinematics-based algorithm. *Eur Spine J,* 14**,** 381-92.

SHIRAZI-ADL, A., SADOUK, S., PARIANPOUR, M., POP, D., EL-RICH, M. (2002). "Muscle force evaluation and the role of posture in human lumbar spine under compression." Eur Spine J **11**: 519-526.

STAUDENMANN, D., POTVIN, J. R., KINGMA, I., STEGEMAN, D. F. & VAN DIEEN, J. H. (2007) Effects of EMG processing on biomechanical models of muscle joint systems: sensitivity of trunk muscle moments, spinal forces, and stability. *J Biomech,* 40**,** 900-9.

WINTER, D. A. (2005) *Biomechanics and motor control of human movement,* Hoboken, NJ, Wiley

ZEINALI-DAVARANI, S., HEMAMI, H., BARIN, K., SHIRAZI-ADL, A. & PARNIANPOUR, M. (2008) Dynamic stability of spine using stability-based optimization and muscle spindle reflex. *IEEE Trans Neural Syst Rehabil Eng,* 16**,** 106-18.

Chapter 5 - Methods of Simulation Study

Skeletal Model

The model represents the spine as a system consisting of 6 rigid bodies. The 6 bodies are 5 lumbar vertebrae (L5, L4, L3, L2, and L1) and the thorax (thoracic and cervical spine, i.e., T12-C1 vertebrae). The physical geometry of the complete system is similar to a lumped mass system with 6 rigid bodies stacked on a pelvis (Cholewicki and McGill, 1996), as shown in Figure 5.1. Each body has 3 degrees of freedom. The kinematics of each are represented by one rotational and two translational degrees of freedom in the sagittal plane, which are measured in the body-fixed coordinate system. The global coordinate system is fixed at the pelvis. The origins of the local coordinate systems are based at the centers of the bottom end plate of each rigid body. The z-axis is orthogonal to the transverse plane, pointing upward; the y-axis is orthogonal to the frontal plane and points in the anterior direction; the x-axis is orthogonal to the sagittal plane, pointing to the right. Each vertebra is modelled as a disc with elliptical cross section, as described in Franklin and Granata (2007). Facet joints are ignored to reduce the complexity of the model.

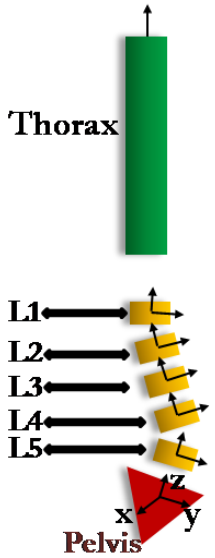

Figure 5.1: Sagittal plane representation of rigid body model in the upright position

Kinematics

The kinematic vectors are estimated from recorded experimental data of the flexion and extension task experiments and optimization. The experimental data provide the sagittal plane angles of the lower back and thorax. The rotations of each vertebra are calculated as certain percentages of the lumbar angle (McGill and Norman, 1986). They are calculated as shown in equation 5.1. Then finite differences are used to obtain the velocity and acceleration vectors of angular displacements as shown in equation 5.2. The translations of each vertebra are calculated with the aid of optimization.

The equations of motion for the model are obtained using Lagrange's equations. The detailed description is given in the following section. The equations of motion give 18 equations with 63 unknowns (45 unknowns in muscle activations and 12 unknowns in translational displacements). An optimization routine is used to find the unknown kinematics vectors that satisfy the developed equations of motion. Constrained optimization is used such that the translational displacements fall in the physiological range reported in a previous study (Sun et al., 2004). The translational displacements that are obtained from this method are essentially the displacements of an upper body with respect to the lower body in the local coordinate system of the lower body.

$$\theta_i = x_i \times LA \tag{5.1}$$

where θ_i = sagittal angle of ith vertebra

x_i = proportion of flexion attributed to the ith vertebra (0.132 to L1 and L2; 0.210 to L3; 0.290 to L4; 0.236 to L5)

LA = lumbar angle

$$\dot{\theta}_i(t_j) = \frac{\theta_i(t_{j+1}) - \theta_i(t_{j-1})}{2\Delta t} \quad , \quad \ddot{\theta}_i(t_j) = \frac{\theta_i(t_{j+1}) - 2\theta_i(t_j) + \theta_i(t_{j-1})}{(\Delta t)^2} \tag{5.2}$$

where $\Delta t = t_{j+1} - t_j = t_j - t_{j-1}$ and an overdot denotes differentiation with respect to time.

Since the rotations of the vertebrae are restricted to the sagittal plane, the angles of each vertebra obtained from the above method are measured in the global coordinate system with the origin on the stationary pelvis. The coordinates of the origins of each body are defined as follows.

$$
\left.
\begin{aligned}
&\text{Origin of pelvis (the global coordinate system) } O = Orp = \{0,0,0\} \\
&\text{Origin of L5 vertebra } Or5 = Orp + \{0,\ y_5,\ z_5\} \\
&\text{Origin of L4 vertebra } Or4 = Or5 + \{0, y_4,\ z_4 + h_5\}^* R_5 \\
&\qquad \text{Origin of L3 vertebra } Or3 = Or4 + \{0, y_3,\ z_3 + h_4\}^* R_4 \\
&\text{Origin of L2 vertebra } Or2 = Or3 + \{0, y_2,\ z_2 + h_3\}^* R_3 \\
&\text{Origin of L1 vertebra } Or1 = Or2 + \{0, y_1,\ z_1 + h_2\}^* R_2 \\
&\text{Origin of torso } Or0 = Or1 + \{0, y_0,\ z_0 + h_1\}^* R_1
\end{aligned}
\right\} \qquad (5.3)
$$

where h_i is the height of the i^{th} vertebra and R_i is the rotation matrix of coordinate system of the i^{th} vertebra and is given as $R_i = \begin{bmatrix} 1 & 0 & 0 \\ 0 & \cos(\theta_i) & \sin(\theta_i) \\ 0 & -\sin(\theta_i) & \cos(\theta_i) \end{bmatrix}$, where θ_i is the sagittal angle of the i^{th} vertebra.

The schematic illustration of kinematic measurements is shown in Figure 5.2 with an example of the L4 vertebral kinematics with respect to the L5 vertebra.

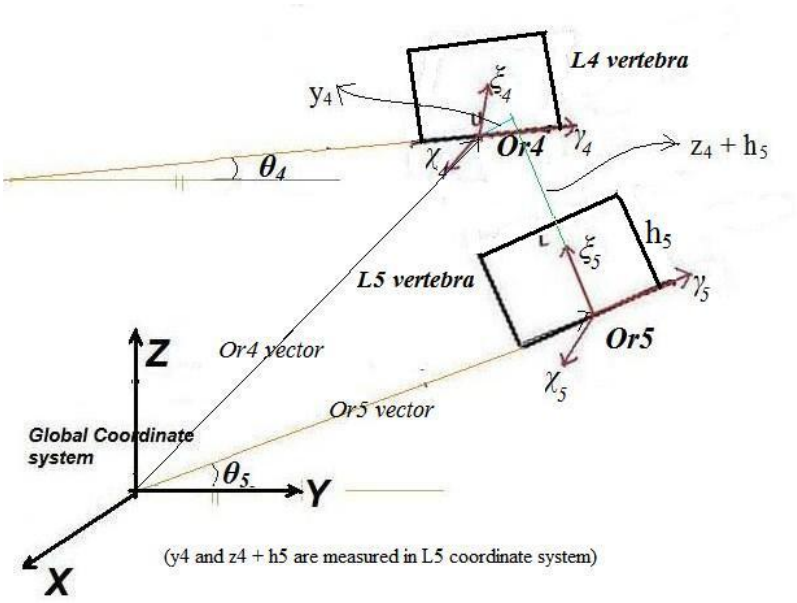

Figure 5.2: Representation of kinematic of 4th lumbar vertebra: the kinematics of L4 vertebra are measured in local coordinate system fixed at Or5 on L5 vertebra

Intervertebral Discs

The viscoelastic behavior of intervertebral discs (IVDs) is modelled using 3 springs and 3 dampers. The model has 2 translational springs and 1 torsional spring and the same type of dampers, associated with the 3 degrees of freedom in the sagittal plane. The torsional spring and damper account for the moment in the IVD due to sagittal plane rotation about the *X* - axis. The 2 translational springs and dampers account for the forces in the IVD due to axial compression and shear. Figure 5.3 shows a schematic illustration of the IVD model with axial, shearing, and torsional springs. The stiffness of the axial spring, kt, is taken as 200N/mm (Izambert et al., 2003; Vresilovic et al., 2006), and for the shear spring ks is taken as 150N/mm (Costi et al., 2008; Gardner-Morse and Stokes, 2004). The rotational stiffness kr is taken as 50 Nm/rad (Stokes et al., 2002). However, these studies did not report damping coefficients. One study (Izambert et al., 2003) investigated the damping coefficients. According to this study, at low-frequency oscillations the damping coefficients were less than the stiffness by approximately 2 orders of magnitude. Hence the damping coefficients for axial, shear, and rotational dampers are taken as

2Ns/mm, 1.5Ns/mm, and 0.5Ns/m-rad, respectively. The energy associated with an IVD is given by

$$E_{ivd} = \sum \left[\frac{1}{2} \cdot K_i \left(l_i - l_{ri} \right)^2 + \frac{1}{2} \cdot C_i \cdot \dot{l}_i^2 \right] \tag{5.4}$$

where K_i are the spring stiffnesses of the 3 springs, C_i are the damping coefficients of the 3 dampers, l_i are the relative displacements between 2 vertebral end plates, l_{ri} are the rest lengths/rotation of the springs, and an overdot denotes differentiation with respect to time. The process of calculating the relative displacements and IVD spring rest lengths/rotations is described in the following pages.

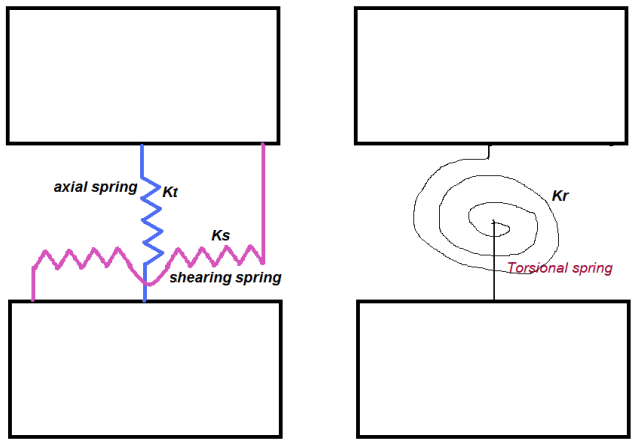

Figure 5.3: IVD model with axial, shearing, and torsional springs (dampers are not included for better visualization)

The shearing and translations of the IVD are measured as described in (Cholewicki and McGill, 1992). The motion of the upper vertebra is calculated relative to the lower vertebra. As shown in Figure 5.4, the shear deformation is measured using the component of ***LU*** along the X_d- axis, and axial deformation is measured using the component of ***LU*** along the Y_d-axis that is orthogonal to the X_d - axis. The X_d -axis is taken such that it bisects the angle 'A' formed by the end plates of the two vertebrae. The rest lengths of the IVD springs are not available in the

literature. The following procedure is used to find the rest lengths of the IVD springs. The equilibrium equations for the spine model in the standing posture are developed without any muscle or external forces. This gives 18 equations with 18 unknowns, the unknowns being the rest lengths and angles of the springs that are used to model the IVDs. This procedure is justified by calculating the compressive loads on the IVDs from these rest length values for the standing posture. The compressive loads are in the physiological range reported in the literature. The procedure will now be described in detail.

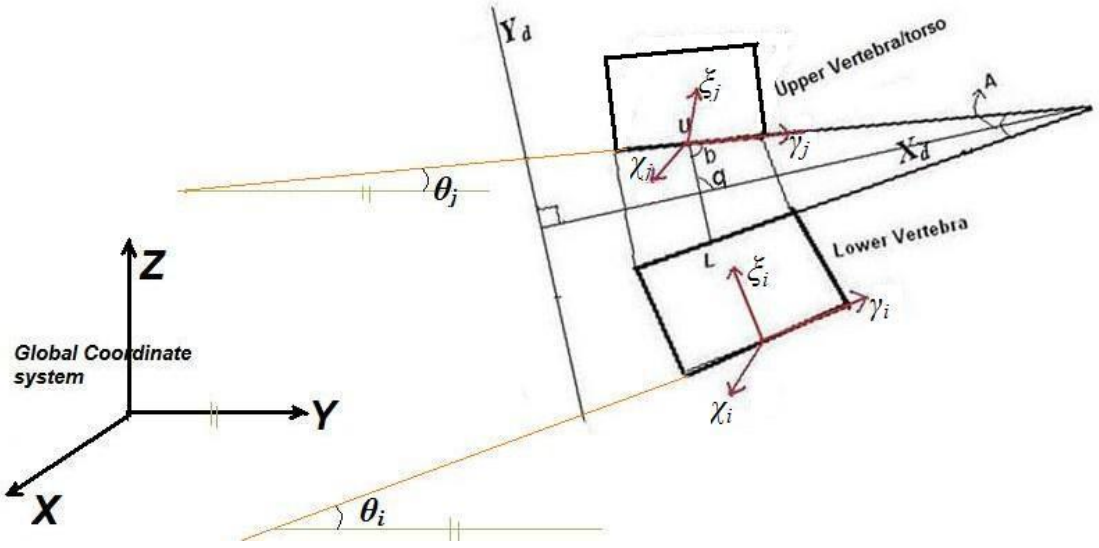

Figure 5.4: Shear and axial translations of IVD: the component of LU on Y_d axis is axial translation and the component of LU on X_d axis is the shear translation. X_d axis bisects the angle A and Y_d axis is perpendicular to X_d axis

Analytical description of IVD energies and rest length calculations:

$$\left.\begin{aligned} &\text{IVD axial displacement } l_y = \boldsymbol{LU}*\sin(q) \\ &\text{IVD shear displacement } l_x = \boldsymbol{LU}*\cos(q) \end{aligned}\right\} \quad (5.5)$$

where ***LU = OU-OL***

where ***OU*** is the vector of the origin of the upper rigid body of the IVD and ***OL*** is given as ***OL*** = $Or_i + \{0,0,hi\}Ri$ where Or_i, h_i, and R_i are the origin, height, and rotation matrix corresponding to the lower vertebra of the IVD, respectively.

To find the angle '*q*':

Angle $A = \theta_j - \theta_i$

where θ_i and θ_j are the sagittal angles of the i^{th} (lower) and j^{th} (upper) vertebrae in the global coordinate system, respectively.

Angle *'q'* = $\pi - (A/2 + b)$

Angle 'b' between the ***LU*** and $\boldsymbol{y_j}$ vectors is given by the inverse cosine of the dot product of the unit vectors in the directions of these two vectors.

The potential energy and damping energy associated with an IVD are given by:

$$\left.\begin{aligned} V_{ivd} &= \frac{1}{2}K_t\left(l_y - l_{yr}\right)^2 + \frac{1}{2}K_s\left(l_x - l_{xr}\right)^2 + \frac{1}{2}K_r\left(\theta_j - \theta_i - \theta_r\right)^2 \\ C_{ivd} &= \frac{1}{2}C_t(\dot{l}_y)^2 + \frac{1}{2}C_s(\dot{l}_x)^2 + \frac{1}{2}C_r(\dot{\theta}_j - \dot{\theta}_i)^2 \end{aligned}\right\} \quad (5.6)$$

where l_{yr}, l_{xr}, and θ_r are the rest length of the translational spring, the rest length of the shearing spring, and the rest angle of the torsional spring, respectively, and the overdot represents the time derivative. For the IVD between the pelvis and the L5 vertebra, $\theta_i = 0$.

<u>To find the rest lengths from the equilibrium position:</u>

Kinetic energy:

$$T_{eq} = \sum_{i=0}^{5}\left[\frac{1}{2}m_i Vg_i^T \cdot Vg_i + \frac{1}{2}\omega_i^T \cdot I_{g_i} \cdot \omega_i\right] = 0 \quad (5.7)$$

where $Vg_i = \frac{d}{dt}\left[\left\{0,0,\frac{h_i}{2}\right\}R_i\right]$ are the velocities of the centers of mass of the rigid bodies,

$\omega_i = \dot{\theta}_i$ are the angular velocities of the rigid bodies, and m_i and Ig_i are the mass and inertia matrices of the rigid bodies, respectively.

Potential energy:

$$V_{eq} = \sum_{i=0}^{5}\left[m_i g \cdot H_i + \frac{1}{2}K_t\left(l_{yi_{eq}} - l_{yri}\right)^2 + \frac{1}{2}K_s\left(l_{xi_{eq}} - l_{xri}\right)^2 + \frac{1}{2}K_r\left(\theta_{i+1_{eq}} - \theta_{i_{eq}} - \theta_{ri}\right)^2 \right] \tag{5.8}$$

where H_i is the height of the center of mass of the ith rigid body measured with the pelvis (origin of the global coordinate system) as the datum.

Damping energy:

$$C_{eq} = \sum_{i=0}^{5}\left[\frac{1}{2}C_t\dot{l}_{yi}^2 + \frac{1}{2}C_s\dot{l}_{xi}^2 + \frac{1}{2}C_r(\dot{\theta}_{i+1} - \dot{\theta}_i)^2 \right] = 0 \tag{5.9}$$

The IVD lengths l_{xi} and l_{yi} and their corresponding derivatives are functions of the state variables.

States $\bar{q} = \left\{\theta_0, y_0, z_0, \theta_1, y_1, z_1, \ldots, \theta_5, y_5, z_5, \dot{\theta}_0, \dot{y}_0, \dot{z}_0, \dot{\theta}_1, \dot{y}_1, \dot{z}_1, \ldots, \dot{\theta}_5, \dot{y}_5, \dot{z}_5\right\}$

where the subscript '*0*' represents the torso's state variable and the numbered subscripts represent the number of the lumbar vertebra.

Then $\left.\frac{\partial V_{eq}}{\partial q_i} = 0\right|_{i=1\text{–}18}$ gives 18 linear equations in 18 unknowns (the rest lengths of the IVDs). Solving these equations gives the IVD rest lengths (Appendix C).

Muscle Model

The muscle model that is adopted here is the one used by Cholewicki and McGill (1996) and Franklin and Granata (2007). The muscle element that generates the tension in the muscle by shortening or lengthening the muscle is called the contractile element (Winter, 2005). This contractile element is surrounded by passive muscle tissue. The force-length and force-velocity characteristics of muscle are affected by both the contractile element and the passive tissue (Winter, 2005). In the current study, a Hill-type muscle model (Hill, 1938) is used (Figure 5.5), which consists of a contractile element in parallel with a spring and a damper. This muscle model accounts for a steady-state contractile muscle force and viscoelastic behavior of the muscle tissue (Franklin and Granata, 2007). In this study, along with the origin and insertion points, the muscles are assigned via points on the vertebral structure to account for muscle curvature, unlike Bergmark's model.

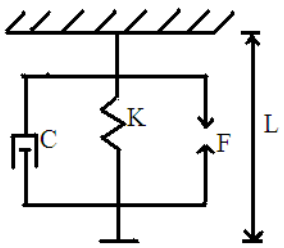

Figure 5.5: Hill-type muscle model with length L and parallel stiffness K and damping C. K = q F/L, C = b F/L, and F = f_o $\alpha(t)$

The force exerted by this muscle model is given by

$$f_m = f_\circ \alpha(t)\left(q\left(\frac{L_m(t) - L_{mo}}{L_{mo}} \right) + c\frac{L_m'(t)}{L_{mo}} + 1 \right) \tag{5.10}$$

where

f_o = maximum muscle force, defined as the maximum muscle stress of F_s = 46N/cm^2 multiplied by the muscle cross-sectional area (Gardner-Morse et al., 1995a).

$\alpha(t)$ = muscle activation

q = dimensionless intrinsic muscle stiffness gain (Bergmark, 1989b)

b = intrinsic muscle damping gain

L_m = muscle length

L_{mo} = muscle rest length

Equation 5.10 gives the tension in each muscle. The force vector acting at each node of the muscle is estimated using the muscle path formula developed by Gao et al. (2002). The force vector acting at a node (or muscle attachment) is estimated as shown in Figure 5.6, with the aid of equation 5.11:

$$F_{node} = f_m \left[\frac{V_1}{\|V_1\|} + \frac{V_2}{\|V_2\|} \right] \tag{5.11}$$

where $V_1 = P_{i-1} - P_i$ and $V_2 = P_{i+1} - P_i$

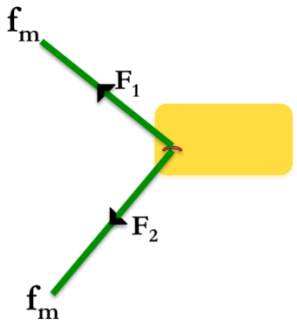

Figure 5. 6: Force acting at a node with muscle tension f_m

The model consists of 45 pairs of muscles (Cholewicki and McGill, 1996). It is believed that these 45 pairs of muscles essentially influence the global movement of the torso. Since the goal of the present study is to build a model of flexion and extension movements, it is appropriate to just model these sets of muscles.

Lagrange's Equations

The dynamic equations of motion of the trunk are developed using Lagrange's equations. Each body is considered as a rigid body with 3 degrees of freedom. Hence the system has a total of 18 degrees of freedom. The equations of motion are given by

$$\frac{d}{dt}\left(\frac{\partial T}{\partial \dot{q}_i}\right) - \frac{\partial T}{\partial q_i} + \frac{\partial V}{\partial q_i} + \frac{\partial D}{\partial \dot{q}_i} = Q_i \tag{5.12}$$

where

T = kinetic energy

V = potential energy

D = Rayleigh's dissipation function

q_i = generalized coordinates

Q_i = generalized forces

The energies and generalized forces are defined as follows:

$$V = \sum_{i\&m=0}^{5}\left[m_i g \cdot H_i + \frac{1}{2} q_i^T \cdot k_{i\,m} \cdot q_m\right] \tag{5.13}$$

$$D = \sum_{i\&m=0}^{5}\left[\frac{1}{2}\dot{q}_i^T \cdot C_{im} \cdot \dot{q}_m\right] \tag{5.14}$$

$$T = \sum_{i\&m=0}^{5}\left[\frac{1}{2} m_i V_{g_i}^T \cdot V_{g_i} + \frac{1}{2}\omega_i^T \cdot I_{im} \cdot \omega_m\right] \tag{5.15}$$

$$Q_i = \sum_{j=1}^{6}\left[\left(\left(\sum_{k=1}^{m_j} F_{j\,k}\right) \cdot \frac{\partial v_j}{\partial \dot{q}_i}\right) + \left(\left(\sum_{k=1}^{m_j} r_{j\,k} \times F_{j\,k}\right) \cdot \frac{\partial \omega_j}{\partial \dot{q}_i}\right)\right] \tag{5.16}$$

where

g = gravity vector

M = mass matrix **I**=inertia matrix

K = stiffness matrix

C = damping matrix

i = DOF (index)

j = body (index)

k = forces acting on body j (index)

F_{jk} = force k acting on body j

r_{jk} = moment arm of force F_{jk}

v_j = linear velocity of the origin of body j

λ_j = angular velocity of body j

q_i = DOF i

Q_i = generalized forces for DOF i

The potential energy of the system consists of the energy due to gravity and the springs connecting the inter-vertebral discs. The dissipation energy consists of the energy due to the dampers between the inter-vertebral discs. The kinetic energy is the sum of the translational kinetic energy due to translational velocity and the rotational energy due to angular velocity. The generalized forces consist of muscle forces and moments. The inertia matrix for the calculation of the kinetic energy is estimated as follows.

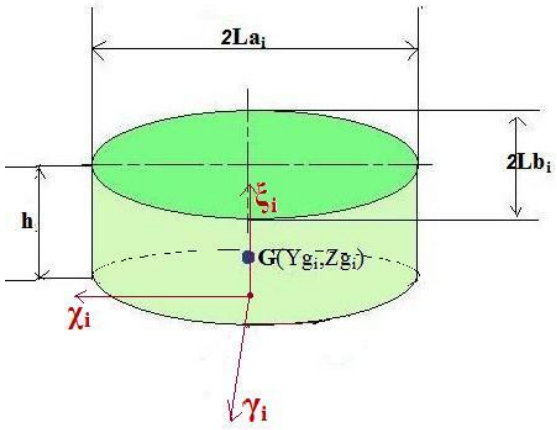

Figure 5.7: Vertebra model for moments of inertia

For the inertial properties, each rigid body is modelled as a disc with elliptical cross section as shown in Figure 5.7. The inertia matrix of the i^{th} rigid body about the center of mass is given by

$$I_{g_i} = \begin{bmatrix} \frac{1}{4}m_i L_b^2 + \frac{1}{12}m_i h_i^2 & 0 & 0 \\ 0 & \frac{1}{4}m_i L_a^2 + \frac{1}{12}m_i h_i^2 & 0 \\ 0 & 0 & \frac{1}{4}m_i L_b^2 + \frac{1}{4}m_i L_a^2 \end{bmatrix} \tag{5.17}$$

Once the rotational kinematics are determined, they are substituted into the equations of motion (5.12) to give a system of equations for the unknown muscle activations. However, these equations are not deterministic, with the number of equations being less than the number of unknowns. The muscle activations are estimated with the help of constrained optimization.

Optimization

Biomechanical models of the spine are often developed to estimate the muscle forces from indeterminate equations. Optimization techniques are commonly used to solve the indeterminate equations, which are redundant in muscle activations. Optimization techniques help one calculate the best possible solution, i.e., one that satisfies certain conditions. Three optimization approaches are commonly used in spine biomechanics: 1. mathematical optimization, 2. the EMG-assisted approach, and 3. ENG-assisted quadratic optimization (Gagnon et al., 2001). A mathematical optimization technique similar to that used in Franklin and Granata (2007) is applied here to compute the time-dependent activation vectors. The fmincon function optimization toolbox of Matlab R2007 is utilized in the optimization routine. The equations of motion provide the equality conditions for the problem (18 equations with 45 unknowns in muscle activations). The inequality condition is that the muscle activations are bound to the domain [0,1]. The metabolic power is used as the cost function of the problem and is minimized. The metabolic power $p(\alpha_o)$ is given by

$$p(\alpha_o) = m\left[37\sin\left(\frac{\alpha_0 \cdot \pi}{2}\right) + 55.5\left(1 - \cos\left(\frac{\alpha_0 \cdot \pi}{2}\right)\right)\right] \tag{5.18}$$

(Anderson and Pandy, 1999; Franklin and Granata, 2007). This program produces muscle activations discretely at each time step of the flexion and extension cycle. Including a stability constraint similar to that in the model of Franklin and Granata (2007) would increase the computational time by at least 2 times, and therefore was not included in this study. The optimization routine at each time step of a trial (each trial has 60 time steps) took on average 7 hours of computational time on an Intel® Core™2 Duo Processor computer with 1GB memory.

Limitations of the model

The 2-D model described in the previous sections is an important step forward in the field of dynamic spine modeling. However, certain assumptions and some simplified methods are employed to address the computational expenses. The vertebrae are assumed to be rigid bodies and the thorax is approximated as one rigid body. The facet joints are ignored and the vertebrae are modeled as cylinders with elliptical cross sections. The Hill-type muscle model used is a linear model even though the dynamic spine is a nonlinear system. The mathematical optimization techniques used in this model produce mechanically valid muscle forces and less accurate physiological results compared to EMG-assisted optimization approaches (Gagnon et al., 2001).

References

ANDERSON, F. C. & PANDY, M. G. (1999) A dynamic optimization solution for vertical jumping in three dimensions. *Comput Methods Biomech Biomed Engin,* 2**,** 201-231.

BERGMARK, A. (1989) Stability of the lumbar spine. A study in mechanical engineering. *Acta Orthop Scand Suppl,* 60**,** 1-54.

CHOLEWICKI, J. & MCGILL, S. M. (1992) Lumbar posterior ligament involvement during extremely heavy lifts estimated from fluoroscopic measurements. *J Biomech,* 25**,** 17-28.

CHOLEWICKI, J. & MCGILL, S. M. (1996) Mechanical stability of the in vivo lumbar spine: implications for injury and chronic low back pain. *Clin Biomech,* 11**,** 1-15.

COSTI, J. J., STOKES, I. A., GARDNER-MORSE, M. G. & IATRIDIS, J. C. (2008) Frequency-dependent behavior of the intervertebral disc in response to each of six degree of freedom dynamic loading - solid phase and fluid phase contributions. *Spine,* 33**,** 1731-8.

FRANKLIN, T. C. & GRANATA, K. P. (2007) Role of reflex gain and reflex delay in spinal stability--a dynamic simulation. *J Biomech,* 40**,** 1762-7.

GAGNON, D., LARIVIERE, C. & LOISEL, P. (2001) Comparative ability of EMG, optimization, and hybrid modeling approaches to predict trunk muscle forces and lumbar spine loading during dynamic sagittal plane lifting. *Clin Biomech,* 16**,** 359-72.

GAO, F., DAMSGAARD, M., RASMUSSEN, J., & CHRISTENSEN, S. T. (2002) Computational method for muscle-path representation in musculoskeletal models, *Bio Cyb,* 87, 199–210.

GARDNER-MORSE, M., STOKES, I. A. & LAIBLE, J. P. (1995) Role of muscles in lumbar spine stability in maximum extension efforts. *J Orthop Res,* 13**,** 802-8.

GARDNER-MORSE, M. G. & STOKES, I. A. F. (2004) Structural behavior of human lumbar spinal motion segments. *J Biomech,* 37**,** 205-12.

HILL, A. V. (1938) The heat of shortening and dynamic constants of muscle. *Proc R Soc. Lond B,* 126**,** 136-95.

IZAMBERT, O., MITTON, D., THOUROT, M. & LAVASTE, F. (2003) Dynamic stiffness and damping of human intervertebral disc using axial oscillatory displacement under a free mass system. *Eur Spine J,* 12**,** 562-6.

MCGILL, S. M. & NORMAN, R. W. (1986) Partitioning of the L4-L5 dynamic moment into disc, ligamentous, and muscular components during lifting. *Spine,* 11**,** 666-78.

STOKES, I. A., GARDNER-MORSE, M., CHURCHILL, D. & LAIBLE, J. P. (2002) Measurement of a spinal motion segment stiffness matrix. *J Biomech,* 35**,** 517-21.

SUN, L. W., LEE, R. Y. W., LU, W. & LUK, K. D. K. (2004) Modeling and simulation of the intervertebral movements of the lumbar spine using an inverse kinematic algorithm. *Med Biol Eng Comput,* 42**,** 740-6.

VRESILOVIC, E. J., JOHANNESSEN, W. & ELLIOTT, D. M. (2006) Disc mechanics with trans-endplate partial nucleotomy are not fully restored following cyclic compressive loading and unloaded recovery. *J Biomech Eng,* 128**,** 823-9.

WINTER, D. A. (2005) *Biomechanics and motor control of human movement,* Hoboken, NJ, Wiley.

Chapter 6 - Estimating Dynamic Muscle Forces of the Torso during Flexion and Extension Movements: A Mathematical Simulation

Abstract

Dynamic tasks involving large-angle trunk movements are one of the major risk factors of low back pain. The goal of this study is to determine the time-dependent muscle forces and spinal loads during large-angle flexion-extension movement. A 2-D sagittal-plane lumped parameter model was built. The kinematic data from one flexion-extension movement was input in the model. Mathematical optimization techniques were used to estimate the muscle forces. Muscle recruitment patterns that minimized the metabolic power while satisfying the 18 equations of motions were calculated. Spinal loads were calculated as the vector sum of the muscle forces and the trunk weight. High abdominal activity was observed at the beginning of flexion and the end of extension. Flexion relaxation was seen at large trunk angles. The multifidus and psoas muscle activations increased with lumbar angle. The spinal compression loads were highest at the onset of flexion, and the shear loads were maximum at large trunk angles. In conclusion, the model was successful in predicting the time-dependent muscle activations patterns and spinal loads.

Introduction

Since the beginning of the 21st century, there has been increased emphasis on the dynamic spine research. Lower back mechanics enables the large angular movements of the human torso. Occupational dynamic tasks involving complex trunk movements are considered to be risk factors for low back disorders. Such complex dynamic trunk movements affect various elements of spine mechanics such as muscle activity, spinal strength, and spinal loads (Davis and Marras, 2000). Davis and Marras (2000) concluded that trunk motion might increase muscle coactivity, which in turn decreases spinal strength while increasing the spinal loads.

Mathematical Modeling

Mathematical/computational modeling is a powerful tool to study in vivo spine mechanics. The spine is a complex musculoskeletal system and requires invasive methods to study in vivo mechanics (Bogduk et al., 1992). Biomechanical modeling can be done using forward dynamics or inverse dynamics. In forward dynamics models, assumed internal forces and moments are input to predict the system kinematics. In contrast, with inverse dynamics models the known kinematics and anthropometric data are input to estimate the internal forces and moments (Winter, 2005). Franklin and Granata (2007) used forward dynamics to study the effect of muscle reflexes on spinal stability. Since the spine is a complex system with numerous muscle groups, skeletal parts, and tissues, inverse dynamics analysis is usually used to model the spine (Hansen et al., 2006).

The main purpose of developing mathematical models of the spine is to estimate internal forces such as muscle forces and spinal loads that are not easy to measure experimentally. The surface electromyography (EMG) measurements are not capable of measuring all the individual muscle forces; EMG measurements can only measure the activation levels of muscle groups that are close to the skin surface. However, mathematical modeling increases the versatility of muscle force research. For example, using kinematic data, anthropometric data, and mechanical

properties of the musculoskeletal system, it is possible to quantitatively estimate the forces and activation levels in individual muscles of the torso.

Inverse dynamics models of the trunk always result in indeterminate dynamic equations, therefore optimization techniques are used to solve for internal forces (Hansen et al., 2006). Recently a number of such models of the trunk were built using known kinematics, and muscle forces were estimated using optimization routines (Bazrgari and Shirazi-Adl, 2007; Bazrgari et al., 2008; Franklin and Granata, 2007; Zeinali-Davarani et al., 2008). Franklin and Granata (2007) used small perturbations to study the effect of muscle reflexes on dynamic stability. Zeinali-Davarani et al. (2008) built an inverted pendulum model of the trunk with 3 degrees of freedom. The model was used to estimate muscle recruitment patterns during 60^{o} trunk flexion movement. Bazrgari et al. (2008) developed a finite element model of the trunk to study the effect of flexion-extension movement velocity on muscle recruitment.

However, these studies did not include the translational degrees of freedom between the vertebrae. The present model is an attempt to build a rigid body dynamic model in the sagittal plane including translational degrees of freedom along with sagittal rotations.

Muscle forces and spinal loads

Muscle activity increases with trunk motion (Davis and Marras, 2000). Marras et al. (1987) showed that during dynamic lifting, trunk extension dynamics decreases agnostic muscle activity. Conflicting results have been presented about the muscle activities during trunk twisting activities (Marras and Granata, 1995; McGill, 1992). However, these studies did not investigate the flexion movements of the torso. In 2008, two studies investigated muscle forces/activations during flexion and extension movements of the torso (Bazrgari et al., 2008; Zeinali-Davarani et al., 2008). The effect of inertial forces is greater in the case of faster movements compared to slower movements (Bazrgari et al., 2008). Acceleration of the trunk results in flexor muscle activations, whereas deceleration results in extensor muscle activation

during trunk flexion (Zeinali-Davarani et al., 2008). The muscle forces and spinal loads increased with movement velocity during such movements.

The spinal loads are directly related to trunk muscle forces. The increase in spinal loads beyond the safe limit is identified as a risk for developing low back pain (Garg and Kapellusch, 2009; Granata and Marras, 1993; Marras and Sommerich, 1991a,b). Muscle coactivity changes with the trunk velocity and acceleration, and increases the spinal loads (Bazrgari et al., 2008; Granata and Marras, 1995b). The dynamic spinal loads were found to be 22.5% to 60 % more than the static spinal loads (Marras and Sommerich, 1991a, b).

The main goal of this study is to build a new rigid body model of the torso in the sagittal plane with 18 degrees of freedom. Unlike previous models described in the literature, the current model includes the translational degrees of freedom between the vertebrae. The following specific aims are addressed in this study.

Specific Aims:

1. To build a kinematics driven dynamic model of model flexion and extension movements with both rotational and translational degrees of freedom.

2. To estimate the muscle forces and the spinal loads during dynamic flexion-extension movements using the new rigid body model of the torso.

Methods

Model

The skeletal model of the spine consists of 6 rigid bodies stacked on a stationary pelvis (Cholewicki and McGill, 1996; Franklin and Granata, 2007). The 6 rigid bodies are 5 lumbar vertebrae and the thorax (Figure 6.1). The kinematics of each is represented by 3 degrees of

freedom: one rotational degree of freedom about the x axis and two translational degrees of freedom along the y and z axes in the sagittal plane.

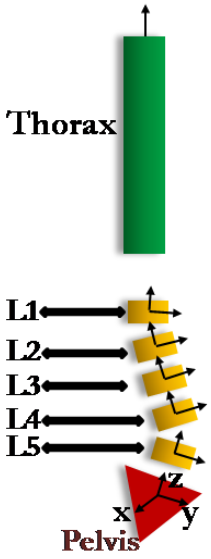

Figure 6.1: Sagittal plane representation of rigid body model in the upright position: 5 lumbar rigid vertebrae and a thorax are stacked on a stationary pelvis

The viscoelastic behavior of each intervertebral disc (IVD) is modeled by 3 springs and dampers: one axial spring and damper, one shear spring and damper, and one rotational spring and damper. The translational springs and dampers account for the axial and shear forces in the IVDs, and the rotational spring and damper account for the IVD moments. The stiffness of the axial spring, kt, is taken as 200N/mm (Izambert et al., 2003; Vresilovic et al., 2006), and for the shear spring, ks is taken as 150N/mm (Costi et al., 2008; Gardner-Morse and Stokes, 2004). The rotational stiffness kr is taken as 50 Nm/rad (Stokes et al., 2002). The damping coefficients for axial, shear, and rotational dampers are taken as 2Ns/mm, 1.5Ns/mm, and 0.5Ns/m-rad, respectively. The axial displacement and shearing of the IVD are calculated according to a method described in (Cholewicki and McGill, 1992). The energy in the IVDs is given by

$$E_{ivd} = \sum \left[\frac{1}{2} \cdot K_i \left(l_i - l_{ri} \right)^2 + \frac{1}{2} \cdot C_i \cdot \dot{l}_i^2 \right] \qquad (6.1)$$

where K_i are the spring stiffnesses of the 3 springs, C_i are the damping coefficients of the 3 dampers, l_i are the relative displacements between 2 vertebral end plates, l_{ri} are the rest lengths/rotations of the springs, and an overdot denotes differentiation with respect to time.

A Hill-type muscle model (Hill, 1938), similar to that of Franklin and Granata (2007) and Cholewicki and McGill (1996), is developed. In this model, along with the origin and insertion points, the muscles are assigned via points on the vertebral structure to account for wrapping of muscles and muscle curvatures around the anatomical structures. The current model uses 45 pairs of muscles (Cholewicki and McGill, 1996). The model consists of a force generator in parallel with a spring and a damper. The force exerted by a muscle is given by

$$f_m = f_\circ \alpha(t)\left(q\left(\frac{L_m(t) - L_{mo}}{L_{mo}} \right) + c\frac{L_m'(t)}{L_{mo}} + 1 \right) \tag{6.2}$$

where

f_o = maximum muscle force, defined as the maximum muscle stress of F = 46N/cm^2 multiplied by the muscle cross-sectional area (Gardner-Morse et al., 1995),

$\alpha(t)$ = muscle activation, q = dimensionless intrinsic muscle stiffness gain (Bergmark, 1989),

c = intrinsic muscle damping gain, L_m = muscle length, L_{mo} = muscle rest length.

Equations of motion

The 18 equations of motion are developed using Lagrange's Equations. The kinetic energy is computed from linear and angular velocities and masses and moments of inertia of the rigid bodies: s

$$T = \sum_{i\&m=0}^{5} \left[\frac{1}{2} m_i V_{g_i}^T \cdot V_{g_i} + \frac{1}{2} \omega_i^T \cdot I_{im} \cdot \omega_m \right] \tag{6.3}$$

The potential energy is computed from the energy due to gravity and the IVD springs:

$$V = \sum_{i\&m=0}^{5} \left[m_i g \cdot H_i + \frac{1}{2} q_i^T \cdot k_{im} \cdot q_m \right] \tag{6.4}$$

The dissipation energy is obtained as the energy due to the IVD dampers:

$$D = \sum_{i\&m=0}^{5} \left[\frac{1}{2} \dot{q}_i^T \cdot C_{im} \cdot \dot{q}_m \right] \tag{6.5}$$

The generalized forces are determined as functions of the muscle forces and moments:

$$Q_i = \sum_{j=1}^{6} \left[\left(\left(\sum_{k=1}^{m_j} F_{jk} \right) \cdot \frac{\partial v_j}{\partial \dot{q}_i} \right) + \left(\left(\sum_{k=1}^{m_j} r_{jk} \times F_{jk} \right) \cdot \frac{\partial \omega_j}{\partial \dot{q}_i} \right) \right] \tag{6.6}$$

where

g = gravity vector, **M** = mass matrix, **I** = inertia matrix, **K** = stiffness matrix, **C** = damping matrix, i = DOF (index), j = body (index), k = forces acting on body j (index), F_{jk} = force k acting on body j, r_{jk} = moment arm of force F_j, v_j = linear velocity of the origin of body j, ω_j = angular velocity of body j, q_i = DOF i, Q_i = generalized force for DOF i.

Kinematics

The kinematic data of one flexion-extension movement for 5 subjects from experiments (Granata and Gottipati, 2008) are used to estimate the kinematic vectors. The experimental data provide the sagittal plane angles of the lower back and thorax. The rotations of each vertebra are calculated as certain percentages of the lumbar angle (McGill and Norman, 1986). Finite differences are used to obtain the velocity and acceleration vectors of angular motions. The translational kinematics of each vertebra are estimated such that they satisfy the developed equations of motion and are within the physiological range reported in the literature (Sun et al., 2004).

Solving for muscle activations

An optimization technique similar to that used in Franklin and Granata (2007) is developed to compute the time-dependent activation vectors. In this model, the muscle activations are chosen

to minimize the metabolic power (cost function) while satisfying the developed indeterminate dynamic equations. The muscle activations are bound to the domain [0, 1]. The cost function $p(\alpha_o)$ is given by

$$p(\alpha_o) = m\left[37\sin\left(\frac{\alpha_0 \cdot \pi}{2}\right) + 55.5\left(1 - \cos\left(\frac{\alpha_0 \cdot \pi}{2}\right)\right)\right] \tag{6.7}$$

(Anderson and Pandy, 1999; Franklin and Granata, 2007). This program produces muscle activations discretely at each time step of the flexion and extension cycle.

Physical properties

The kinematic data for 5 healthy subjects from the experimental study (Granata and Gottipati, 2008) was used to build 5 different subject specific models. The mechanical properties of the rigid bodies of each model are estimated using the subject's weight, trunk height, and gender. The trunk mass and the lumbar vertebral mass are estimated from the total body mass (Winter, 2005). The thorax height and vertebral heights are estimated from the measured trunk height (de Leva, 1996). All 5 lumbar vertebrae are assumed have the same length. Table 6.1 shows the masses and heights of the rigid bodies for each subject. All the subjects are assumed to have the same intervertebral heights in a standing posture, and the heights of the lumbar vertebra are adjusted according to the subject's lumbar length. The heights of S1-L5, L5-L4, L4-L3, L3-L2, L2-L1, and L1-T12 intervertebral discs (the mid-heights of the IVDs) in a standing posture are taken as 9, 11, 11, 11, 9, and 8mm, respectively (Shin et al., 2007; Zhou et al., 2000). Table 6.1 gives the physical properties for each subject's model.

Table 6.1: Physical properties of subjects

Subject	Total mass (kg)	Thorax mass (kg)	Lumbar mass (kg)	Torso length (cm)	Thorax length (cm)	Lumbar length (cm)	Vertebral height (cm)
Sub 1	59.87	16.70	8.32	52.07	27.86	15.93	2.30
Sub 2	70.3	19.61	9.77	49.53	26.50	15.15	2.15
Sub 3	56.7	15.82	7.88	55.88	29.86	17.09	2.38
Sub 4	68.04	18.98	9.46	52.07	30.03	16.27	2.38
Sub 5	77.11	21.51	10.72	63.50	34.04	19.84	2.95

Results

The kinematics of 5 subjects were used in the model to estimate the muscle forces during a single flexion and extension movement. Subjects were asked to maintain a speed of 1 cycle (1 flexion and extension movement) per 2 seconds with the aid of a metronome. However, each subject adopted a different kinematic pattern. The variability in trunk and lumbar angular displacements and velocities can be seen in the following Table 6.2 and Table 6.3 and in graphs (a) and (b) of Figures 6.2, 6.4, 6.6, 6.8, and 6.10. The variability in trunk angle and velocity is smaller than the variability in lumbar angle and velocity. The means (standard deviations) of maximum trunk angle and velocity are 67.86^{o} (4.34) and 119.97^{o}/s (6.71), respectively. The means (standard deviations) of maximum lumbar angle and velocity are 67.38^{o} (5.64) and 142.04^{o}/s (29.02), respectively.

Table 6.2: Maximum and minimum trunk and lumbar angles

	Sub 1	Sub 2	Sub 3	Sub 4	Sub 5	Mean (Std)
Max. Trunk Angle	63.32^{o}	73.24^{o}	67.26^{o}	64.18^{o}	71.29^{o}	67.86^{o} (4.34)
Min. Trunk Angle	1.23^{o}	8.34^{o}	0.68^{o}	5.40^{o}	3.99^{o}	3.93^{o} (3.14)
Max. Lumbar Angle	58.10^{o}	69.11^{o}	72.10^{o}	66.28^{o}	72.42^{o}	67.38^{o} (5.64)
Min. Lumbar Angle	17.24^{o}	3.68^{o}	12.76^{o}	11.23^{o}	4.71^{o}	9.96^{o} (5.64)

Table 6.3: Maximum and minimum trunk and lumbar angular velocities

	Sub 1	**Sub 2**	**Sub 3**	**Sub 4**	**Sub 5**	**Mean (Std)**
Max. Trunk Velocity (^{o}/s)	116.90	121.05	127.79	110.32	123.87	119.97 (6.71)
Min. Trunk Velocity (^{o}/s)	-111.52	-129.15	-113.25	-122.38	-116.09	-118.48 (7.26)
Max. Lumbar Velocity (^{o}/s)	139.26	129.87	183.52	104.89	152.67	142.04 (29.02)
Min. Lumbar Velocity (^{o}/s)	-127.00	-118.15	-133.25	-105.78	-101.80	-117.16 (13.41)

All the subjects exhibited similar muscle activation patterns with small exceptions, which may be due to the differences in kinematic patterns. Figures 6.2 to 6.11 present the activation profiles of all five subjects. Table 6.4 gives the maximum activation levels of each muscle group for each subject. The rectus abdominus (RA) muscle was activated at the onset of flexion and the end of the extension with average maximum activation of 19.49% (8.08). Two sets of external obliques (EO1 and EO2) and internal obliques muscles (IO1 and IO2) were modeled. The EO1 was activated at the end of flexion and/or the beginning of extension with average maximum activation of 34.20 (14.62). The EO2 was activated at the beginning of flexion and end of extension with average maximum activation of 88.84% (18.58). A similar trend was observed in the case of Internal obliques with IO1 activation and IO2 activation with average maximum activations of 94.68 (7.11) and 55.69 (25.37), respectively. The erector spinae (ES) muscles had an average maximum activation level of 33.12 (9.92) at the onset of flexion and end of extension. The latissimus dorsi (LD) muscle had no activation at peak angles, and had almost constant activation at lower angles. The mean maximum activation of LD was 32.56 (3.97). The multifidus (MF) and psoas (PS) muscles were activated throughout the flexion-extension movement, with higher activation at peak angles and with average maximum activations 56.90 (3.41) and 54.54 (3.08), respectively. Little or no activation was seen in pars lumborum muscles.

Table 6.4: Maximum muscle activation percentages

Muscle	Sub1	Sub2	Sub3	Sub4	Sub5	Mean (std.)
RA	14.52	15.37	30.98	9.64	26.95	19.49 (8.08)
EO1	12.88	43.29	54.91	35.76	24.16	34.20 (14.62)
EO2	100.00	52.21	91.98	100.00	100.00	88.84 (18.58)
IO1	82.20	91.20	100.00	100.00	100.00	94.68 (7.11)
IO2	29.86	91.73	77.38	51.44	28.05	55.69 (25.37)
ES	41.72	21.42	46.75	32.36	23.36	33.12 (9.92)
LD	25.91	31.07	34.44	37.84	33.56	32.56 (3.97)
MF	55.40	57.09	56.24	52.72	63.06	56.90 (3.41)
PS	58.09	56.48	54.29	54.86	48.99	54.54 (3.08)

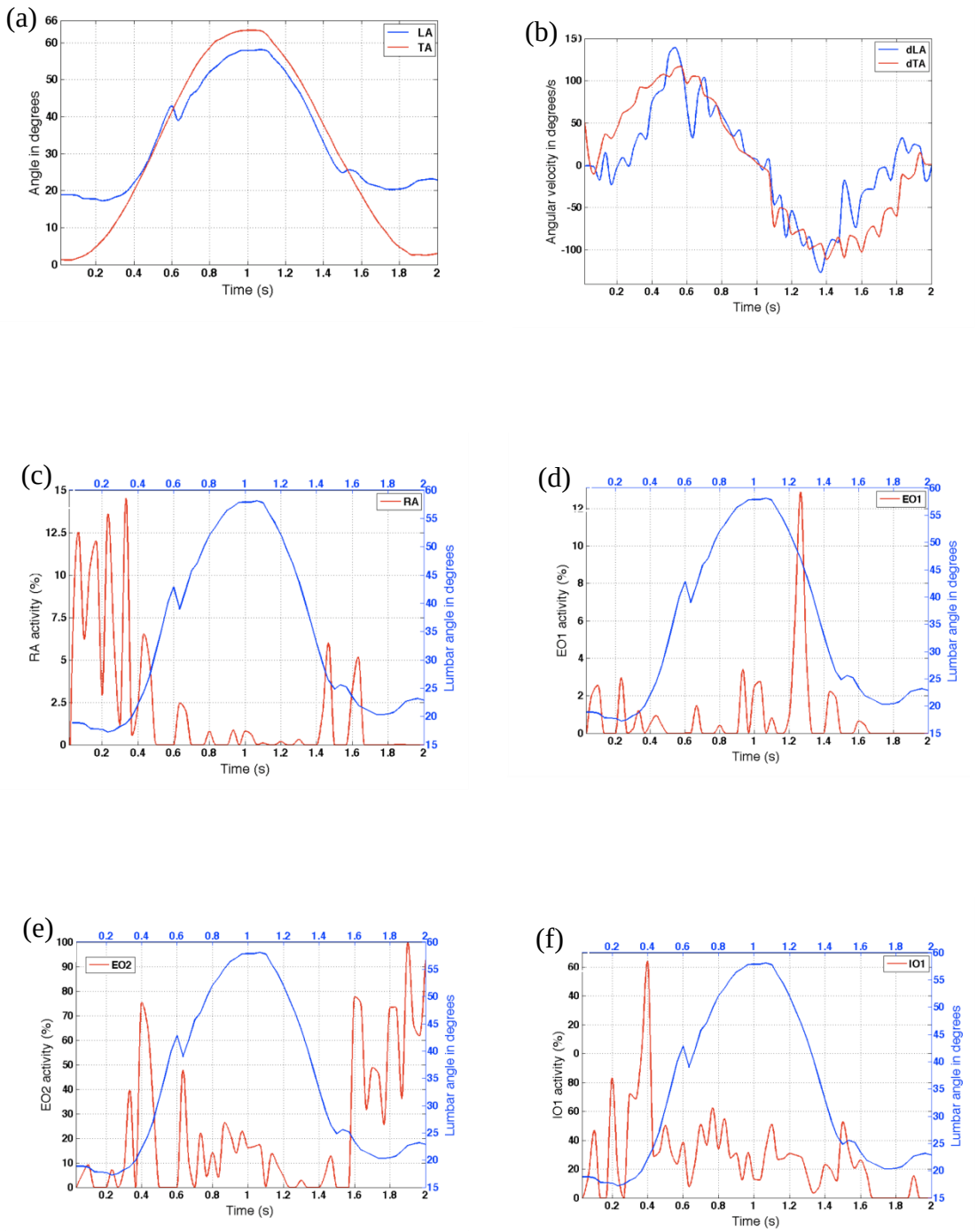

Figure 6.2: Results for subject 1 - (a): Trunk angle (TA) and Lumbar angle (LA) vs. time; (b): Trunk velocity and Lumbar velocity vs. time; (c), (d), (e), and (f): % Muscle activations vs. time (RA – Rectus abdominus; EO1 and EO2 - External oblique; IO1- Internal oblique).

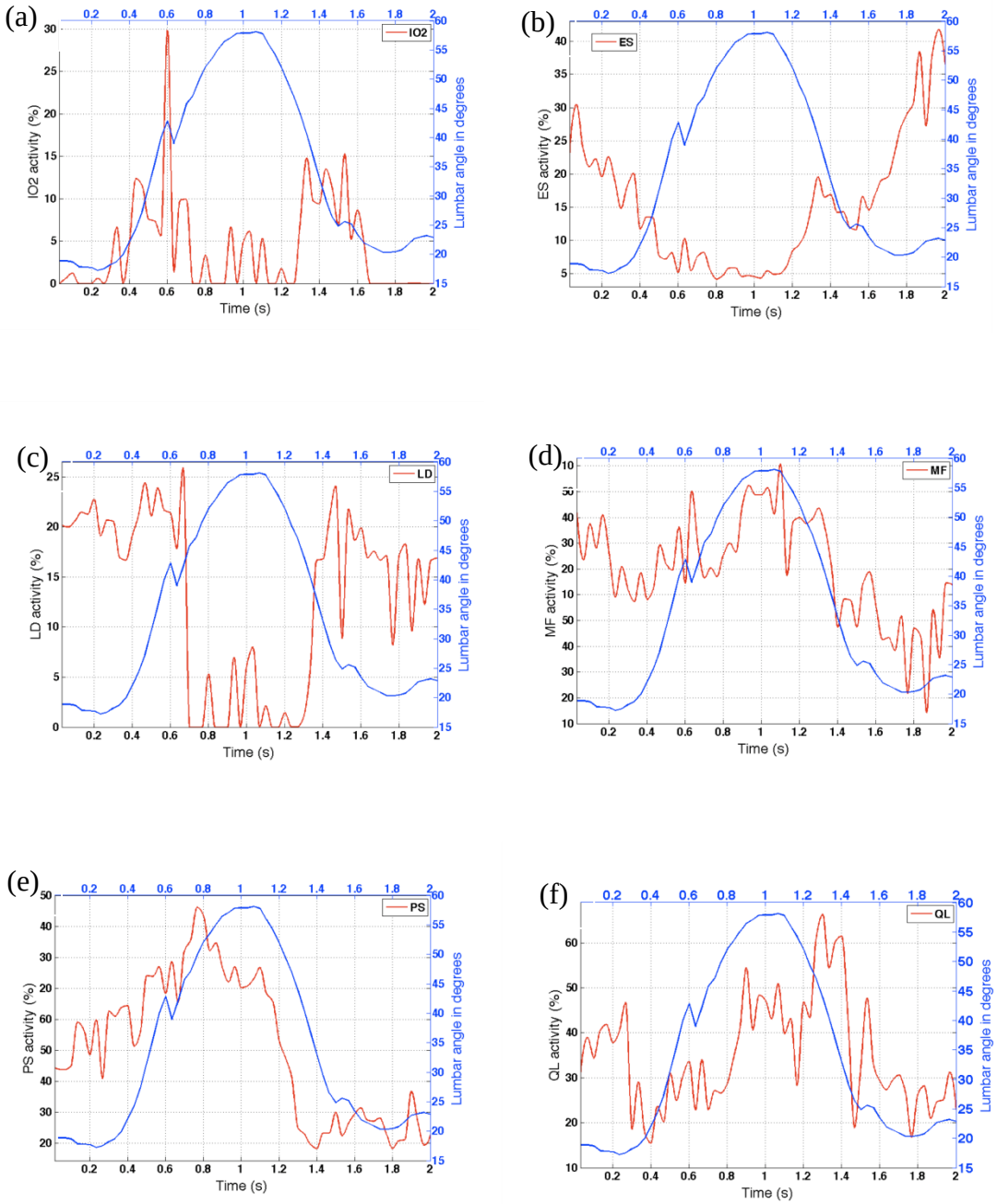

Figure 6.3: Results for subject 1 – (a), (b), (c), (d), (e), and (f): % Muscle activations vs. time (IO2 – Internal oblique, ES – erector spinae, LD – Latissimus dorsi, MF – Multifidus, PS – Psoas, QL – Quadratus lumborum).

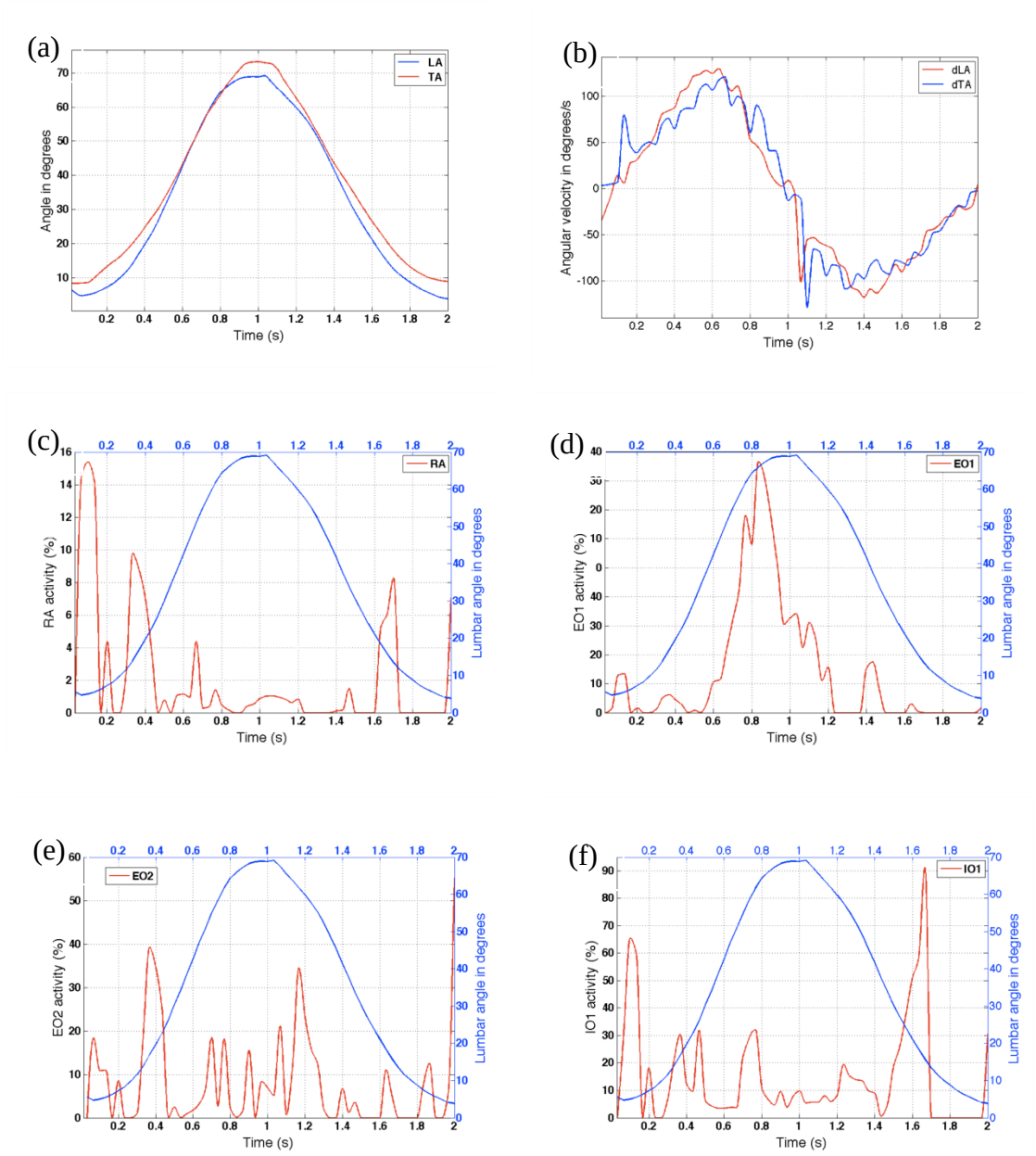

Figure 6.4: Results for subject 2 - (a): Trunk angle (TA) and Lumbar angle (LA) vs. time; (b): Trunk velocity and Lumbar velocity vs. time; (c), (d), (e), and (f): % Muscle activations vs. time (RA – Rectus abdominus; EO1 and EO2 - External oblique; IO1 – Internal oblique).

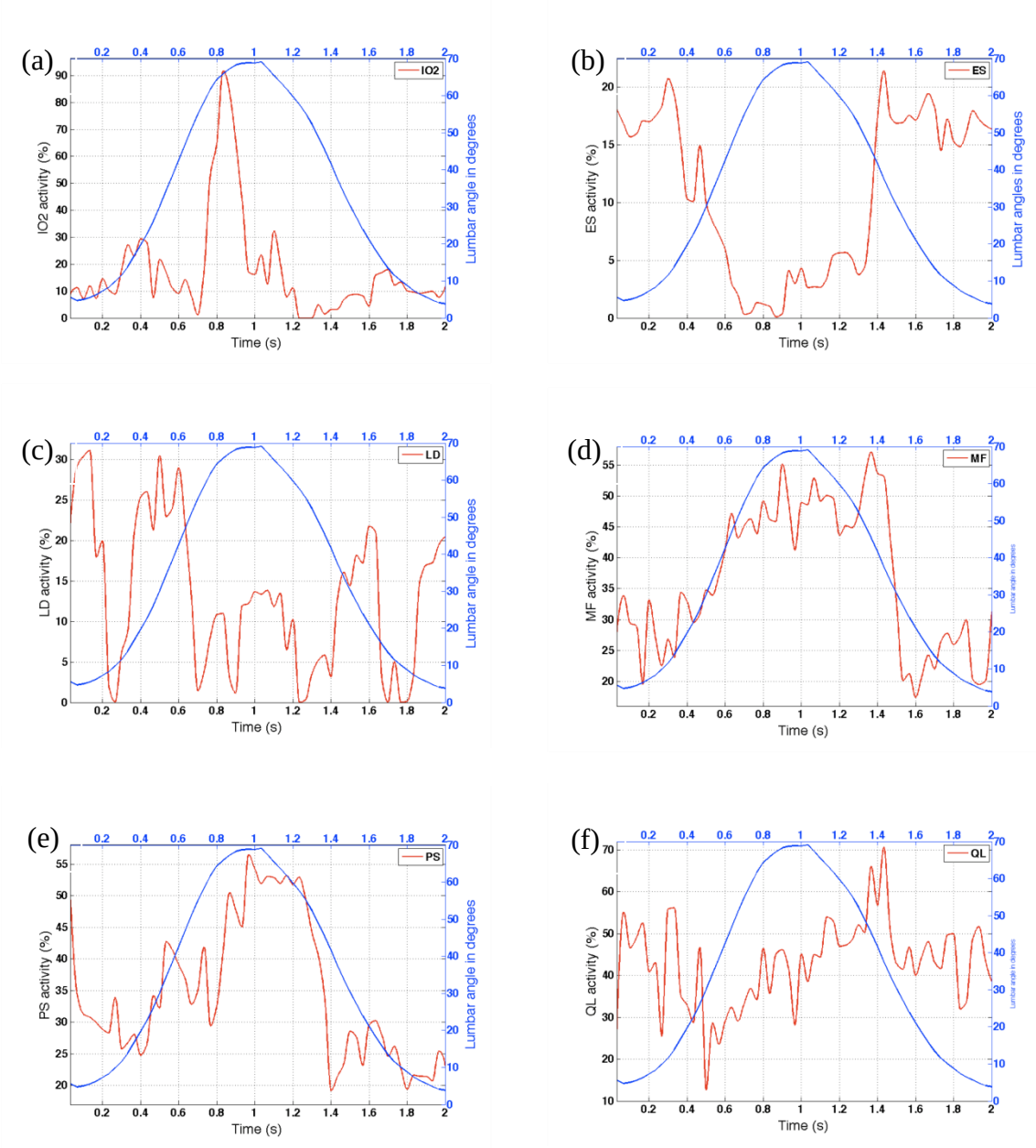

Figure 6.5: Results for subject 2 – (a), (b), (c), (d), (e), and (f): % Muscle activations vs. time (IO2 – Internal oblique, ES – erector spinae, LD – Latissimus dorsi, MF – Multifidus, PS – Psoas, QL – Quadratus lumborum).

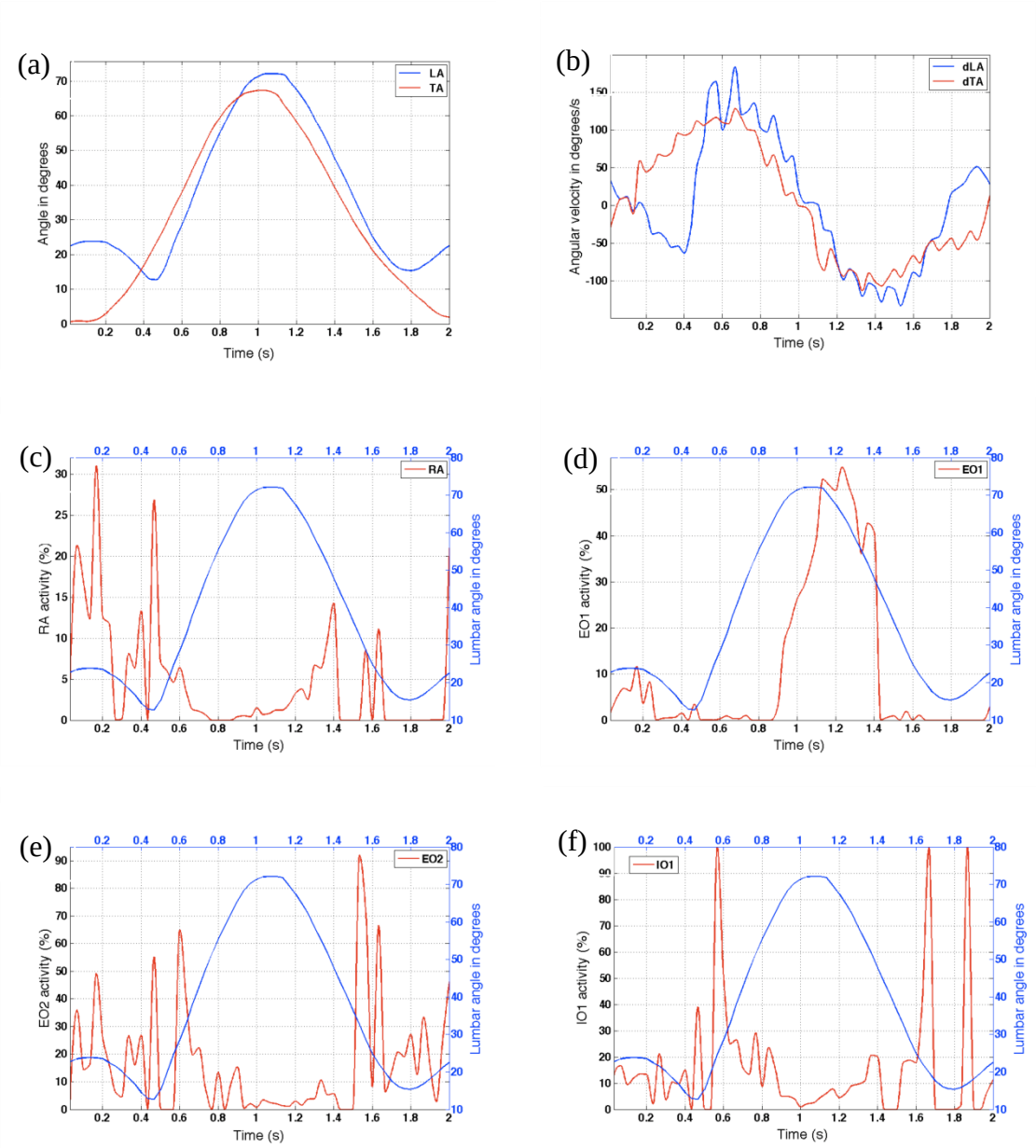

Figure 6.6: Results for subject 3 - (a): Trunk angle (TA) and Lumbar angle (LA) vs. time; (b): Trunk velocity and Lumbar velocity vs. time; (c), (d), (e), and (f): % Muscle activations vs. time (RA – Rectus abdominus; EO1 and EO2 - External oblique; IO1 – Internal oblique).

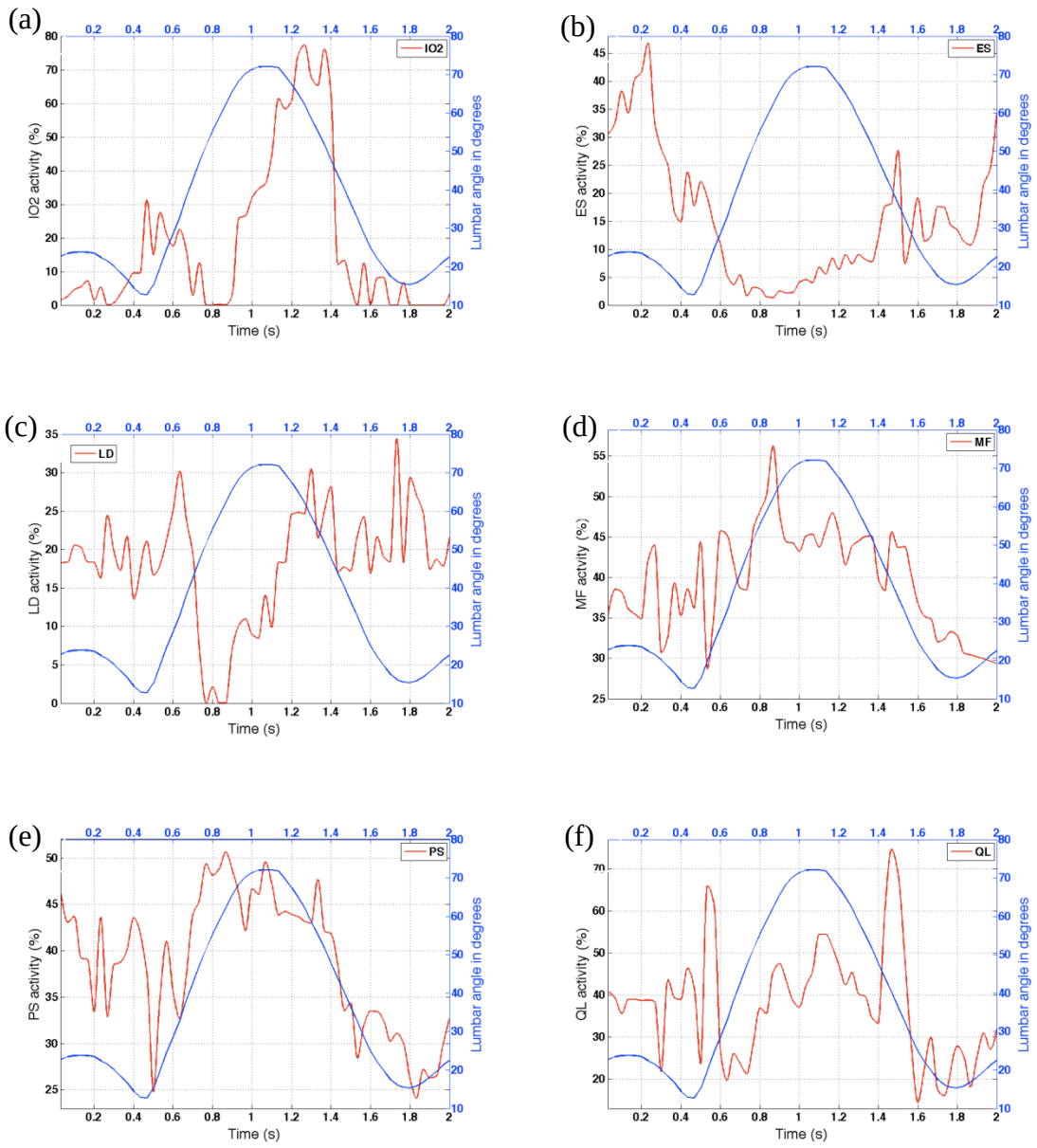

Figure 6.7: Results for subject 3 – (a), (b), (c), (d), (e), and (f): % Muscle activations vs. time (IO2 – Internal oblique, ES – erector spinae, LD – Latissimus dorsi, MF – Multifidus, PS – Psoas, QL – Quadratus lumborum).

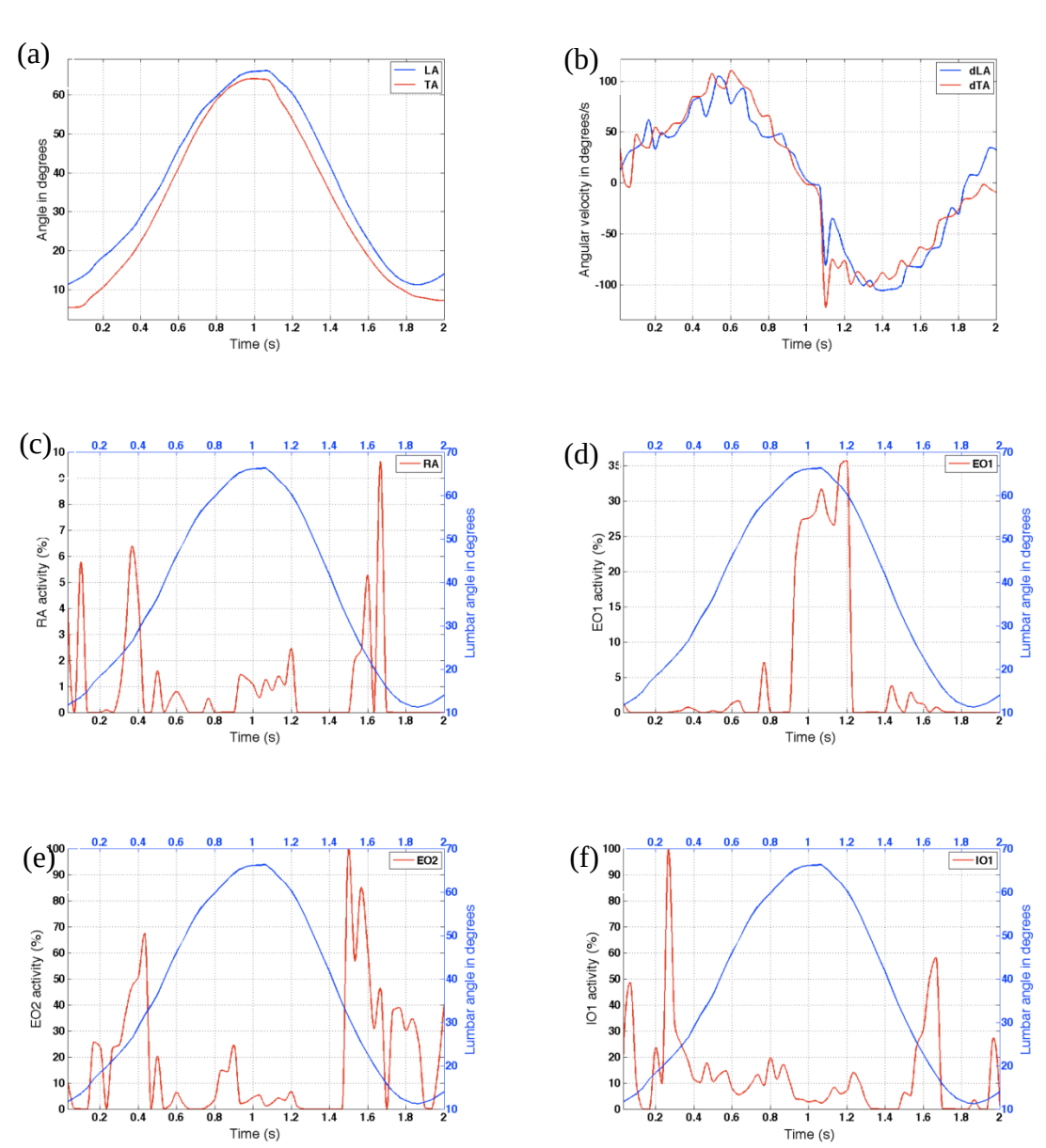

Figure 6.8: Results for subject 4 - (a): Trunk angle (TA) and Lumbar angle (LA) vs. time; (b): Trunk velocity and Lumbar velocity vs. time; (c), (d), (e), and (f): % Muscle activations vs. time (RA – Rectus abdominus; EO1 and EO2 - External oblique; IO1 – internal oblique).

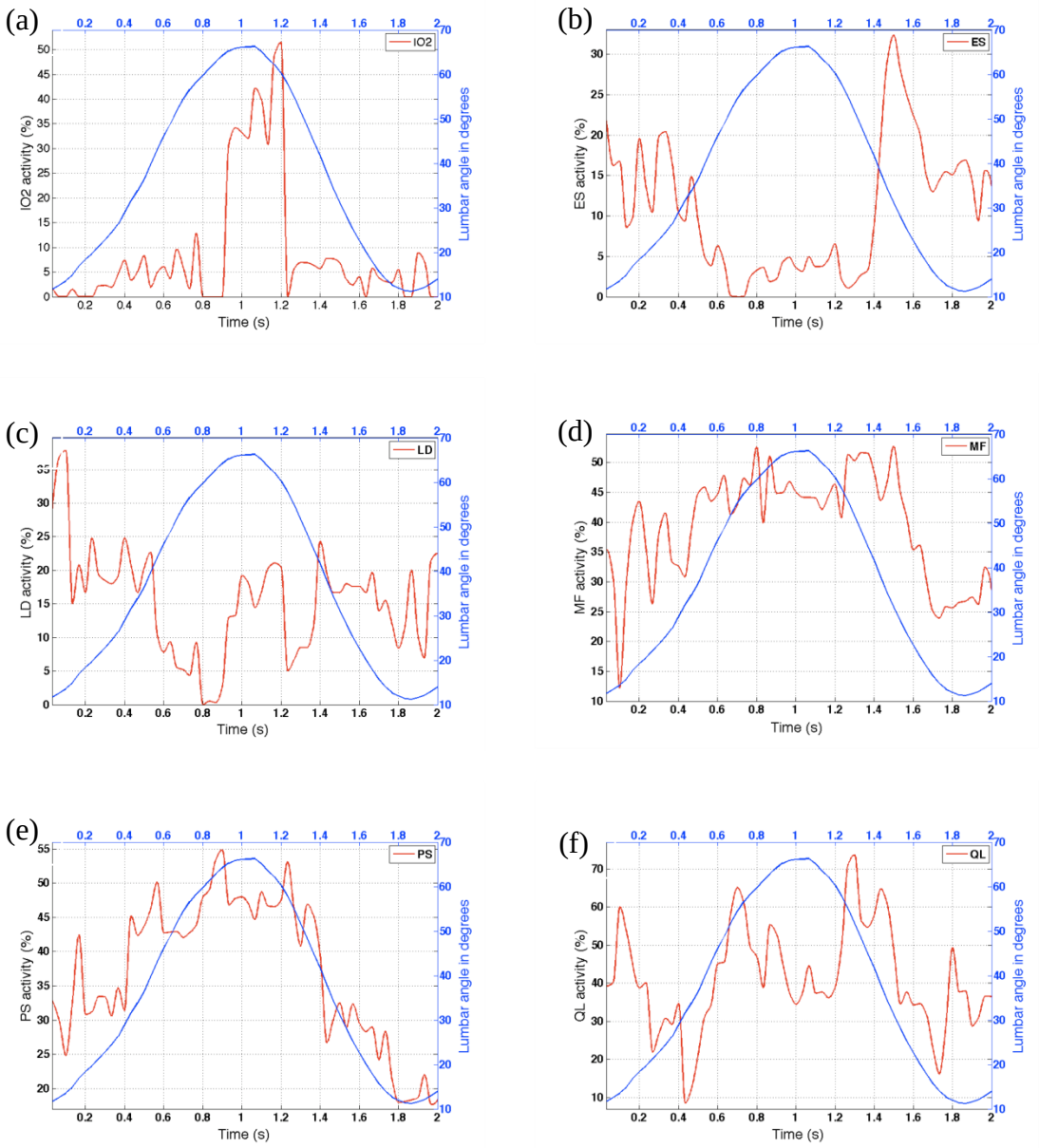

Figure 6.9: Results for subject 4 – (a), (b), (c), (d), (e), and (f): % Muscle activations vs. time (IO2 – Internal oblique, ES – erector spinae, LD – Latissimus dorsi, MF – Multifidus, PS – Psoas, QL – Quadratus lumborum).

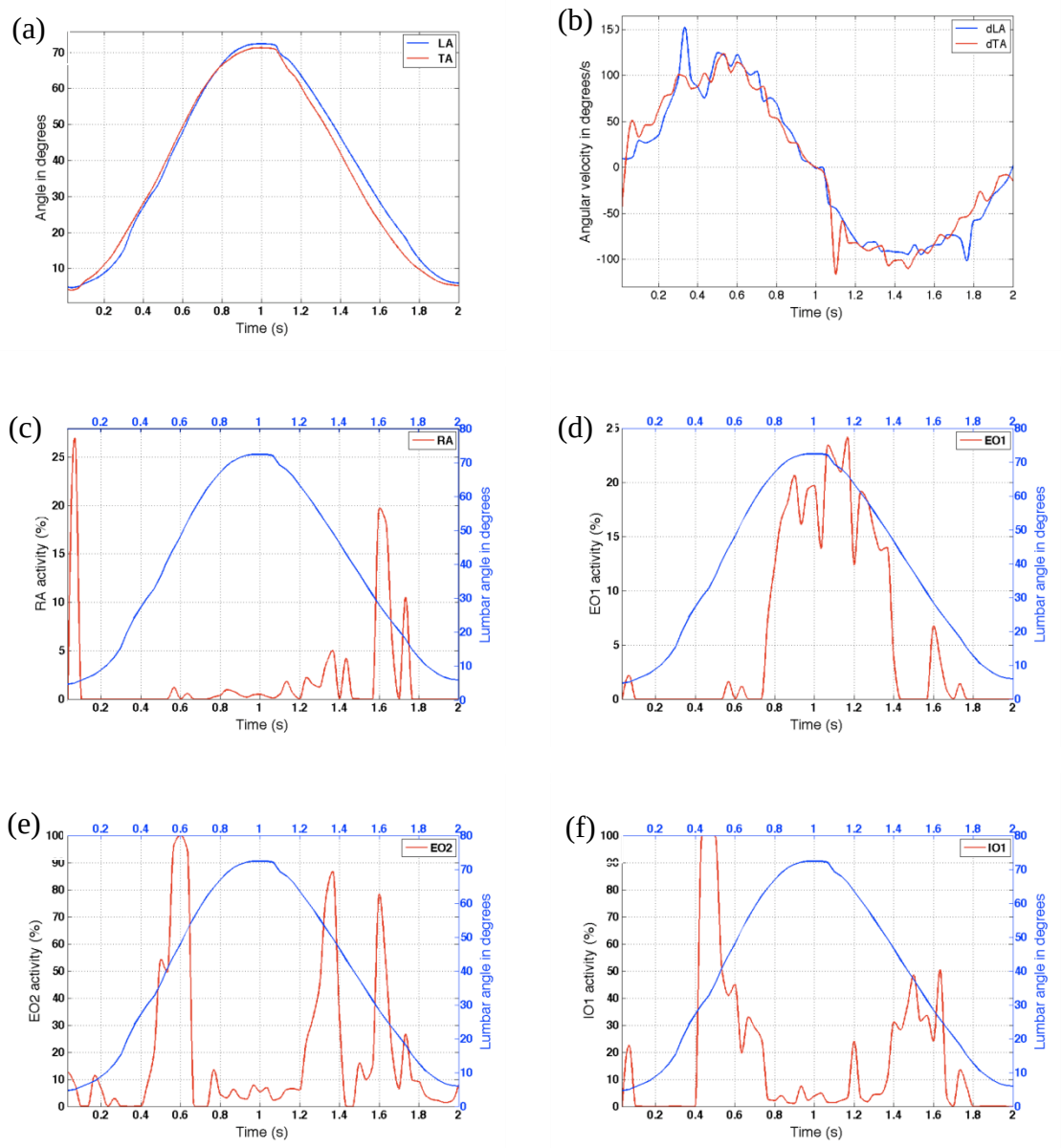

Figure 6.10: Results for subject 5 - (a): Trunk angle (TA) and Lumbar angle (LA) vs. time; (b): Trunk velocity and Lumbar velocity vs. time; (c), (d), (e), and (f): % Muscle activations vs. time (RA – Rectus abdominus; EO1 and EO2 - External oblique; IO1- internal oblique).

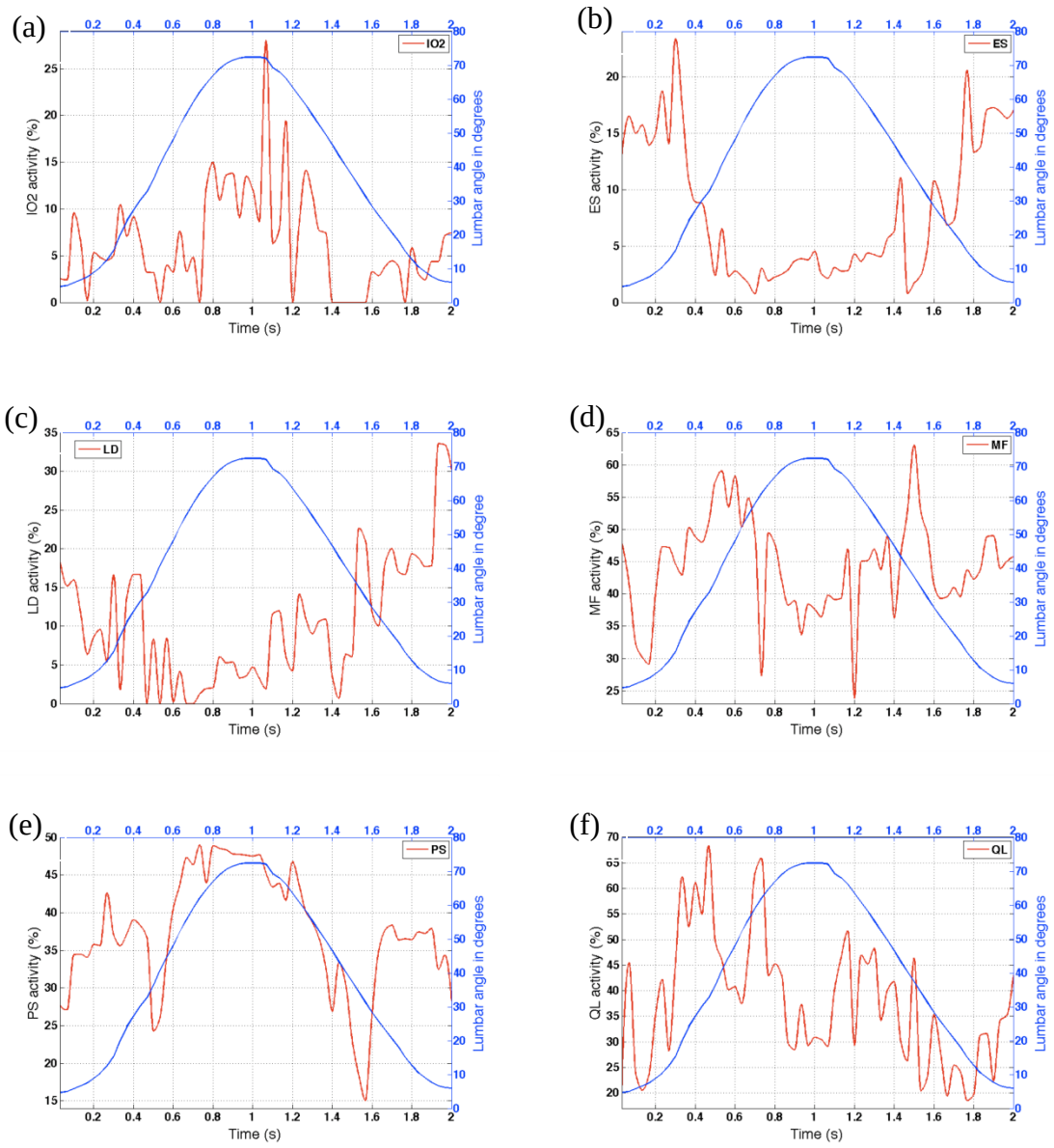

Figure 6.11: Results for subject 5 – (a), (b), (c), (d), (e), and (f): % Muscle activations vs. time (IO2 – Internal oblique, ES – erector spinae, LD – Latissimus dorsi, MF – Multifidus, PS – Psoas, QL – Quadratus lumborum).

The spinal loads on pelvis (S1) were calculated as the vector sum of muscle forces and trunk weight (Granata and Marras, 1995; Granata and Wilson, 2001). The compressive loads reached maximum values at the onset of flexion for all the subjects except for subject 2. In general there was small increase compressive load at the peak flexion and the subject 2 had the highest compressive load at the peak flexion (Figure 6.12). The mean (standard deviation) of maximum compressive load is 1337.32 N (191.01). The shear loads (Figure 6.13) reached maximum values at the peak flexion with mean (standard deviation) value of 707.708 N (120.38) (Appendix C). Figures 6.12(f) and 6.13(f) show the least square fit plots of the spinal loads of all the subjects. This demonstrates the overall trend of time dependent dynamic spinal loads.

Table 6.5: Maximum Compression and Shear loads

	Maximum Compression load (N)	**Maximum Shear load (N)**
Subject 1	1543.50	697.35
Subject 2	1289.90	661.89
Subject 3	1430.10	673.08
Subject 4	1386.10	594.31
Subject 5	1037.00	911.91
Mean (Standard deviation)	1337.32 (191.01)	707.708 (120.38)

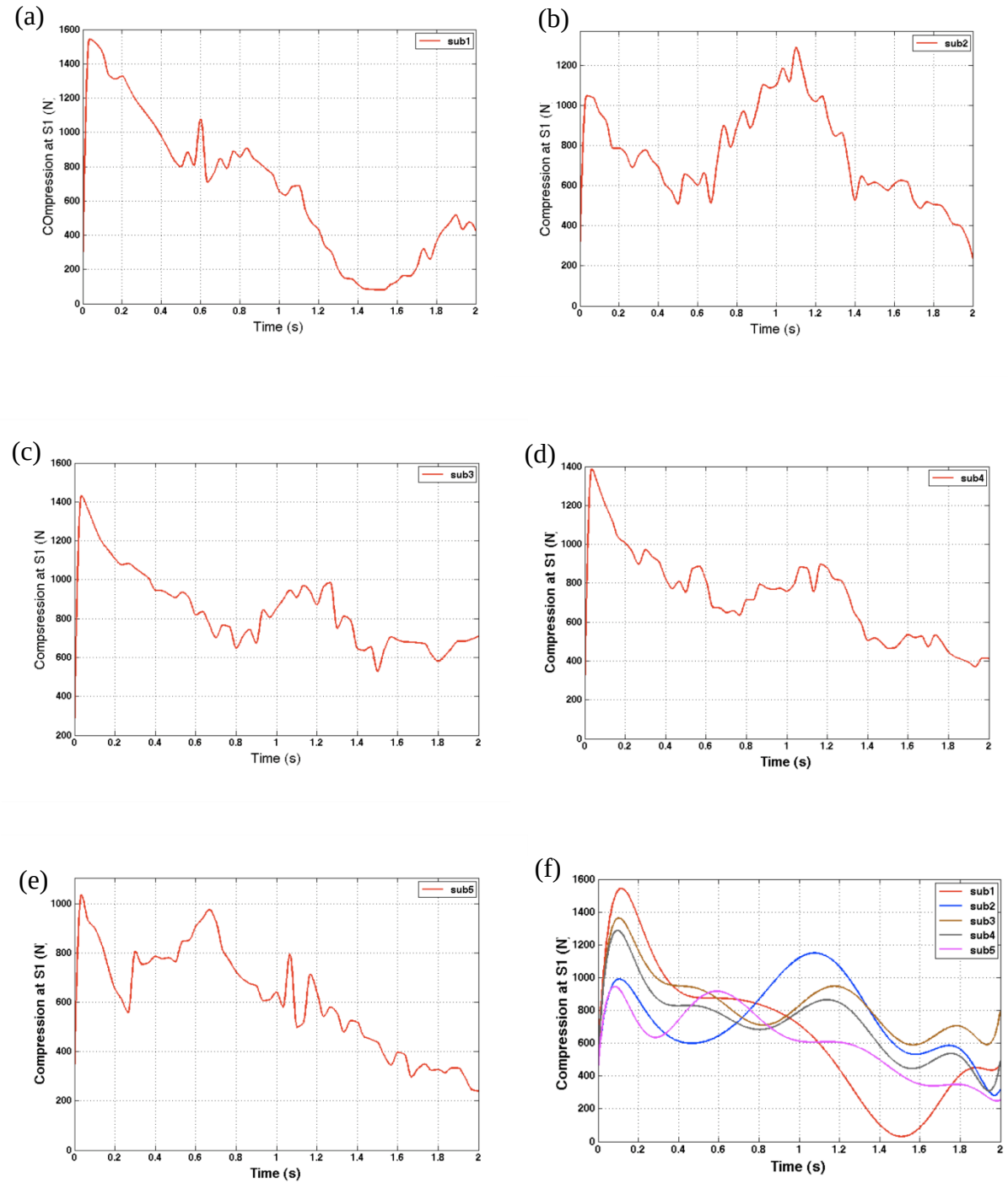

Figure 6.12: Compression load at Pelvis (S1) vs. time: compressive loads are highest at the onset of the flexion except in subject 2

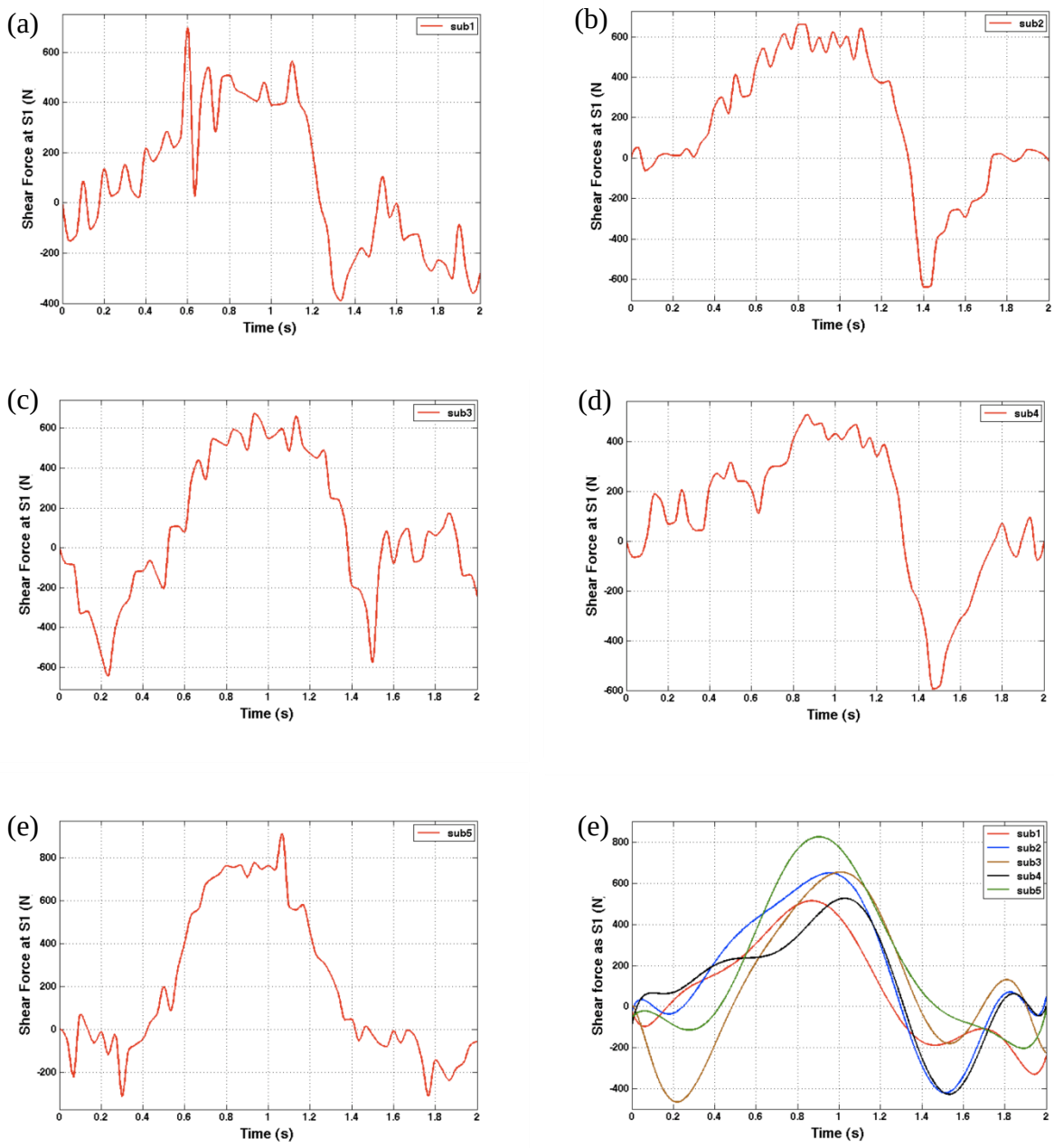

Figure 6.13: Shear load at Pelvis (S1) vs. time: shear loads are highest at maximum flexion angle

Discussion

The human torso is a dynamic system and the lower back enables dynamic movements of the torso. Low back injuries are the most prevalent health issue in the United States and often occur during dynamic tasks such as lifting external loads. Such tasks involve large angular displacements of the torso, including flexion and extension movements. However, most of the dynamic models of the torso in the past have investigated the dynamics of small-angle perturbations. This was the motivation for the present investigation of the dynamics of large flexion-extension movements of the torso.

In the present study, a kinematics driven, sagittal plane, lumped parameter model of flexion-extension movement was developed. The inputs for the model are the rotational kinematics from a single flexion-extension movement. The 2-dimensional model with 18 degrees of freedom in the sagittal plane accounted for the rigid body dynamics of the vertebrae, the viscoelastic behavior of the intervertebral discs, and the muscle dynamics to estimate the torso muscle forces.

The data of five out of ten subjects who participated in flexion-extension exercises (Granata and Gottipati, 2008) were used in this study. The five subjects were selected such that their thoracic kinematics are similar. The range of flexion depends on the subject's height and sex, and hence changes from subject to subject (Gatton and Pearcy, 1999). Gatton and Pearcy (1999) also showed that an individual could adopt at least four different movement sequences or patterns to perform flexion movement. Subjects in the current study exhibited different lumbar movement patterns. The subjects were asked to perform one flexion-extension movement in 2 seconds with the aid of a metronome. However, subject-to-subject kinematic variability was observed in both trunk and lumbar kinematics. The variability in lumbar kinematics is even more prominent than that in trunk kinematics. The activation levels varied from subject to subject, even though they have similar patterns. For example, the RA muscle was activated at the initial and final stages of movement in all the subjects. All the subjects exhibited RA activation at lumbar angles ranging from 20^{o} to 40^{o} except in one case: in the first half of the movement, subject 5 had activation only at the onset of flexion. A similar trend was observed in other muscle groups, i.e., the muscle

activation profiles are similar in all the subjects, with different peak values of activations. The velocity and acceleration of the movements are known to affect the muscle forces both quantitatively and qualitatively (Bazrgari et al., 2008; Zeinali-Davarani et al., 2008), which might have resulted in slight subject-to-subject variations in activation profiles.

Muscle activations

A high degree of abdominal activity was observed at the initial stage of flexion and the final stage of extension. RA, EO2, and IO1 had minimum or no activation levels at lumbar angles above 40^{o}. These results agree with those of Zenaili-Deverani et al. (2008). EO1 and IO2 were activated at the lumbar angles above 35^{o}. Contraction of abdominal muscles at peak flexion protects the spine against hyperflexion (Paquet et al., 1994). The reduction in activation of global extensor muscles can be accompanied by an increase in activation of abdominal muscles to accomplish large-angle lumbar flexion (Bazrgari et al., 2008; Olson et al., 2004). However, in this study, the increase in activation was seen only in EO1 and IO2 muscles.

The ES muscles had higher activation levels in the first and second halves of flexion and extension, respectively. The ES showed minimum activation at large flexion angles. The activation of erector spinae is known to decrease as the trunk approaches maximum flexion angles and completely ceases at full flexion (Floyd and Silver, 1955; Holleran et al., 1995; Schultz et al., 1985). This phenomenon is called flexion-relaxation. Schultz et al. (1985) showed that flexion-relaxation starts at flexion angles as low as 40^{o}. The trunk velocities in the current study lie between the intermediate and the fast movement velocities reported by Bazrgari et al. (2008), where flexion-relaxation was observed for intermediate velocities.

The multifidus muscles were activated throughout the flexion-extension movement, with increasing activation levels with lumbar angle. The multifidus muscles are identified as the powerful spine stabilizers (Arokoski et al., 2004; Ward et al., 2009). Ward et al. (2009) also showed that the architecture of these muscles produces large forces to stabilize the spine, and they

become intrinsically stronger with increase in lumbar flexion angle. The spine is known to be more stable at large flexion angles, and this stability is accomplished with the help of the passive stiffness of spinal segments (Arjmand and Shirazi-Adl, 2006). The higher activation levels of multifidus muscles suggest that they may contribute to spinal stability at large flexion angles. However, further investigation with stability analyses is necessary to understand the effect of multifidus activity on spinal stability.

The quadratus lumborum (QL) muscles were activated throughout the flexion-extension movement. Evidence suggests that QL plays an important role during lumbar flexion (Andersson et al., 1996). Andersson et al. (1996) reported a reduction in the activity of superficial erector spinae muscles and increased involvement of QL muscles with an increase in lumbar flexion. McGill (1998) also suggested that QL activation depends on lumbar sagittal movement and plays a role in spinal stability in the sagittal plane.

Contrary to Zeinali-Davarani et al. (2008), the current study found that the psoas muscles were activated throughout the flexion-extension movement. The activation levels of the muscles increased with lumbar flexion angle. The psoas muscles' lines of action do not depend on hip flexion, but depend on spine orientation (McGill, 1998). In the current study, the pelvis was fixed and the spine was sagittally flexed, which caused large relative motion between the lumbar vertebrae and the pelvis. This relative motion might have caused the higher activation levels in the psoas muscles. Sit-up exercises also cause a similar relative motion between the spine and pelvis; sit-up exercises with/without bent knees produce higher activation levels in the psoas muscles (Juker et al., 1998).

Spinal loads

Large dynamic compression and shear spinal loads are identified as risk factors for low back pain (Adams et al., 1996; Granata and Marras, 1995a,b; Shirazi-Adl, 1991). Axial compressive loads on the spine, determined from a fundamental static biomechanical model, were found to be

considerably lower than the dynamic compression loads (Granata and Marras, 1999). The model developed in this study is used to estimate the time-dependent spinal loads. Compared to the results published in the literature, the spinal loads computed in this study are lower in value (Granata and Marras, 1995a,b; Granata and Wilson, 2001). The model presented in this study did not consider the spinal stability analysis and is restricted to the sagittal plane. This might have resulted in lower values of spinal loads compared to the ones published in the literature. However, the qualitative information of these spinal loads can be useful to understand the spine mechanics. The maximum shear loads occurred at higher flexion angles and the maximum compression loads occurred at the onset of flexion. The onset of flexion from static standing posture can usually be jerky and may cause higher compression loads. At high flexion angles, the spine injury risk may be due to shear loads, and at the onset of flexion or during jerky movements the risk could be due to compression loads.

Shortcomings of the model

The motion monitoring system used to record the kinematics data was not capable of recording all the kinematics of the rigid bodies. The lumbar vertebral rotations and translational kinematics of all the bodies were estimated computationally. Mathematical optimization techniques were used in this model to predict the muscle forces. It was concluded that mathematical optimization gives mechanically valid results and less accurate physiological results compared to EMG-assisted optimization approaches (Gagnon et al., 2001). The EMG-assisted optimization techniques may produce more accurate results with the current model. The optimization routines used in this study are computationally very expensive. Each flexion-extension cycle had 60 time steps, and each time step took an average of 5 hours of computational time. Hence, even though the model developed here was a nonlinear dynamic model, a linear muscle model was used.

Conclusions

A rigid body, lumped parameter model was developed successfully to estimate the torso muscle forces. The predicted activity of abdominal muscles and erector spinae seem to agree well with

results in the published literature. The multifidus muscles, quadratus lumborum, and psoas muscles were found to play an important role in the dynamics of trunk flexion-extension movements. The model predicted that the spine is more vulnerable to compressive loads at the onset of flexion and to shear loads at large flexion angles. Further studies are required to see if the quantitative measures of spinal loads can predict the onset of low back injuries. In spite of having many limitations, this model can be considered as a progressive step in the research on dynamic assessment of the spine.

References

ADAMS, M. A., MCMILLAN, D. W., GREEN, T. P. & DOLAN, P. (1996) Sustained loading generates stress concentrations in lumbar intervertebral discs. *Spine* , 21**,** 434-8.

ANDERSON, F. C. & PANDY, M. G. (1999) A dynamic optimization solution for vertical jumping in three dimensions. *Comput Methods Biomech Biomed Engin,* 2**,** 201-231.

ANDERSSON, E. A., ODDSSON, L. I. E., GRUNDSTROM, H., NILSSON, J. & THORSTENSSON, A. (1996) EMG activities of the quadratus lumborum and erector spinae muscles during flexion - Relaxation and other motor tasks. *Clinical Biomechanics,* 11**,** 392-400.

ARJMAND, N. & SHIRAZI-ADL, A. (2006) Model and in vivo studies on human trunk load partitioning and stability in isometric forward flexions. *J Biomech,* 39**,** 510-21.

AROKOSKI, J. P., VALTA, T., KANKAANPAA, M. & AIRAKSINEN, O. (2004) Activation of lumbar paraspinal and abdominal muscles during therapeutic exercises in chronic low back pain patients. *Arch Phys Med Rehabil,* 85**,** 823-32.

BAZRGARI, B. & SHIRAZI-ADL, A. (2007) Spinal stability and role of passive stiffness in dynamic squat and stoop lifts. *Comput Methods Biomech Biomed Engin,* 10**,** 351-60.

BAZRGARI, B., SHIRAZI-ADL, A., TROTTIER, M. & MATHIEU, P. (2008) Computation of trunk equilibrium and stability in free flexion-extension movements at different velocities. *J Biomech,* 41**,** 412-21.

BERGMARK, A. (1989) Stability of the lumbar spine. A study in mechanical engineering. *Acta Orthop Scand Suppl,* 60**,** 1-54.

BOGDUK, N., MACINTOSH, J. E. & PEARCY, M. J. (1992) A universal model of the lumbar back muscles in the upright position. *Spine* , 17**,** 897-913.

CHOLEWICKI, J. & MCGILL, S. M. (1992) Lumbar posterior ligament involvement during extremely heavy lifts estimated from fluoroscopic measurements. *J Biomech,* 25**,** 17-28.

CHOLEWICKI, J. & MCGILL, S. M. (1996) Mechanical stability of the in vivo lumbar spine: implications for injury and chronic low back pain. *Clin Biomech,* 11**,** 1-15.

COSTI, J. J., STOKES, I. A., GARDNER-MORSE, M. G. & IATRIDIS, J. C. (2008) Frequency-dependent behavior of the intervertebral disc in response to each of six degree of freedom dynamic loading - solid phase and fluid phase contributions. *Spine,* 33**,** 1731-8.

DAVIS, K. G. & MARRAS, W. S. (2000) The effects of motion on trunk biomechanics. *Clin Biomech ,* 15**,** 703-17.

DE LEVA, P. (1996) Adjustments to Zatsiorsky-Seluyanov's segment inertia parameters. *J Biomech,* 29**,** 1223-30.

FLOYD, W. F. & SILVER, P. H. (1955) The function of the erectores spinae muscles in certain movements and postures in man. *J Physiol,* 129**,** 184-203.

FRANKLIN, T. C. & GRANATA, K. P. (2007) Role of reflex gain and reflex delay in spinal stability--a dynamic simulation. *J Biomech,* 40**,** 1762-7.

GAGNON, D., LARIVIERE, C. & LOISEL, P. (2001) Comparative ability of EMG, optimization, and hybrid modeling approaches to predict trunk muscle forces and lumbar spine loading during dynamic sagittal plane lifting. *Clin Biomech ,* 16**,** 359-72.

GARDNER-MORSE, M., STOKES, I. A. & LAIBLE, J. P. (1995) Role of muscles in lumbar spine stability in maximum extension efforts. *J Orthop Res,* 13**,** 802-8.

GARDNER-MORSE, M. G. & STOKES, I. A. F. (2004) Structural behavior of human lumbar spinal motion segments. *J Biomech,* 37**,** 205-12.

GARG, A. & KAPELLUSCH, J. M. (2009) Applications of biomechanics for prevention of work-related musculoskeletal disorders. *Ergonom,* 52**,** 36-59.

GATTON, M. L. & PEARCY, M. J. (1999) Kinematics and movement sequencing during flexion of the lumbar spine. *Clin Biomech ,* 14**,** 376-83.

GRANATA, K. P. & GOTTIPATI, P. (2008) Fatigue influences the dynamic stability of the torso. *Ergonom,* 51**,** 1258-71.

GRANATA, K. P. & MARRAS, W. S. (1993) An EMG-assisted model of loads on the lumbar spine during asymmetric trunk extensions. *J Biomech,* 26**,** 1429-38.

GRANATA, K. P. & MARRAS, W. S. (1995a) An EMG-assisted model of trunk loading during free-dynamic lifting. *J Biomech,* 28**,** 1309-17.

GRANATA, K. P. & MARRAS, W. S. (1995b) The influence of trunk muscle coactivity on dynamic spinal loads. *Spine ,* 20**,** 913-9.

GRANATA, K. P. & MARRAS, W. S. (1999) Relation between spinal load factors and the high-risk probability of occupational low-back disorder. *Ergonom,* 42**,** 1187-99.

GRANATA, K. P. & WILSON, S. E. (2001) Trunk posture and spinal stability. *Clin Biomech ,* 16**,** 650-9.

HANSEN, L., DE ZEE, M., RASMUSSEN, J., ANDERSEN, T. B., WONG, C. & SIMONSEN, E. B. (2006) Anatomy and biomechanics of the back muscles in the lumbar spine with reference to biomechanical modeling. *Spine ,* 31**,** 1888-99.

HILL, A. V. (1938) The heat of shortening and dynamic constants of muscle. *Proc. R. Soc. B.,* 126**,** 136-195.

HOLLERAN, K., POPE, M., HAUGH, L. & ABSHER, R. (1995) The response of the flexion-relaxation phenomenon in the low back to loading. *Iowa Orthop J,* 15**,** 24-8.

IZAMBERT, O., MITTON, D., THOUROT, M. & LAVASTE, F. (2003) Dynamic stiffness and damping of human intervertebral disc using axial oscillatory displacement under a free mass system. *Eur Spine J,* 12**,** 562-6.

JUKER, D., MCGILL, S., KROPF, P. & STEFFEN, T. (1998) Quantitative intramuscular myoelectric activity of lumbar portions of psoas and the abdominal wall during a wide variety of tasks. *Med Sci Sports Exer,* 30**,** 301-10.

MARRAS, W. S. & GRANATA, K. P. (1995) A biomechanical assessment and model of axial twisting in the thoracolumbar spine. *Spine ,* 20**,** 1440-51.

MARRAS, W. S., RANGARAJULU, S. L. & WONGSAM, P. E. (1987) TRUNK FORCE DEVELOPMENT DURING STATIC AND DYNAMIC LIFTS. *Human Factors,* 29**,** 19-29.

MARRAS, W. S. & SOMMERICH, C. M. (1991a) A three-dimensional motion model of loads on the lumbar spine: I. Model structure. *Hum Factors,* 33**,** 123-37.

MARRAS, W. S. & SOMMERICH, C. M. (1991b) A three-dimensional motion model of loads on the lumbar spine: II. Model validation. *Hum Factors,* 33**,** 139-49.

MCGILL, S. M. (1992) A myoelectrically based dynamic three-dimensional model to predict loads on lumbar spine tissues during lateral bending. *J Biomech,* 25**,** 395-414.

MCGILL, S. M. (1998) Low back exercises: evidence for improving exercise regimens. *Phys Ther,* 78**,** 754-65.

MCGILL, S. M. & NORMAN, R. W. (1986) Partitioning of the L4-L5 dynamic moment into disc, ligamentous, and muscular components during lifting. *Spine,* 11**,** 666-78.

OLSON, M. W., LI, L. & SOLOMONOW, M. (2004) Flexion-relaxation response to cyclic lumbar flexion. *Clin Biomech ,* 19**,** 769-76.

PAQUET, N., MALOUIN, F. & RICHARDS, C. L. (1994) Hip-spine movement interaction and muscle activation patterns during sagittal trunk movements in low back pain patients. *Spine,* 19**,** 596-603.

SCHULTZ, A. B., HADERSPECK-GRIB, K., SINKORA, G. & WARWICK, D. N. (1985) Quantitative studies of the flexion-relaxation phenomenon in the back muscles. *J Orthop Res,* 3**,** 189-97.

SHIN, D. S., LEE, K. & KIM, D. (2007) Biomechanical study of lumbar spine with dynamic stabilization device using finite element method. *Computer-Aided Design,* 39**,** 559-567.

SHIRAZI-ADL, A. (1991) Finite-element evaluation of contact loads on facets of an L2-L3 lumbar segment in complex loads. *Spine ,* 16**,** 533-41.

STOKES, I. A., GARDNER-MORSE, M., CHURCHILL, D. & LAIBLE, J. P. (2002) Measurement of a spinal motion segment stiffness matrix. *J Biomech,* 35**,** 517-21.

SUN, L. W., LEE, R. Y. W., LU, W. & LUK, K. D. K. (2004) Modeling and simulation of the intervertebral movements of the lumbar spine using an inverse kinematic algorithm. *Med Biol Eng Comput,* 42**,** 740-6.

VRESILOVIC, E. J., JOHANNESSEN, W. & ELLIOTT, D. M. (2006) Disc mechanics with trans-endplate partial nucleotomy are not fully restored following cyclic compressive loading and unloaded recovery. *J Biomech Eng,* 128**,** 823-9.

WARD, S. R., KIM, C. W., ENG, C. M., GOTTSCHALK, L. J. T., TOMIYA, A., GARFIN, S. R. & LIEBER, R. L. (2009) Architectural analysis and intraoperative measurements demonstrate the unique design of the multifidus muscle for lumbar spine stability. *J Bone Joint Surg Am,* 91**,** 176-85.

WINTER, D. A. (2005) *Biomechanics and motor control of human movement,* Hoboken, NJ, John Wiley & Sons, Inc.

ZEINALI-DAVARANI, S., HEMAMI, H., BARIN, K., SHIRAZI-ADL, A. & PARNIANPOUR, M. (2008) Dynamic stability of spine using stability-based optimization and muscle spindle reflex. *IEEE Trans Neural Syst Rehabil Eng,* 16**,** 106-18.

ZHOU, S. H., MCCARTHY, I. D., MCGREGOR, A. H., COOMBS, R. R. & HUGHES, S. P. (2000) Geometrical dimensions of the lower lumbar vertebrae--analysis of data from digitised CT images. *Eur Spine J,* 9**,** 242-8.

Chapter 7 – Conclusions and Future Work

Conclusions

The main goal behind the research presented in this dissertation was to investigate the dynamic behavior of the human trunk. In particular, the dynamic stability and time-dependent muscle forces of trunk flexion-extension movements were investigated. The work includes an experimental study and a mathematical simulation study.

The experimental study investigated the fatigue-stability relations of dynamic trunk movements. The participants performed symmetric and asymmetric repetitive flexion-extension movement trials before and after trunk muscle fatigue. Another condition that was implemented was the constraint on the pelvis. Trials were performed with and without restraining the pelvic movements. Muscle fatigue significantly decreased the dynamic stability of torso movement. The asymmetric movements were found to be more stable than the symmetric movements when the pelvic movement was restrained. This is the first known study to empirically investigate the effect of muscle fatigue on dynamic movements of the torso (Granata and Gottipati, 2008).

The simulation study investigated the time-dependent muscle forces of dynamic trunk movements. A rigid body, lumped parameter model of flexion-extension movement of the trunk in the sagittal plane was developed. The 5 lumbar vertebrae and the thorax were modeled as rigid bodies stacked on a stationary pelvis. The intervertebral discs were modeled as translational and rotational springs. A total of 45 pairs of trunk muscles were used. Kinematics driven optimization was applied to estimate the dynamic muscle forces of the torso during one flexion-extension movement. This is one of the first lumped parameter models that investigated muscle forces during large angular displacements of the torso. The time-dependent muscle activation patterns that were estimated from this study were in good agreement with those in the published literature. The study showed that psoas muscles play an important role during trunk flexion-extension movements when pelvic movements are restrained.

Future Work

Experimental work

The nonlinear dynamic methods used in this study to quantify the dynamic stability can be used in various experiments. These methods can be used to study the changes in dynamic stability of the torso while lifting a range of external loads. Occupational lifting tasks are considered as a risk factor for low back pain (Norman et al., 1998). Moreover, the movement velocity is known to affect the dynamic stability of the torso (Granata and England, 2006). The effect of movement velocity on dynamic stability while lifting external loads can also be investigated. The methods can be expanded to accommodate for testing patients with chronic low-back pain. This may give insight into how low back disorders affect the stability of the spine.

Computational work

Computational modeling of biomechanical systems opens doors to investigate various mechanisms that cannot be studied experimentally. The model presented in Chapters 5 and 6 can be used to study muscle forces during dynamic lifting exercises. External loads can be included in the model as generalized forces. The muscle reflexes and reflex delays affect the dynamic stability of the torso (Brown and McGill, 2009; Franklin and Granata, 2007). The dynamic muscle reflex mechanism can be studied by using a muscle reflex model similar to the one published in the literature (Franklin and Granata, 2007). However, the reflex model can be computationally very expensive, and efficient computing resources would be required.

More general results can be achieved by expanding the model to 3 dimensions. This expansion to 3 dimensions will help study the lateral rotation and twisting of the trunk. Faster computational resources should be used to study how stability affects the muscle recruitment patterns. Further, EMG-assisted optimization can be used to get more physiologically accurate results (Gagnon et al., 2001). Muscle fatigue conditions can be included in the model (Granata et al., 2004). This will help to study the effect of muscle fatigue on muscle recruitment patterns.

The EMG-assisted optimization will give better results in this case compared to the mathematical optimization.

References

BROWN, S. H. M. & MCGILL, S. M. (2009) The intrinsic stiffness of the in vivo lumbar spine in response to quick releases: implications for reflexive requirements. *J Electromyogr Kinesiol,* 19**,** 727-36.

FRANKLIN, T. C. & GRANATA, K. P. (2007) Role of reflex gain and reflex delay in spinal stability--a dynamic simulation. *J Biomech,* 40**,** 1762-7.

GAGNON, D., LARIVIERE, C. & LOISEL, P. (2001) Comparative ability of EMG, optimization, and hybrid modeling approaches to predict trunk muscle forces and lumbar spine loading during dynamic sagittal plane lifting. *Clin Biomech* , 16**,** 359-72.

GRANATA, K. P. & GOTTIPATI, P. (2008) Fatigue influences the dynamic stability of the torso. *Ergonom,* 51**,** 1258-71.

GRANATA, K. P. & ENGLAND, S. A. (2006) Stability of dynamic trunk movement. *Spine,* 31**,** E271-6.

GRANATA, K. P., SLOTA, G. P. & WILSON, S. E. (2004) Influence of fatigue in neuromuscular control of spinal stability. *Hum Factors,* 46**,** 81-91.

NORMAN, R., WELLS, R., NEUMANN, P., FRANK, J., SHANNON, H. & KERR, M. (1998) A comparison of peak vs cumulative physical work exposure risk factors for the reporting of low back pain in the automotive industry. *Clin Biomech* , 13**,** 561-573.

Appendix A

IRB Approval

Virginia Tech
VIRGINIA POLYTECHNIC INSTITUTE AND STATE UNIVERSITY

Institutional Review Board

Dr. David M. Moore
IRB (Human Subjects) Chair
Assistant Vice President for Research Compliance
1880 Pratt Drive, Suite 2006(0497), Blacksburg, VA 24061
Office: 540/231-4991; FAX: 540/231-0959
email: moored@vt.edu

DATE: December 16, 2005

MEMORANDUM

TO: Kevin P. Granata Engineering Science & Mechanics 0219

FROM: David Moore

SUBJECT: **IRB Expedited Continuation**: "Musculoskeletal Biomechanics of Movement and Control " IRB # 05-769 ref 04-635, 03-632

This memo is regarding the above referenced protocol which was previously granted expedited approval by the IRB on January 21, 2005. The proposed research is eligible for expedited review according to the specifications authorized by 45 CFR 46.110 and 21 CFR 56.110. Pursuant to your request of last week, as Chair of the Virginia Tech Institutional Review Board, I have granted approval for extension of the study for a period of 12 months, effective as of January 21, 2006.

Approval of your research by the IRB provides the appropriate review as required by federal and state laws regarding human subject research. It is your responsibility to report to the IRB any adverse reactions that can be attributed to this study.

To continue the project past the 12-month approval period, a continuing review application must be submitted (30) days prior to the anniversary of the original approval date and a summary of the project to date must be provided. Our office will send you a reminder of this (60) days prior to the anniversary date.

Virginia Tech has an approved Federal Wide Assurance (FWA00000572, exp. 7/20/07) on file with OHRP, and its IRB Registration Number is IRB00000667.

cc: File

Informed Consent

Informed Consent for Participation in Research Projects Involving Human Subjects

Title of Project: Musculoskeletal Biomechanics of Movement and Control

Investigators: K.P. Granata

Purpose of this Research

To understand musculoskeletal injury and improve clinical diagnoses of injury it is necessary to understand how muscles control force and movement. The purpose of this study is to measure the relation between human movement, force generation and muscle activity. We are also interested in observing how gender, fatigue and physical conditioning influence these parameters. Throughout the course of this project more than 450 subject volunteers will participate including healthy individuals from the age of 18 to 55.

Procedures

We will tape adhesive markers and sensors on your skin around your trunk, legs and arms. These sensors are EMG electrodes that measure the activity of your muscles and position sensors to measure how you move. After some preliminary warm up stretches, we may ask you to push and/or pull as hard as you can against a resistance. We may then ask you to hold or lift a weight or weighted-box and to bend forward and back. We may also ask you to do some fatiguing exertions such as holding or lifting a heavy weight or pushing/pulling against a bar or cable for several minutes. We may also apply a quick but small force to record reflexes. You may be requested to return for repeated testing. Between test sessions you may be asked to participate in specified physical conditioning as per the American College of Sports Medicine recommended guidelines.

Risks

The risks of this study are minor. They include a potential skin irritation to the adhesives used in the tape and electrode markers. You may also feel some temporary muscle soreness such as might occur after exercising. Subjects participating in physical conditioning may experience muscle soreness and/or musculoskeletal injury associated with inherent risks of cardiovascular, strength training and therapeutic exercise. To minimize these risks you will be asked to warm-up before the tasks and tell us if you are aware of any history of skin-reaction to tape, history of musculeoskeletal injury, cardiovascular limitations.

Benefits

By participating in this study, you will help to increase our understanding musculeoskeletal control of movement and musculoskeletal injury mechanisms. We hope to make this research experience interesting and enjoyable for you where you may learn experimental procedures in biomechanical sciences. We do not guarantee or promise that you will receive any of these benefits and no promise of benefits has been made to encourage your participation.

Anonymity and Confidentiality

Experimental data collected from your participation will be coded and matched to this consent form so only members of the research team can determine your identity. Your identity will not be divulged to unauthorized people or agencies. Digital video recorded during the experimental trials will be used to track the movement of the sensors by means of computer analyses and is insufficient video quality to observe individual participant identifying characteristics. Secondary VHS-style video may be recorded to validate the digital motion data. This camera angle is placed to avoid facial or other identifying characteristics. Sometimes it is necessary for an investigator to break confidentiality if a significant health or safety concern is perceived or the participant is believed to be a threat to himself/herself or others.

Compensation

Participants required to return for multiple test sessions or participate in physical conditioning for this protocol will receive payment per the number of test sessions as well as a bonus for full completion of the multi-session research protocol. Subjects participating in experiments as part of course or laboratory procedures will receive appropriate credit for analysis of specified data as described in the course syllabus but not for personal performance during the experimental session. If course credit is involved and the subject chooses not to participate alternative means for earning equivalent credit will be established with the course instructor.

Informed Consent for Participation in Research Projects Involving Human Subjects

Freedom to Withdraw

You are free to withdraw from a study at any time without penalty. If you choose to withdraw, you will be compensated for the portion of the time of the study (if financial compensation is involved). If you choose to withdraw, you will not be penalized by reduction in points or grade in a course (if course credit is involved). You are free not to answer any questions or respond to experimental situations that they choose without penalty.

There may be circumstances under which the investigator may determine that you should not continue as a subject. You will be compensated for the portion of the project completed

Approval of Research

This research project has been approved, as required, by the Institutional Review Board for Research Involving Human Subjects at Virginia Polytechnic Institute and State University, by the Department of Engineering science and Mechanics.

21 January 2006
IRB Approval Date

20 January 2007
Approval Expiration Date

Subject's Responsibilities

I voluntarily agree to participate in this study. I have the following responsibilities:

- Inform the investigators of all medical conditions that may influence performance or risk
- Comply to the best of my ability with the experimental and safety instructions
- Inform the investigator of any physical and mental discomfort resulting from the experimental protocol

Subject's Permission

I have read and understand the Informed Consent and conditions of this project. I have had all my questions answered. I hereby acknowledge the above and give my voluntary consent:

Subject Name (Print):_____

Subject signature:_____ Date_____

_____ Date_____
Witness (Optional except for certain classes of subjects)

Should I have any pertinent questions about this research or its conduct, and research subjects' rights, and whom to contact in the event of a research-related injury to the subject, I may contact:

Investigator(s): _____E-mail: _____ Phone 231-2022
Faculty Advisor: K.P. Granata E-mail: Granata@vt.edu Phone 231-7039

Ishwar Puri 231-3243
Departmental Reviewer/Department Head Telephone/e-mail

David M. Moore
Chair, IRB
Office of Research Compliance
Research & Graduate Studies
540-231-4991 / moored@vt.edu

This Informed Consent is valid from 21January 2006 to 20 January 2007.

Subjects must be given a complete copy (or duplicate original) of the signed Informed Consent

Data Collection Sheet

Subject # _____ Date:_____ Time: _____

Age:_____ Gender: _____

Height:_____ Weight:_____ Nationality: _____

Arm length :	Leg length :	Trunk length :
Target location	Z :	Y :

Checklist

□ Signed consent form

□ Birds secured

□ EMG cables secured

1. BEFORE FATIGUE

□ without pelvic support - **right hand**

Trial 1: Trial 2:

□ without pelvic support - **both hands**

Trial 1: Trial 2:

□ with pelvic support - **right hand**

Trial 1: Trial 2:

□ with pelvic support - **both hands**

Trial 1: Trial 2:

FATIGUE PROTOCOL

Total time: ————

% of MVE achieved: ————

Time taken to start the trial: ————

2. AFTER FATIGUE

□ with pelvic support – **right hand**

Trial 1: Trial 2:

□ with pelvic support –**both hands**

Trial 1: Trial 2:

%MVE after w/o pelvic support trials: ————

%MVE achieved after 2nd fatigue test: ————

Total time of 2nd fatigue test: ————

Time taken to start trial: ————

□ without pelvic support – **both hands**

Trial 1: Trial 2:

□ without pelvic support - **right hand**

Trial 1: Trial 2:

% MVE at the end of the experiment: ————

Appendix B

Codes

Matlab code for experimental study

```
clear all
close all

tic
stringfilename1 = ['Z:\testsnewsub\NF1\NF1tr1','.exp'];
data1 = dlmread(stringfilename1,'\t',9,0); % read the data file
t = length(data1);

marker1 = data1(:,2:10); % data from sensor on T10 vertebra
marker2 = data1(:,11:19); % data from sensor on S1 vertebra

k = 1:t;
for i = 1:2
    if i ==1
       data = marker1;
   elseif i == 2
      data = marker2;
   end

   for j = 1:t
      RM = [data(j,1:3); data(j,4:6);data(j,7:9)]; % rotation matrix
      if j ==1
         R = transpose(RM);
```

```
        end
        RMnew = R*RM;
        Z(i,j) = atan(RMnew(2,1)/RMnew(1,1))*180/pi; % computing the Euler angles
        Y(i,j) = asin(-RMnew(3,1))*180/pi;
        X(i,j) = atan(RMnew(3,2)/RMnew(3,3))*180/pi;
    end
end

% save the Euler angles
nametosave=['tr1'];

newfilenameZ=['Z:\testsnewsub\NF1\' nametosave 'Z.txt'];
newfilenameY=['Z:\testsnewsub\NF1\' nametosave 'Y.txt'];
newfilenameX=['Z:\testsnewsub\NF1\' nametosave 'X.txt'];

save(newfilenameZ,'Z','-ascii','-tabs','-double')
save(newfilenameY,'Y','-ascii','-tabs','-double')
save(newfilenameX,'X','-ascii','-tabs','-double')

newfilenameM1EA=[nametosave 'Z.txt'];
newfilenameM2EA=[nametosave 'Y.txt'];
newfilenameLA=[nametosave 'X.txt'];

%%
t = 60000;
Z1 = Z(1,:);
Z2 = Z(2,:);

Y1 = Y(1,:);
Y2 =Y(2,:);
```

```
X1 = X(1,:);
X2 =X(2,:);

        rawdata(:,2)=Z1;
          rawdata(:,3)=Y1;
          rawdata(:,4)=X1;

          rawdata(:,5)=Z2;
          rawdata(:,6)=Y2;
          rawdata(:,7)=X2;

          %%%FILTER HERE
          fs = 100; % Sampling Frequency in hertz
          fn = fs/2; % Nyquist Frequency
          fc = 10; % Cut-off frequency for 2nd order butterworth filter
          [b,a] = butter(2, fc/fn);
          fdata = filtfilt(b,a,rawdata);

          Z1=fdata(:,2);
Y1=fdata(:,3);
X1=fdata(:,4);
Z2=fdata(:,5);
Y2=fdata(:,6);
X2=fdata(:,7);
%%
% Select the peaks and spline in between them to get 20 cycles for each trial
                    plot(k,Z1)
                    pause
                    [X,Y]=ginput(2);
                    [uselesspeak,I]=min(Z1(round(X(1)):round(X(2))));
                    hold on
```

```
 plot(I+round(X(1))-1,uselesspeak,'rX')
 timeofpeaks=[I+round(X(1))-1];
 uselesspeaks=uselesspeak;
  [X,Y]=ginput(2);
 [uselesspeak,I]=min(Z1(round(X(1)):round(X(2))));
 hold on
 plot(I+round(X(1))-1,uselesspeak,'rX')
 timeofpeaks1=[I+round(X(1))-1];
 uselesspeaks1=uselesspeak;
 hold off
plot((timeofpeaks:timeofpeaks1),Z1(timeofpeaks:timeofpeaks1))
Z1 = Z1(timeofpeaks:timeofpeaks1);
z1length = length(Z1);
l=z1length;
L = 40000/l;

figure(5)
  x=L:L:40000; y= Z1;
 xx =1:40000;
 yy = spline(x,y,xx);
 subplot(3,1,1)
 plot(xx,yy)
 title('Marker 1 EA1')
 xlabel('Time')
 ylabel('Displacement')
 Z1 = yy';

 figure(1)
plot(k,Y1)
pause
[X,Y]=ginput(2);
```

```
[uselesspeak,I]=min(Y1(round(X(1)):round(X(2))));
hold on
plot(I+round(X(1))-1,uselesspeak,'rX')
timeofpeaks=[I+round(X(1))-1];
uselesspeaks=uselesspeak;
 [X,Y]=ginput(2);
[uselesspeak,I]=min(Y1(round(X(1)):round(X(2))));
hold on
plot(I+round(X(1))-1,uselesspeak,'rX')
timeofpeaks1=[I+round(X(1))-1];
uselesspeaks1=uselesspeak;
plot((timeofpeaks:timeofpeaks1),Y1(timeofpeaks:timeofpeaks1))
Y1 = Y1(timeofpeaks:timeofpeaks1);
y1length = length(Y1);
l= y1length;
L=40000/l;

x=L:L:40000; y= Y1;
xx =1:40000;
yy = spline(x,y,xx);
subplot(3,1,2)
plot(xx,yy)
title('Marker 1 EA2')
xlabel('Time')
ylabel('Displacement')
Y1 = yy';

figure(1)
plot(k,X1)
pause
   [X,Y]=ginput(2);
```

```
[uselesspeak,I]=max(X1(round(X(1)):round(X(2))));
hold on
plot(I+round(X(1))-1,uselesspeak,'rX')
timeofpeaks=[I+round(X(1))-1];
uselesspeaks=uselesspeak;
 [X,Y]=ginput(2);
[uselesspeak,I]=max(X1(round(X(1)):round(X(2))));
hold on
plot(I+round(X(1))-1,uselesspeak,'rX')
timeofpeaks1=[I+round(X(1))-1];
uselesspeaks1=uselesspeak;
plot((timeofpeaks:timeofpeaks1),X1(timeofpeaks:timeofpeaks1))
X1 = X1(timeofpeaks:timeofpeaks1);
x1length = length(X1);
l = x1length;
L = 40000/l;

 x=L:L:40000; y= X1;
 xx =1:40000;
 yy = spline(x,y,xx);
 subplot(3,1,3)
 plot(xx,yy)
 title('Marker 1 EA3')
 xlabel('Time')
 ylabel('Displacement')
 X1 = yy';

 figure(1)
 plot(k,Z2)
 pause
 [X,Y]=ginput(2);
```

```
 [uselesspeak,I]=min(Z2(round(X(1)):round(X(2))));
 hold on
 plot(I+round(X(1))-1,uselesspeak,'rX')
 timeofpeaks=[I+round(X(1))-1];
 uselesspeaks=uselesspeak;
  [X,Y]=ginput(2);
 [uselesspeak,I]=min(Z2(round(X(1)):round(X(2))));
 hold on
 plot(I+round(X(1))-1,uselesspeak,'rX')
 timeofpeaks1=[I+round(X(1))-1];
 uselesspeaks1=uselesspeak;
 hold off
plot((timeofpeaks:timeofpeaks1),Z2(timeofpeaks:timeofpeaks1))
Z2= Z2(timeofpeaks:timeofpeaks1);
z2length = length(Z2);
l=z2length;
L =40000/l;

figure(5)
 x=L:L:40000; y= Z2;
 xx =1:40000;
 yy = spline(x,y,xx);
 subplot(3,1,1)
 plot(xx,yy)
 title('Marker 2 EA1')
 xlabel('Time')
 ylabel('Displacement')
 Z2 = yy';

figure(1)
 plot(k,Y2)
```

```
pause
[X,Y]=ginput(2);
 [uselesspeak,I]=min(Y2(round(X(1)):round(X(2))));
 hold on
 plot(I+round(X(1))-1,uselesspeak,'rX')
 timeofpeaks=[I+round(X(1))-1];
 uselesspeaks=uselesspeak;
  [X,Y]=ginput(2);
 [uselesspeak,I]=min(Y2(round(X(1)):round(X(2))));
 hold on
 plot(I+round(X(1))-1,uselesspeak,'rX')
 timeofpeaks1=[I+round(X(1))-1];
 uselesspeaks1=uselesspeak;
 hold off
plot((timeofpeaks:timeofpeaks1),Y2(timeofpeaks:timeofpeaks1))
Y2 = Y2(timeofpeaks:timeofpeaks1);
y2length = length(Y2);
l = y2length;
L = 40000/l;

 x=L:L:40000; y= Y2;
 xx =1:40000;
 yy = spline(x,y,xx);
 subplot(3,1,2)
 plot(xx,yy)
 title('Marker 2 EA2')
 xlabel('Time')
 ylabel('Displacement')
Y2 = yy';

figure(1)
```

```
plot(k,X2)
pause
   [X,Y]=ginput(2);
[uselesspeak,I]=max(X2(round(X(1)):round(X(2))));
hold on
plot(I+round(X(1))-1,uselesspeak,'rX')
timeofpeaks=[I+round(X(1))-1];
uselesspeaks=uselesspeak;
 [X,Y]=ginput(2);
[uselesspeak,I]=max(X2(round(X(1)):round(X(2))));
hold on
plot(I+round(X(1))-1,uselesspeak,'rX')
timeofpeaks1=[I+round(X(1))-1];
uselesspeaks1=uselesspeak;
hold off
plot((timeofpeaks:timeofpeaks1),X2(timeofpeaks:timeofpeaks1))
X2 = X2(timeofpeaks:timeofpeaks1);
x2length = length(X2);
l = x2length;
L = 40000/l;

x=L:L:40000; y= X2;
xx =1:40000;
yy = spline(x,y,xx);
subplot(3,1,3)
plot(xx,yy)
title('Marker 2 EA3')
xlabel('Time')
ylabel('Displacement')
X2 = yy';
```

```
M1EA = sqrt(Z1.^2+Y1.^2+X1.^2);
M2EA = sqrt(Z2.^2+Y2.^2+X2.^2);

LA = sqrt((Z1-Z2).^2+(Y1-Y2).^2+(X1-X2).^2);

%reduce the number of data points in each data set
figure(5)
x=3/20:3/20:6000; y= M1EA;
xx =1:6000;
yy = spline(x,y,xx);
subplot(5,1,1)
plot(xx,yy)
title('Marker 1 EA')
xlabel('Time')
ylabel('Displacement')
M1EA = yy';

x=3/20:3/20:6000; y= M2EA;
xx =1:6000;
yy = spline(x,y,xx);
subplot(5,1,2)
plot(xx,yy)
title('Marker 2 EA')
xlabel('Time')
ylabel('Displacement')
M2EA = yy';

x=3/20:3/20:6000; y= LA;
xx =1:6000;
yy = spline(x,y,xx);
subplot(5,1,5)
```

```
plot(xx,yy)
title('LA')
%xlabel('Time')
ylabel('Displacement')
LA = yy';

% Save the data
nametosave=['tr1'];

newfilenameM1EA=['Z:\testsnewsub\NF1\' nametosave 'M1EA.txt'];
newfilenameM2EA=['Z:\testsnewsub\NF1\' nametosave 'M2EA.txt'];
newfilenameLA=['Z:\testsnewsub\NF1\' nametosave 'LA.txt'];

save(newfilenameM1EA,'M1EA','-ascii','-tabs','-double')
save(newfilenameM2EA,'M2EA','-ascii','-tabs','-double')
save(newfilenameLA,'LA','-ascii','-tabs','-double')

newfilenameM1EA=[nametosave 'M1EA.txt'];
newfilenameM2EA=[nametosave 'M2EA.txt'];
newfilenameLA=[nametosave 'LA.txt'];
toc

 stringfilename3 = ['Z:\testsnewsub\NF1\tr1LA.l1'];  % read the logarithmic divergence vectors
produced from Rosenstein's algorithm
data3 = dlmread(stringfilename3,'\t',0,0);
time = data3(:,1)/150;
L1LA=2;
figure(12)
plot(time,data3(:,L1LA))
title('L1LA')
xlabel('cycles')
```

```
ylabel('<ln(d)>')
Ymax=max(data3(:,L1LA));
Ymin=min(data3(:,L1LA));

% approximate the linear region of the logarithmic divergence curve of nearest neighbors plotted against time as largest Lyapunov exponent
timeminusone=abs(time-1.5);
[subtractone,m]=min(timeminusone);
LstLA1=polyfit(time(1:m),data3(1:length(time(1:m)),L1LA),1);
hold on
plot(time(1:m),LstLA1(1)*time(1:m)+LstLA1(2),'r')
axis([0,4,Ymin,Ymax])
LyapunovexponentLA1=LstLA1(1);
grid on
```

Mathematica code to produce dynamic equations of motion

```
(* ~~~ Change to local directory ~~~ *)

ClearAll["Global`*"];
Remove["Global`*"];
Directory["Documents"]

(*Define rotation matrix*)
R1[q_] := {{1, 0, 0}, {0, Cos[q], -Sin[q]}, {0, Sin[q], Cos[q]}};

(*Definitions*)

Len[Vtr_, Vor_] := Sqrt[(Vtr - Vor).(Vtr - Vor) ];
Lsqr[Vtr_, Vor_] := (Vtr - Vor).(Vtr - Vor) ;
Vec[Vtr_, Vor_] := (Vtr - Vor);
```

```
Mag[V_] := Sqrt[V.V];

(*Global coordinate system*)

n1 = {1, 0, 0};
n2 = {0, 1, 0};
n3 = {0, 0, 1};

(*  1=X,2=Y,3=Z *)

Cp1 = Transpose[R1[Tp]].n1;
Cp2 = Transpose[R1[Tp]].n2;
Cp3 = Transpose[R1[Tp]].n3;
C51 = Transpose[R1[T5[t]]].n1;
C52 = Transpose[R1[T5[t]]].n2;
C53 = Transpose[R1[T5[t]]].n3;
C41 = Transpose[R1[T4[t]]].n1;
C42 = Transpose[R1[T4[t]]].n2;
C43 = Transpose[R1[T4[t]]].n3;
C31 = Transpose[R1[T3[t]]].n1;
C32 = Transpose[R1[T3[t]]].n2;
C33 = Transpose[R1[T3[t]]].n3;
C21 = Transpose[R1[T2[t]]].n1;
C22 = Transpose[R1[T2[t]]].n2;
C23 = Transpose[R1[T2[t]]].n3;
C11 = Transpose[R1[T1[t]]].n1;
C12 = Transpose[R1[T1[t]]].n2;
C13 = Transpose[R1[T1[t]]].n3;
CT1 = Transpose[R1[Tt[t]]].n1;
CT2 = Transpose[R1[Tt[t]]].n2;
CT3 = Transpose[R1[Tt[t]]].n3

(* Define origins of body *)
```

```
Orp = xp[t]*n1 + yp[t]*n2 + zp[t]*n3;
Or5 = Orp + x5[t]*Cp1 + y5[t]*Cp2 + z5[t]*Cp3;
Or4 = Or5 + x4[t]*C51 + y4[t]*C52 + (z4[t] + L5)*C53;
Or3 = Or4 + x3[t]*C41 + y3[t]*C42 + (z3[t] + L4)*C43;
Or2 = Or3 + x2[t]*C31 + y2[t]*C32 + (z2[t] + L3)*C33;
Or1 = Or2 + x1[t]*C21 + y1[t]*C22 + (z1[t] + L2)*C23;
Ort = Or1 + xt[t]*C11 + yt[t]*C12 + (zt[t] + L1)*C13;

(*Define angular velocities*)

NwL5 = {T5'[t], 0, 0};
NwL4 = {T4'[t], 0, 0};
NwL3 = {T3'[t], 0, 0};
NwL2 = {T2'[t], 0, 0};
NwL1 = {T1'[t], 0, 0};
NwT = {Tt'[t], 0, 0};

(* Define Center of mass of each body *)

G5 = Or5 + Cx5*C51 + Cy5*C52 + Cz5*C53;
G4 = Or4 + Cx4*C41 + Cy4*C42 + Cz4*C43;
G3 = Or3 + Cx3*C31 + Cy3*C32 + Cz3*C33;
G2 = Or2 + Cx2*C21 + Cy2*C22 + Cz2*C23;
G1 = Or1 + Cx1*C11 + Cy1*C12 + Cz1*C13;
GT = Ort + Cxt*CT1 + Cyt*CT2 + Czt*CT3;

(* Define translational velocities *)

vG5 = D[G5, t];
vG4 = D[G4, t];
vG3 = D[G3, t];
vG2 = D[G2, t];
```

```
vG1 = D[G1, t];
vGT = D[GT, t];

(*Inertial about G, approximated as a disc with elliptical cross section (lb>la, radii)*)

I5 = {{1/4 m5 lb^2 + 1/12 m5 L5^2, 0, 0}, {0, 1/4 m5 la^2 + 1/12 m5 L5^2,
   0}, {0, 0, 1/4 m5 (la^2 + lb^2)}};
I4 = {{1/4 m4 lb^2 + 1/12 m4 L4^2, 0, 0}, {0, 1/4 m4 la^2 + 1/12 m4 L4^2,
   0}, {0, 0, 1/4 m4 (la^2 + lb^2)}};
I3 = {{1/4 m3 lb^2 + 1/12 m3 L3^2, 0, 0}, {0, 1/4 m3 la^2 + 1/12 m3 L3^2,
   0}, {0, 0, 1/4 m3 (la^2 + lb^2)}};
I2 = {{1/4 m2 lb^2 + 1/12 m2 L2^2, 0, 0}, {0, 1/4 m2 la^2 + 1/12 m2 L2^2,
   0}, {0, 0, 1/4 m2 (la^2 + lb^2)}};
I1 = {{1/4 m1 lb^2 + 1/12 m1 L1^2, 0, 0}, {0, 1/4 m1 la^2 + 1/12 m1 L1^2,
   0}, {0, 0, 1/4 m1 (la^2 + lb^2)}};
IT = {{1/4 mt lb^2 + 1/12 mt Lt^2, 0, 0}, {0, 1/4 mt la^2 + 1/12 mt Lt^2,
   0}, {0, 0, 1/4 mt (la^2 + lb^2)}};

(*IVD attachments  - origins, terminals and the vector UL*)

IVDP5o = Orp;          IVDP5t = Or5;          IVDP5l = IVDP5t - IVDP5o;
IVD54o = Or5 + L5*C53; IVD54t = Or4;          IVD54l = IVD54t - IVD54o;
IVD43o = Or4 + L4*C43; IVD43t = Or3;          IVD43l = IVD43t - IVD43o;
IVD32o = Or3 + L3*C33; IVD32t = Or2;          IVD32l = IVD32t - IVD32o;
IVD21o = Or2 + L2*C23; IVD21t = Or1;          IVD21l = IVD21t - IVD21o;
IVD1To = Or1 + L1*C13; IVD1Tt = Ort;          IVD1Tl = IVD1Tt - IVD1To;

(*Define Angle ‘b’*)

EPp = 0*Cp1 + Cp2 + 0*Cp3;

EP51 = C52 + 0*C53;
 A5 = ArcCos[(IVDP5l.EP51)/(Mag[IVDP5l]*Mag[EP51])];
```

```
EP41 = C42 + 0*C43;
A4 = ArcCos[(IVD54l.EP41)/(Mag[IVD54l]*Mag[EP41])];
EP31 = C32 + 0*C33;
A3 = ArcCos[(IVD43l.EP31)/(Mag[IVD43l]*Mag[EP31])];
EP21 = C22 + 0*C23;
A2 = ArcCos[(IVD32l.EP21)/(Mag[IVD32l]*Mag[EP21])];
EP11 = C12 + 0*C13;
A1 = ArcCos[(IVD21l.EP11)/(Mag[IVD21l]*Mag[EP11])];
EPT1 = CT2 + 0*CT3;
AT = ArcCos[(IVD1Tl.EPT1)/(Mag[IVD1Tl]*Mag[EPT1])];
```

```
(*Define angle A/2*)
ang5 = T5[t]/2;                ang4 = (T4[t] - T5[t])/2;      ang3 = (T3[t] - T4[t])/2;
ang2 = (T2[t] - T3[t])/2;      ang1 = (T1[t] - T2[t])/2;
angT = (Tt[t] - T1[t])/2;
```

```
(*Define angle 'q'*)
Ang5 = pi - A5 - ang5;
Ang4 = pi - A4 - ang4;
Ang3 = pi - A3 - ang3;
Ang2 = pi - A2 - ang2;
Ang1 = pi - A1 - ang1;
AngT = pi - AT - angT;
```

```
(*Magnitude of vector UL*)
IVD5l = Mag[IVDP5l];      IVD4l = Mag[IVD54l];      IVD3l = Mag[IVD43l];
IVD2l = Mag[IVD32l];      IVD1l = Mag[IVD21l];      IVDTl = Mag[IVD1Tl];
```

```
(*Shear displacement of IVD*)
```

```
IVD5ly = IVD5l*Cos[Ang5];
IVD4ly = IVD4l*Cos[Ang4];
IVD3ly = IVD3l*Cos[Ang3];
IVD2ly = IVD2l*Cos[Ang2];
IVD1ly = IVD1l*Cos[Ang1];
IVDTly = IVDTl*Cos[AngT];

(*Axial displacement of IVD*)

IVD4lz = IVD4l*Sin[Ang4];
IVD3lz = IVD3l*Sin[Ang3];
IVD2lz = IVD2l*Sin[Ang2];
IVD1lz = IVD1l*Sin[Ang1];
IVDTlz = IVDTl*Sin[AngT];


(*IVD energies*)
VKZ = 0.5*KZ*(IVD5lz - rlz5)^2 + 0.5*KZ*(IVD4lz - rlz4)^2 +
        0.5*KZ*(IVD3lz - rlz3)^2 + 0.5*KZ*(IVD2lz - rlz2)^2 +
        0.5*KZ*(IVD1lz - rlz1)^2 + 0.5*KZ*(IVDTlz - rlzt)^2;

VKY = 0.5*KY*(IVD5ly - rly5)^2 + 0.5*KY*(IVD4ly - rly4)^2 +
         0.5*KY*(IVD3ly - rly3)^2 + 0.5*KY*(IVD2ly - rly2)^2 +
        0.5*KY*(IVD1ly - rly1)^2 + 0.5*KY*(IVDTly - rlyt)^2;

VKT = 0.5*KT*(T5[t] - rt5)^2 + 0.5*KT*(T5[t] - T4[t] - rt4)^2 +
        0.5*KT*(T4[t] - T3[t] - rt3)^2 + 0.5*KT*(T3[t] - T2[t] - rt2)^2 +
        0.5*KT*(T2[t] - T1[t] - rt1)^2 + 0.5*KT*(T1[t] - Tt[t] - rtt)^2;

VCZ = 0.5*CZ*(D[IVD5lz, t])^2 + 0.5*CZ*(D[IVD4lz, t])^2 +
        0.5*CZ*(D[IVD3lz, t])^2 + 0.5*CZ*(D[IVD2lz, t])^2 +
        0.5*CZ*(D[IVD1lz, t])^2 + 0.5*CZ*(D[IVDTlz, t])^2 ;
```

```
VCY = 0.5*CY*(D[IVD5ly, t])^2 + 0.5*CY*(D[IVD4ly, t])^2 +
        0.5*CY*(D[IVD3ly, t])^2 + 0.5*CY*(D[IVD2ly, t])^2 +
        0.5*CY*(D[IVD1ly, t])^2 + 0.5*CY*(D[IVDTly, t])^2 ;

VCT = 0.5*CT*(D[T5[t], t])^2 + 0.5*CT*(D[T5[t] - T4[t], t])^2 +
        0.5*CT*(D[T4[t] - T3[t], t])^2 + 0.5*CT*(D[T3[t] - T2[t], t])^2 +
        0.5*CT*(D[T2[t] - T1[t], t])^2 + 0.5*CT*(D[T1[t] - Tt[t], t])^2 ;

(* Kinetic energy *)
T = 1/2*m5*vG5.vG5 + 1/2*m4*vG4.vG4 + 1/2*m3*vG3.vG3 + 1/2*m2*vG2.vG2 +
  1/2*m1*vG1.vG1 +1/2*mt*vGT.vGT + 1/2*NwL5.I5.NwL5 + 1/2*NwL4.I4.NwL4 +
1/2*NwL3.I3.NwL3 +1/2*NwL2.I2.NwL2 + 1/2*NwL1.I1.NwL1 + 1/2*NwT.IT.NwT ;

(*Potential energy*)

g = {gx, gy, gz}; (*gravity vector*)
V = m5*g.G5 + m4*g.G4 + m3*g.G3 + m2*g.G2 + m1*g.G1 + mt*g.GT + VKZ + VKY +
  VKT;

(*Dissipation energy*)

Dm =  VCZ + VCY + VCT;

(*LAGRANGE DERIVATIVE*)
(*Define Lagrange derivative*)

EL[q_] := D[D[T, q'[t]], t] - D[T, q[t]] + D[V, q[t]] + D[Dm, q'[t]];

(*Calculate Lagrange derivative*)
```

```
ELy5 = EL[y5];      ELz5 = EL[z5];      ELT5 = EL[T5];
ELy4 = EL[y4];      ELz4 = EL[z4];      ELT4 = EL[T4];
ELy3 = EL[y3];      ELz3 = EL[z3];      ELT3 = EL[T3];
ELy2 = EL[y2];      ELz2 = EL[z2];      ELT2 = EL[T2];
ELy1 = EL[y1];      ELz1 = EL[z1];      ELT1 = EL[T1];
ELyT = EL[yt];      ELzT = EL[zt];      ELTT = EL[Tt];
```

```
<< ToMatlab.m (*execute the convertor file to create an m-file (matlab file) of mathematica expression*)

(*create an m-file of Lagrange derivatives*)

WriteMatlab[ELM, "ELM1.m", "ELM", 2000]


(*MUSCLE FILE CREATION*)

(*Define muscle attachments*)

musOr = {Ox, Oy, Oz}*0.01;
musTer = {Tx, Ty, Tz}*0.01;
ins1 = {in1x, in1y, in1z}*0.01;
ins2 = {in2x, in2y, in2z}*0.01;
ins3 = {in3x, in3y, in3z}*0.01;
ins4 = {in4x, in4y, in4z}*0.01;
ins5 = {in5x, in5y, in5z}*0.01;


(*Muscles with origins on pelvis and terminals on ribs*)

terminalR = Ort + musTer.{CT1, CT2, CT3};
momR = musTer.{CT1, CT2, CT3};
LenR = Len[terminalR, musOr];
LsR = Lsqr[terminalR, musOr];
dLenR = D[LenR, t];
```

```
(*Define force vector*)

forceR = fo *csa* ( q*((L - Lo)/Lo) + b*(dL/Lo) + 1)*Vec[ musOr, terminalR]/L;


(*Write the m-file of force vector*)

WriteMatlab[forceR, "forceR.m", "forceR", 2000]
```

Matlab code for simulation study

```
tic
load data  %load the data set

T = 1/150:1/150:2+2/150;
t = T(1:length(A1));

% divide the lumbar angle into lumbar vertebral angles
T5 = 0*pi/180+0.236*A1;
T4 = 0.29*A1+T5;
T3 = 0.21*A1+T4;
T2 = 0.132*A1+T3;
T1 = 0.132*A1+T2;
Tt = A2; % thorax angle

% compute the velocities and accelerations for one flexion and extension cycle
for i = 1:301
   dt = t(i+1)-t(i);
   if i == 1
      dTt(i) = (Tt(i+1)-Tt(i))/dt; dT1(i) = (T1(i+1)-T1(i))/dt; dT2(i) = (T2(i+1)-T2(i))/dt;
      dT3(i) = (T3(i+1)-T3(i))/dt; dT4(i) = (T4(i+1)-T4(i))/dt; dT5(i) = (T5(i+1)-T5(i))/dt;
```

```
    else
        dTt(i) = (Tt(i+1)-Tt(i-1))/2/dt; dT1(i) = (T1(i+1)-T1(i-1))/2/dt; dT2(i) = (T2(i+1)-T2(i-
1))/2/dt;
        dT3(i) = (T3(i+1)-T3(i-1))/2/dt; dT4(i) = (T4(i+1)-T4(i-1))/2/dt; dT5(i) = (T5(i+1)-T5(i-
1))/2/dt;
    end
end

for i = 1:300
    dt = t(i+1)-t(i);
    if i == 1
        ddTt(i) = (dTt(i+1)-dTt(i))/dt; ddT1(i) = (dT1(i+1)-dT1(i))/dt; ddT2(i) = (dT2(i+1)-
dT2(i))/dt;
        ddT3(i) = (dT3(i+1)-dT3(i))/dt; ddT4(i) = (dT4(i+1)-dT4(i))/dt; ddT5(i) = (dT5(i+1)-
dT5(i))/dt;

    else
        ddTt(i) = (dTt(i+1)-dTt(i-1))/2/dt; ddT1(i) = (dT1(i+1)-dT1(i-1))/2/dt; ddT2(i) = (dT2(i+1)-
dT2(i-1))/2/dt;
        ddT3(i) = (dT3(i+1)-dT3(i-1))/2/dt; ddT4(i) = (dT4(i+1)-dT4(i-1))/2/dt; ddT5(i) =
(dT5(i+1)-dT5(i-1))/2/dt;
    end
end

V1 = dlmread('muscles2.dat'); % load the muscle data
properties = csvread('properties1.csv'); % load the physical properties of torso segments

%%
load main12_5 % load the results from the previous time step
```

```
%initial guess for the optimization taken from previous step
aa0=XX;
clear XX*
XX0 = aa0;
Y1=  aa0(46:51);
Vy1=aa0(52:57);
fy1=aa0(58:63);
 Z1=aa0(64:69);
 Vz1=aa0(70:75);
fz1=aa0(76:81);

% Velocities and acceleration are computed as function previous step values and time
for ii=1:6
    aa0(ii+51)=Vy1(ii)+(fy1(ii)+aa0(57+ii))/60;
    aa0(ii+69)=Vz1(ii)+(fz1(ii)+aa0(75+ii))/60;
end

for ii=1:6
    aa0(ii+45)=Y1(ii)+(Vy1(ii)+aa0(51+ii))/60+(fy1(ii)+aa0(57+ii))*(1/30)^2/4;
    aa0(ii+63)=Z1(ii)+(Vz1(ii)+aa0(69+ii))/60+(fz1(ii)+aa0(75+ii))*(1/30)^2/4;
end

ml = V1(1:45,34); csa = V1(1:45,35); % read the length and cross sectional area of each muscle

% time steps at increment of 5s are used in the simulation
thetas = [Tt(10), T1(10), T2(10), T3(10), T4(10), T5(10), dTt(10), dT1(10), dT2(10), dT3(10),
dT4(10), dT5(10), ddTt(10), ddT1(10), ddT2(10), ddT3(10), ddT4(10), ddT5(10)];

% setting lower and upper bounds
LB(1:45,1) = zeros(45,1);
LB(46:51,1) =[-.002 -0.0033 -.0038 -.0029 -.0014 -0.0006]+0.000000002;
```

```
LB(52:57,1) = -ones(6,1)*(0.009);
LB(58:63,1) = ones(6,1)*(-0.7);
LB(64:69,1) = 0.001*[5 6 7 6.5 7 5.5];
LB(70:75,1) = ones(6,1)*(-0.005);
LB(76:81,1) = ones(6,1)*(-0.1);

UB(1:45,1) = ones(45,1);
UB(46:51,1) = ones(6,1)*(0.006);
UB(52:57,1) = ones(6,1)*(0.02);
UB(58:63,1) = ones(6,1)*(0.7);
UB(64:69,1) = ones(6,1)*(0.02);
UB(70:75,1) = ones(6,1)*(0.005);
UB(76:81,1) = ones(6,1)*(0.1);

A = []; B = [];

options=optimset('LargeScale','off','MaxFunEvals',1e5,'MaxIter',500,'TolX',1e-12,'TolFun',1e-
8,'TolCon',1e-9,'Display','iter','MaxSQPIter',2000,'gradobj','off'); % show progress after each
iteration

XX = fmincon('obj2_15',aa0,A,B,A,B,LB,UB,'mycon1',options,thetas, XX0);
save main12_10
toc

%%%%%%%%%%%%%%%%%%%%%%%%%%%%%%%%%%%%%%%%%%%%%
% Objective function
function P = obj2_15(XX,thetas, csa, ml,XX0)

thetat = thetas(1); theta1 = thetas(2); theta2 = thetas(3); theta3 = thetas(4); theta4 = thetas(5);
theta5 = thetas(6);
dthetat = thetas(7); dtheta1 = thetas(8); dtheta2 = thetas(9); dtheta3 = thetas(10); dtheta4 =
```

```
thetas(11); dtheta5 = thetas(12);
ddthetat = thetas(13); ddtheta1 = thetas(14); ddtheta2 = thetas(15); ddtheta3 = thetas(16);
ddtheta4 = thetas(17); ddtheta5 = thetas(18);

Yt= XX(46);  Y1=XX(47); Y2=XX(48); Y3 = XX(49); Y4= XX(50); Y5= XX(51);
dYt= XX(52);  dY1= XX(53); dY2= XX(54); dY3 = XX(55); dY4= XX(56); dY5= XX(57);
ddYt= XX(58);  ddY1= XX(59); ddY2= XX(60); ddY3 = XX(61); ddY4= XX(62); ddY5=
XX(63);
 Zt= XX(64);  Z1=XX(65); Z2=XX(66); Z3 = XX(67); Z4= XX(68); Z5= XX(69);
dZt= XX(70);  dZ1= XX(71); dZ2= XX(72); dZ3 = XX(73); dZ4= XX(74); dZ5= XX(75);
ddZt= XX(76);  ddZ1= XX(77); ddZ2= XX(78); ddZ3 = XX(79); ddZ4= XX(80); ddZ5=
XX(81);

properties = csvread('properties1.csv');

A = genfor2(thetat, theta1, theta2, theta3, theta4, theta5,Yt, Y1, Y2, Y3, Y4, Y5, Zt, Z1, Z2,
Z3,Z4, Z5,dthetat, dtheta1, dtheta2,dtheta3, dtheta4, dtheta5,dYt, dY1, dY2, dY3, dY4, dY5,
dZt, dZ1, dZ2, dZ3,dZ4, dZ5); % computing the generalized force matrix, the LHS of the
equation Aeq* alphas = Beq

Beq = ELM1(thetat, theta1, theta2, theta3, theta4, theta5,Yt, Y1, Y2, Y3, Y4, Y5, Zt, Z1, Z2,
Z3,Z4, Z5,dthetat, dtheta1, dtheta2,dtheta3, dtheta4, dtheta5,dYt, dY1, dY2, dY3, dY4, dY5,
dZt, dZ1, dZ2, dZ3,dZ4, dZ5, ddthetat, ddtheta1, ddtheta2,ddtheta3, ddtheta4, ddtheta5,ddYt,
ddY1, ddY2, ddY3, ddY4, ddY5, ddZt, ddZ1, ddZ2, ddZ3,ddZ4, ddZ5, properties)';  %
computing the RHS matrix of the equation Aeq* aplhas = Beq

for i=1:length(ml)
   m(i) = 1000*(csa(i))*ml(i)/1000000; % calculating the mass of the muscles
end
p = m.*((74/4)*sin(a*pi/2)+(111/2)*(1-cos(a*pi/2))); % the metabolic power function (cost
function)
```

```
p = sum(p);
q = 0;

for ii = 1:18
    q = q+(Aeq(ii,:)*a' - Beq(ii))^2;
end

P= p+10^6*q;
```

Appendix C

The Lyapunov Exponents

Abbreviations:

sub = subject gen = gender

bf = before fatigue af = after fatigue

as = asymmetric trial s = asymmetric trial

nps = no pelvic restraint

sub	gen	as1-bf	as2-bf	s1-bf	s2-bf	as1-bf-nps	as2-bf-nps	s1-bf-nps	s2-bf-nps
1	f	0.95	0.86	0.68	0.78	0.68	0.86	0.75	0.79
2	f	0.98	1.04	1.12	1.24	0.89	0.91	0.93	0.9
3	f	1.1	0.88	1.08	0.96	0.91	0.88	0.93	0.92
4	f	0.65	0.67	0.85	0.81	0.77	0.89	0.82	0.97
5	f	0.61	0.71	0.87	0.92	0.95	0.99	0.79	0.79
1	m	0.76	0.8	0.85	0.82	0.79	0.81	0.78	0.8
2	m	0.76	0.87	0.79	0.86	0.98	0.9	0.94	0.98
3	m	0.79	0.66	1.15	0.96	0.81	0.89	0.96	0.93
4	m	0.84	0.85	0.9	0.95	0.72	0.9	0.74	0.69
5	m	0.98	0.97	0.84	0.98	0.9	0.88	0.8	0.85

sub	gen	as1-af	as2-af	s1-af	s2-af	as1-af-nps	as2-af-nps	s1-af-nps	s2-af-nps
1	f	0.87	1.01	0.99	0.85	0.89	1.06	0.84	0.89
2	f	1.18	0.97	0.93	1.19	0.9	1	0.93	0.91
3	f	1.13	0.93	1.1	1.04	0.9	0.74	0.78	0.73
4	f	0.7	0.83	0.88	0.86	0.98	0.83	0.89	1.04
5	f	1.1	1	0.9	0.93	0.97	0.99	0.88	0.98
1	m	0.82	0.82	0.81	0.86	0.78	0.9	0.83	0.85
2	m	1.08	0.98	1.01	1.28	0.89	1.03	1.08	0.94
3	m	0.95	1.15	0.84	1.03	0.82	0.93	0.92	1.15
4	m	0.82	0.97	0.85	1.14	0.83	1	0.93	1.06
5	m	1.03	0.95	0.88	0.99	0.99	0.93	0.95	0.94

IVD Rest Lengths

Abbreviations:

Th = thorax P = pelvis

St.Eq.L = standing posture in equilibrium Sub = subject

IVD	St. Eq. L (mm)	Rest lengths (mm)				
		Sub 1	Sub 2	Sub 3	Sub 4	Sub 5
Th - L1	8.00	8.80	8.94	8.76	8.91	9.04
L1 - L2	9.00	9.80	9.94	9.76	9.91	10.03
L2 - L3	11.00	12.04	12.22	11.98	12.18	12.34
L3 - L4	11.00	12.12	12.31	12.06	12.27	12.44
L4 _ L5	11.00	12.11	12.31	12.05	12.26	12.44
L5 - P	9.00	10.28	10.50	10.21	10.46	10.65

Spinal Loads in Standing Equilibrium Position

	Sub 1	Sub 2	Sub 3	Sub 4	Sub 5
Comp. Load (N)	245.43	288.21	232.50	278.98	316.40
Shear load (N)	0.17	0.12	0.12	0.13	0.12